INVESTIGATING THE FUNCTION OF 36K – A MAJOR CNS MYELIN PROTEIN IN ZEBRAFISH

Dissertation

zur

Erlangung des Doktorgrades (Dr. rer. nat.)

der

Mathematisch-Naturwissenschaftlichen Fakultät

der

Rheinischen Friedrich-Wilhelms-Universität Bonn

vorgelegt von

Bhuvaneswari Nagarajan

aus

Chennai

Bonn 2018

Angefertigt mit Genehmigung der Mathematisch-Naturwissenschaftlichen Fakultät der Rheinischen Friedrich-Wilhelms-Universität Bonn

1. Gutachter: Prof. Dr. Benjamin Odermatt

2. Gutachter: Prof. Dr. Ulrich Kubitscheck

Tag der Promotion: 31.01.2019

Erscheinungsjahr: 2019

Abstract

Zebrafish can regenerate and remyelinate CNS axons following injury in contrast to humans and other mammals. Common myelin proteins like Mbp, Plp1/DM20 are conserved across species from zebrafish to humans. In addition to the conserved myelin proteins, there are other major myelin proteins like ClaudinK, Zwilling, 36K identified in teleosts. 36K is one of the most abundant CNS myelin proteins in zebrafish brain while it is absent as protein in mammals. Despite the abundance, its function remains unknown. Understanding the function of 36K during development is essential to study the function during remyelination. This study focusses on investigating the function of 36K during development in zebrafish. Translation blocking Morpholinos have been designed to address the function by knocking down the expression of 36K. 36K knockdown larvae have reduced body-length, disrupted myelin and fewer differentiated OPCs. The phenotypes could be rescued when *36k* mRNA was co-injected with the Morpholino, suggesting the specificity of the Morpholino. With a mRNA microarray analysis, an upregulation of Notch targets has been found in 36K knockdown larvae. Further confirming that 36K acts on oligodendrocyte precursor cells through Notch, the phenotypes could be rescued in 36K knockdown larvae when treated with a gamma secretase inhibitor. This inhibitor indirectly inhibits Notch, by preventing the release of Notch intracellular domain, the step crucial for Notch activation. As 36K belongs to the short chain dehydrogenase family and is present in cell membrane, we further hypothesised that 36K alters membrane lipids and hence regulates the activity of gamma secretase. Thin layer chromatography and liquid chromatography-mass spectrometry experiments could confirm alteration in lipids in 36K knockdown larvae. In summary, 36K regulates membrane lipid composition and hence activity of gamma secretase and Notch ligands. This in turn has an influence on Notch activity and oligodendrocyte differentiation and hence myelination. Further studies will have to be carried out to investigate the role of 36K in compact myelin as well as its role on OPC differentiation during remyelination, which might help in developing potential strategies for remyelination in humans.

Zusammenfassung

Die Myelinscheide besteht aus Ausläufern der Plasmamembran von Gliazellen, welche sich um Axone wickeln. Im zentralen Nervensystem (ZNS) wird die Myelinscheide von Oligodendrozyten und im peripheren Nervensystem von Schwann Zellen gebildet. Eine Störung der Myelinscheide im ZNS kann die Folge verschiedener demyelinisierender Erkrankungen wie z.B. der Multiplen Sklerose sein und tritt häufig auch im Zusammenhang mit weiteren neurodegenerativen Erkrankungen auf. In dieser Arbeit wurde die Funktion eines wichtigen ZNS-Myelinproteins während der frühen Zebrafisch Entwicklung untersucht. Zebrafische sind im Gegensatz zu Menschen und anderen Säugetieren in der Lage Axone des zentralen Nervensystems (ZNS) nach einer Verletzung erfolgreich zu regenerieren und zu remyelinisieren. Neben bekannten Myelinproteinen wie Mbp, Plp1, P0, ist das Protein 36K, welches im Säugetier bis heute noch nicht identifiziert werden konnte, ein Hauptbestandteil des Zebrafisch ZNS Myelins. Obwohl 36K eines der am stärksten exprimierten Proteine im Gehirn von Zebrafischen ist, ist seine Funktion weitgehend unbekannt. Eine Aufklärung der Rolle von 36K im Zebrafisch Myelin könnte daher wesentlich zur Entwicklung neuer therapeutischer Strategien zur Behandlung von demyelinisierenden Erkrankungen beitragen. Um die Funktion von 36K während der Myelinisierung genauer zu untersuchen, wurde im Rahmen dieser Arbeit durch spezifische Translations-blockierende Morpholino-Oligonukleotide (MOs) ein 36K Protein-Knockdown hervorgerufen. Knockdown-Fisch-Larven wiesen eine reduzierte Körperlänge auf und reagierten in Escape-Response Experimenten vermindert. Mittels 2-Photonen-Mikroscopie wurde eine Reduktion der Anzahl von unreifen Oligodendrozyten-Vorläuferzellen sowie differenzierten, myelinisierenden Oligodendrozyten festgestellt. Des Weiteren war die Myelinisierung in den Knockdown-Larven stark beeinträchtigt. Ein Rescue-Experiment, das eine Co-Injektion von 36K MO und *36k* mRNA beinhaltete, konnte die Reduktion der Zellzahlen beheben und somit die Spezifität des MO bestätigen. Die Injektion eines zweiten unabhängigen Translations-blockierenden MO gegen 36K verursachte ebenfalls eine

Reduktion von Oligodendrozyten-Vorläuferzellen, wodurch die Spezifität des ersten MO zusätzlich bewiesen wurde. Mittels mRNA Microarray-Analyse wurde in den Knockdown-Larven eine Hochregulierung des Notch-Targets festgestellt. Knockdown- Larven, die mit einem Gamma-Sekretase-Inhibitor behandelt wurden, der die Ausschüttung der Notch-intrazellulären Domäne und somit die Aktivierung von Notch verhindert, wiesen eine ähnliche Anzahl an Oligodendrozyten-Vorläuferzellen wie die Kontrollen auf. Daraus lässt sich schlussfolgern, dass 36K die Anzahl von Oligodendrozyten-Vorläuferzellen über den Notch-Signalweg reguliert. Da 36K zur Familie der Kurz-Ketten-Dehydrogenasen gehört und in der Zellmembran vorhanden ist, wurde von uns angenommen, dass 36K Membranlipide und damit den Zugang und die Aktivität von Notch-Liganden und der Gamma-Sekretase beeinflussen könnte. Veränderungen in der Lipidzusammensetzung in 36K Knockdown-Fischlarven konnten durch Dünnschicht-Chromatographie und Massenspektrometrie Experimente bestätigt werden. Zusammenfassend implizieren die generierten Daten, dass 36K während der frühen Myelin Entwicklung die Aktivität von Notch-Liganden und Gamma-Sekretase-verarbeitendem Notch innerhalb der Membran verändert, möglicherweise durch Regulierung der Membranlipidzusammensetzung. Des Weiteren wurde festgestellt, dass 36K die Differenzierung von Oligodendrozyten sowie die Myelinisierung während der embryonalen Entwicklung reguliert. Möglicherweise spielen daher diese Signalwege im Zusammenhang mit 36K, die während der Entwicklung auftreten auch unter pathologischen Bedingungen in adulten Lebensphasen eine wichtige Rolle.

Table of Contents

List of Figures and Tables

Abbreviations

oligodendrocyte precursor cells (OPCs)

central nervous system (CNS)

myelin basic protein (MBP)

proteolipid protein (Plp1)

days post fertilization (dpf)

Reverse transcription polymerase chain reaction (RT PCR)

Quantitative Real time polymerase chain reaction (q-rt-PCR, qPCR)

Calibrated Normalized Relative Quantities (CNRQ)

Messenger Ribonucleic acid (mRNA)

36K Morpholino (MO1)

control Morpholino (control MO)

36K Morpholino co-injected with 36K mRNA (MO1+RNA)

second translation blocking Morpholino to 36K (MO2)

TrichostatinA (TSA)

histone deacetylase (HDAC)

Sonic hedgehog (Shh)

Fibroblast growth factor (FGF)

Retinoic acid (RA)

Glial fibrillary acidic protein (Gfap)

Hairy related 4 (Her4)

Deltaa (dla)

Dorsal root ganglion (DRG)

N-[N-(3,5-difluorophenacetyl)-l-alanyl]-S-phenylglycine t-butyl ester (DAPT)

1. Introduction

One of the major goals of neuro-developmental research is to understand the mechanisms that regulate the generation of different individual types of neuronal and glial cells in the central nervous system (CNS). This does not only elucidate normal CNS development, but also helps in unravelling the mechanisms underlying neurological diseases. Neuronal proliferation, differentiation, circuit formation, synaptogenesis, neurotransmission, all of these events seem to involve the activity or participation of glial cells (Barres, 2008). Myelin, extension of plasma membrane of glial cells around some neuronal axons, forms huge part of the CNS (Sherman and Brophy, 2005). The evolution of CNS has been dependent on and accompanied by the acquisition and development of myelin sheath (Zalc, 2016). Disruption of myelin sheath in CNS can happen in various demyelinating diseases like Multiple Sclerosis, myelopathies, leukodystrophies and can occur together with other neurodegenerative diseases involving axonal degeneration (Franklin and Ffrench-Constant, 2008). The importance of myelin proteins and their significance during myelinogenesis and also during remyelination following disease or injury should not be overlooked in maintenance of structural integrity of myelin as well as in the development of glial cells. In this study, the function of a major CNS myelin protein during development in zebrafish is investigated.

1.1. Progenitor patterning and gliogenesis in the spinal cord

During vertebrate embryogenesis, neural development is one of the most complex processes and is also the earliest to start and the last to be completed (Hill, 2012). There are two major classes of neural tube stem cells that give rise to two types of cells, neurons and glia, that make the majority of the nervous system (Murphy et al., 1997). These two classes of cells differentiate into several different types with important and highly specialised functions and shapes. Neurulation starts with the formation of the notochord, which plays a major role in

patterning the initial formation of the nervous system (Nikolopoulou et al., 2017). Notochord is the defining structure in all Chordate embryos. It forms initially as the axial process and then extends as a hollow tube from the primitive pit to the oral membrane (Satoh et al., 2014). The axial process merges with the endodermal layer forming the notochordal plate, which then rises back into the mesodermal layer forming a column of cells which then becomes the Notochord (Hill, 2012; Satoh et al., 2014).

The neural plate is then formed above the notochord from the central portion of the ectoderm that thereafter folds to form the neural tube. This will eventually form the complete central nervous system (CNS) (Smith and Schoenwolf, 1989). Neuronal specification is thought to happen before the neural plate folds stimulated by signals from notochord, mesoderm. There is a bending occurring in the midline in the region forming the neural groove. The neural plate eventually fuses on the dorsal side to form a hollow neural tube. This extends rostrally and caudally, leaving two neuropores at either ends, which close later, forming the ventricles of the brain and spinal cord (William J. Larsen, Lawrence S. Sherman, 2002). Neural stem cells lie in the zone closest to the ventricular layer, which generates both neuroblasts and glioblasts (Hill, 2012). Neuroblasts give rise to neurons and glioblasts give rise to glia. Both these cells undergo complex stages of differentiation, interacting over a long-time period during development, with specific markers for different stages (Delaunay et al., 2008). Vertebrate neurulation is shown in (Figure 1.1A-D).

In zebrafish, instead of folding up the neural plate into a tube, a neural keel is first formed (Lowery and Sive, 2004). The topological arrangement of cells during neural keel formation from the neural plate is similar to that of other vertebrates (Papan and Campos-Ortega, 1999). As part of the so-called secondary neurulation, neural rod formed by fusing of neural keel at the dorsal midline, inflates to form a vertebrate typical tube (Schmitz et al., 1993). Hence, neurulation in fish and mammals leads to the formation of a highly similar structure,

the neural tube (Schmidt et al., 2013). Zebrafish neurulation in hindbrain (Figure 1.2A-D) and spinal cord (Figure 1.2E-H) is depicted in (Figure 1.2).

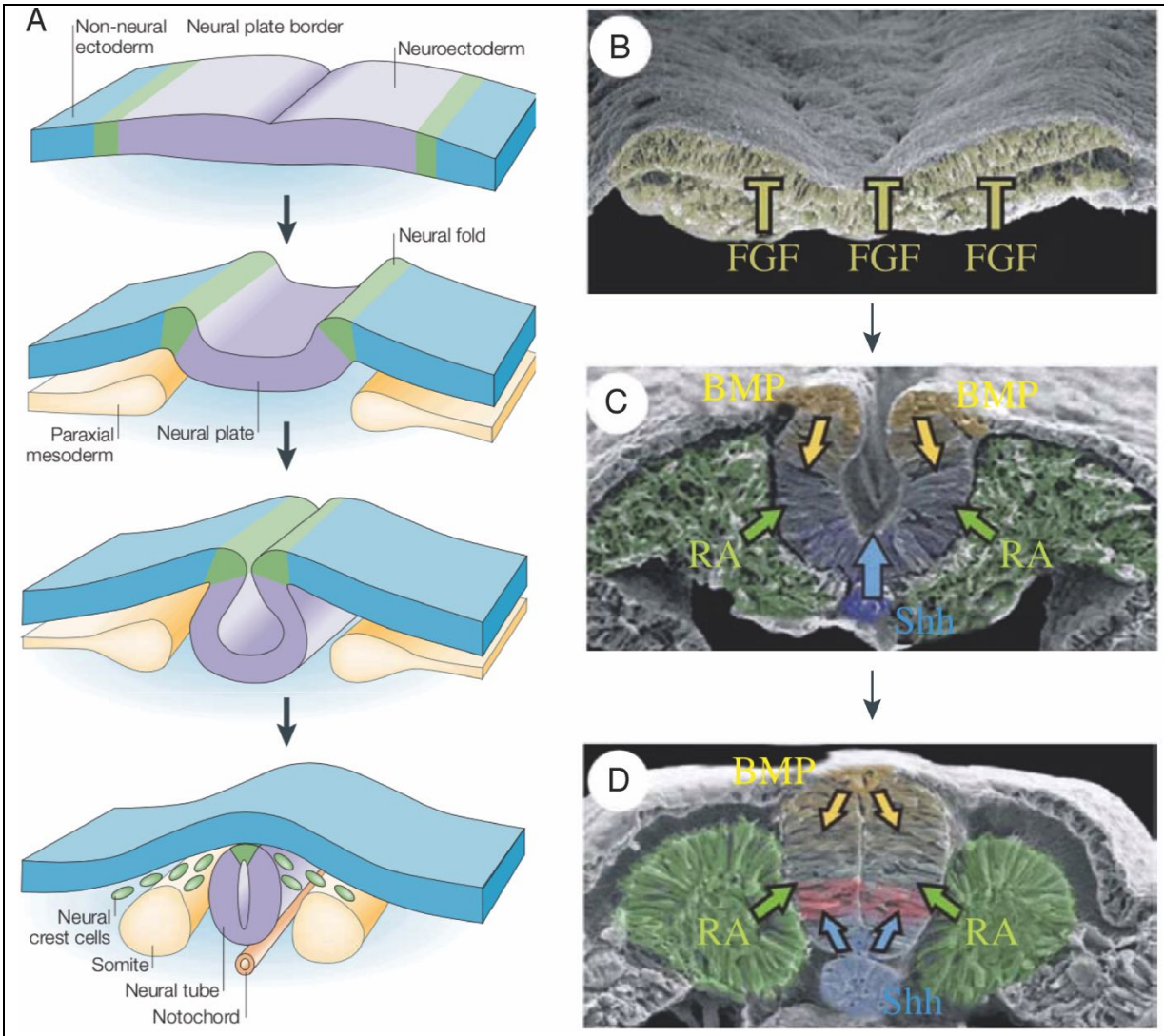

Figure 1.1: Neurulation and signalling pathways. (A) Neural plate borders elevate forming the neural folds, causing the neural plate to roll into the neural tube. Neural crest cells delaminate from the neural folds or dorsal neural tube. Figure adapted from (Gammill and Bronner-Fraser, 2003). (B-D) Scanning electron micrographs of chick neural tube showing different stages of neurulation (B) neural plate (C) neural folds (D) neural tube also depicting the signalling sources. Figure adapted from (Briscoe and Novitch, 2008).

Several signalling pathways decide dorsoventral patterning during early development. The notochord secretes sonic hedgehog (Shh) leading to ventral expression of Shh (Litingtung and Chiang, 2000; Pierani et al., 1999; Sasai et al., 2014). Neural specification requires

Delta/Notch signalling (Grandbarbe, 2003; Louvi and Artavanis-Tsakonas, 2006). Border patterning is through fibroblast growth factor (FGF) and bone morphogenetic protein (BMP) (Kudoh et al., 2002; Liu and Niswander, 2005). Generation of neuronal subtypes in the ventral neural tube occurs in response to a graded Shh/Gli signalling (Briscoe and Novitch, 2008; Lu et al., 2000; Price and Briscoe, 2004). An early dorsoventral patterning leading to five distinct neuronal subtypes emerging in the ventral neural tube in precise spatial order has been identified with various transcription factors and molecular markers involved: MNs and four groups of interneurons V0, V1, V2, V3 (Briscoe and Novitch, 2008) (Figure 1.1B-D).

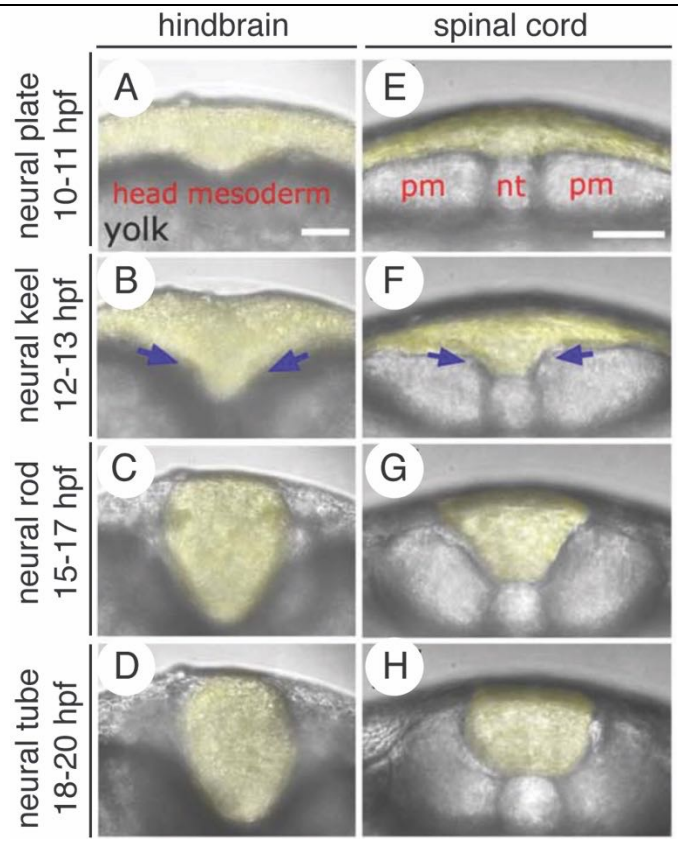

Figure 1.2: Neurulation in zebrafish. Transverse brightfield images showing tissue movements of neurulation in zebrafish in hindbrain (A-D) and spinal cord (E-H) with the neural plate pseudo-coloured in yellow. (A, E) Neural plate is over an underlying mesoderm at 10-11 hpf. (B, F) The neural plate converges toward the midline to generate a neural keel by 12-13 hpf. (C,G) The neural keel changes shape to form the neural rod around 15-17 hpf. (D,H) The neural rod transforms into the neural tube by 18-20 hpf. Figure taken from (Araya et al., 2016).

Floor plate refers to the cells that occupies the ventral midline of the spinal cord. Ventral neural progenitor cells expressing the transcription factors Olig1 and Olig2 are called pMN progenitors. These produce motor neurons and then oligodendrocytes. Progenitor transcription factors can be subdivided into class I and class II proteins based on their mode of regulation by Shh signalling (Price and Briscoe, 2004). Expression of class I proteins is repressed at distinct thresholds of Shh, consequently limiting their ventral borders of expression. On the contrary, expression of class II proteins depends on Shh signalling, so their dorsal expression boundaries are defined by graded Shh signalling. Gli proteins Gli1, Gli2, Gli3 are expressed as repressors in the absence of Shh in the neural tubes in vertebrates (Briscoe and Novitch, 2008; Sasai et al., 2014). In addition to Shh/Gli signalling, FGF signals are present in neural progenitors from the time of formation. This inhibits neural differentiation, and suppresses the expression of class I and II proteins, thus preventing the dorsoventral patterning (Kudoh et al., 2002). Therefore, maturation of neural progenitors depends on evasion from FGF signals coming from the mesodermal layers. Retinoic acid (RA) attenuates the proliferative effects of FGFs and also plays a major role in inducing class I proteins expression, hence offset the ventralising effects of Shh (Kudoh et al., 2002; Maden, 2006). BMPs from the neural folds has prominent roles in the specification of cell fate in the dorsal neural tube (Bond et al., 2012; Lee et al., 2008). Wnt proteins arising from the dorsal midline promote progenitor proliferation throughout the neural tube, and also inhibit Shh signalling (Ulloa and Martı, 2010) Influences of various signalling on cell fate and neuronal development is depicted in (Figure 1.3A-C).

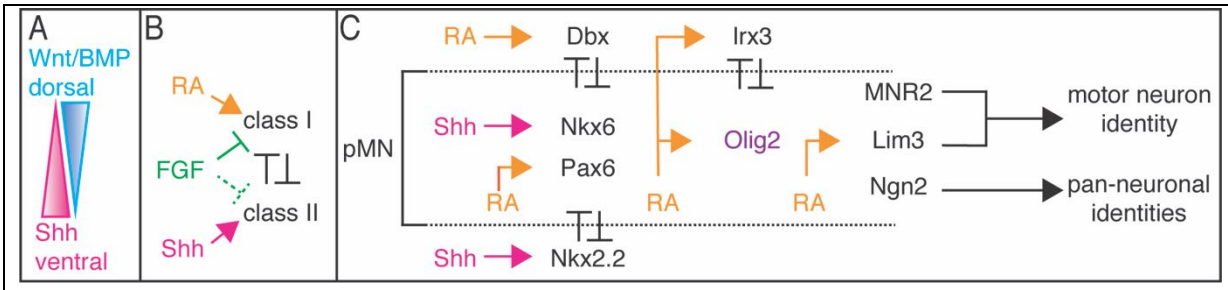

Figure 1.3: Influences of various signalling and transcription factors on cell fate and neuronal development. (A) Shh signalling from the ventral domain is counteracted by Wnt/BMP signalling from the dorsal domain and induces homeodomain expressions. (B) FGF blocks both class I and class II protein expressions and hence prevents dorso-ventral patterning. Shh represses class I expression and induces class II transcription factors expression, while RA causes class I expression. (C). Shh and RA initiate the expression of Nkx6, Pax6 in ventral progenitors. Repressor activities of Nkx6, Pax6 prevent inhibitor expression such as Dbx, Nkx2.2, and activate Olig2 expression. Within pMN, Olig2 represses Irx3 and directs MN differentiation. This repressor activity of Olig2 is in conjunction with RA receptors. Figures adapted from (Briscoe and Novitch, 2008; Ulloa and Martı, 2010).

Expression of several transcription factors mediate cell fate and neuronal differentiation. Olig2 transcription factor expression begins in the early stages in the new neural tube as a response to both Shh and RA signals (Wilson and Maden, 2005). It is found to act downstream of the class II proteins Nkx6.1 and Nkx6.2. Olig2 then plays a role in dorsoventral patterning by repressing class I protein Irx3 from the ventral neural tube. It is a unique marker for MN progenitors. Olig2 orchestrates the expression of Ngn2/NeuroM. A critical step in the differentiation of MNs is the increase in the levels of Ngn2/NeuroM expression so that they can bind to the Hb9 promoter and activate its expression. Otherwise, Olig2 recruits a repressor complex that prevents the expression of Hb9 keeping them in immature progenitor state. Thus, Olig2 appears to coordinate several steps including progenitor patterning, motor neuron (MN) fate determination and neurogenic differentiation (Figure 1.3C). A residual population of Olig2+ cells that did not differentiate into MNs early in development, gives rise to oligodendrocytes later in development. Therefore, the maintenance of undifferentiated Olig2+ progenitors throughout MN development is important

for gliogenesis (Briscoe and Novitch, 2008; Price and Briscoe, 2004). Glial cells have many roles, both in the central and the peripheral nervous system. There is a special type of early developmental glia called radial glia. The other types of glia include macroglial cells namely astrocytes, oligodendrocytes, and microglia in the CNS and Schwann cells in the PNS (Barres, 2008).

1.2. Development of oligodendrocytes and myelination

Proliferating glial precursors are specific to the ventral ventricular zone, dorsal to the floor plate. Following the majority of spinal cord neurogenesis, a subset of these cells generates oligodendrocytes (Noll and Miller, 1993). Most of the oligodendrocytes depend on a growth factor called platelet derived growth factor (PDGF AA) for proliferation and migration (Richardson et al., 1988). Delta-Notch signalling has been shown to play a key role in cell fate determination from pMN region cells by restricting neurogenin expression initially and hence maintain a subset of olig2+ precursor cells which at a later time produce oligodendrocytes (Park and Appel, 2003). Towards the end of motor neuron induction, neurogenins expression is downregulated, allowing the expression of a more ventrally expressed transcription factor Nkx2.2 overlapping the Olig2 domains (Zhou et al., 2001). Cells expressing Nkx2.2 and Olig2 subsequently develop to oligodendrocytes (Zhou et al., 2001). Olig2 is expressed from the early progenitor stage to migration, differentiation and myelination, and is essential for the generation of oligodendrocytes in vertebrates (Park et al., 2002; Zhou et al., 2001). Olig1 is required in rostral CNS regions and at a slightly later stage of differentiation (Lu et al., 2002; Zhou and Anderson, 2002) together with Sox10, which initiates the activation of Mbp promoter expression (Li et al., 2007; Stolt, 2002). Absence of Olig1 and Olig2 expression generates a specific class of interneurons and astrocytes (Zhou and Anderson, 2002). After oligodendrocyte precursor cell (OPC) specification, inactivation of Notch favours oligodendrocyte differentiation from OPCs (Park and Appel, 2003) (Figure 1.4).

Following extensive proliferation, OPCs migrate widely throughout the CNS to presumptive white matter regions by specific directional and substrate cues (Miller, 2010; Ono et al., 1995; Sugimoto et al., 2001). OPC migration and differentiation are closely linked, as differentiated oligodendrocytes are not migratory (Miller, 2010). Towards the end of migration, oligodendrocyte lineage cells withdraw their processes when they contact one another (Kirby et al., 2006). OPC differentiation into a myelinating oligodendrocyte is followed by morphologically complex expansion of uncompacted myelin membrane demanding dynamic cytoskeleton rearrangements of F-actin and microtubules (Bauer et al., 2009; Nawaz et al., 2015; Snaidero et al., 2014; Zuchero et al., 2015). Different stages of oligodendrocyte development are also depicted in (Figure 1.4).

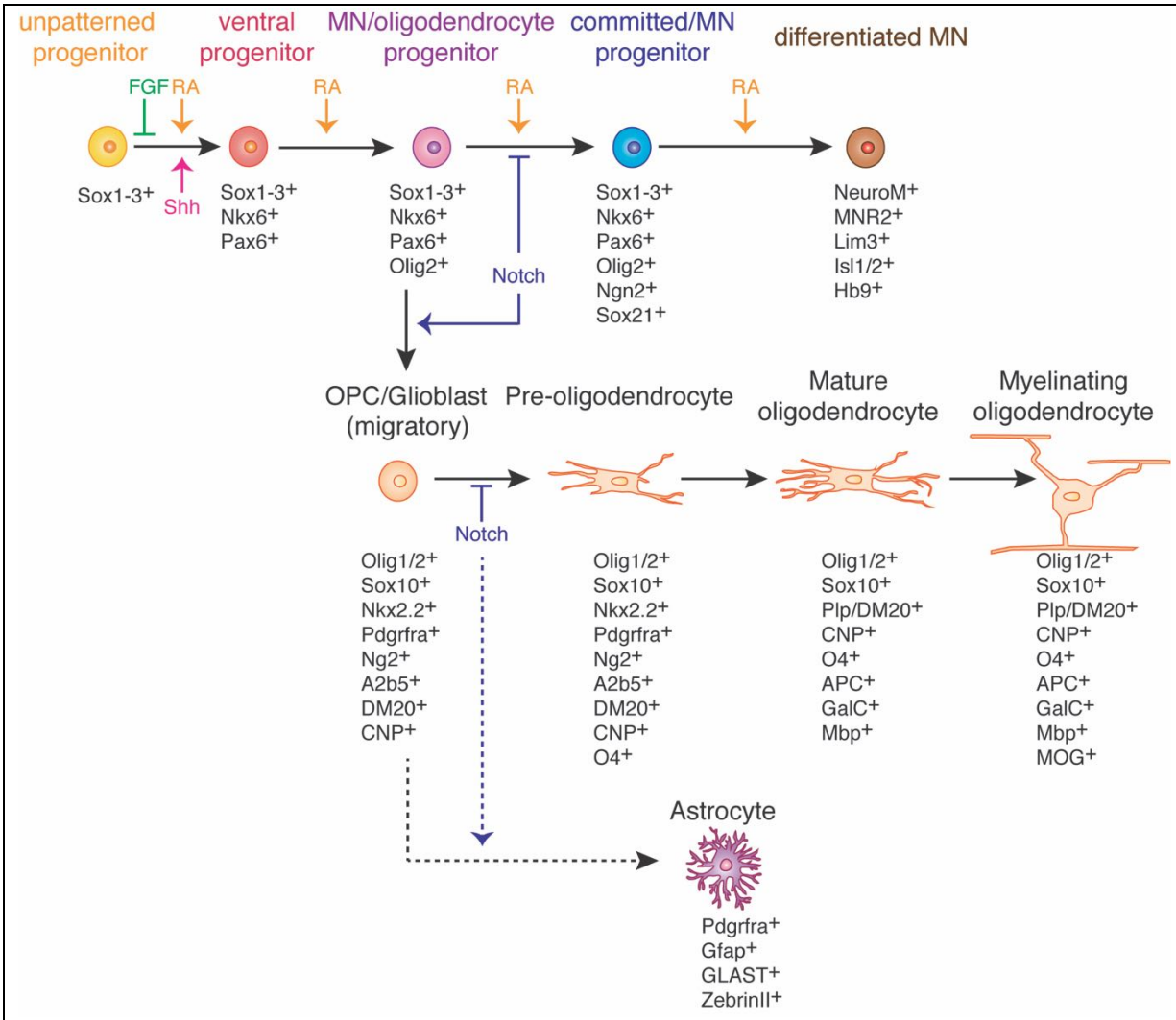

Figure 1.4: Progressive changes in progenitor cells during neurogenesis and gliogenesis. FGFs hold the progenitors in unpatterned progenitor state. Shh and RA ventralise the progenitors and induce transcription factors like Nkx6. Continued Shh and RA exposure lead to Olig2 expression which can develop into motor neurons or glia. In the presence of RA but absence of Notch, Olig2 cells begin to exit cell cycle and differentiate into motor neurons. In the presence of Notch, Olig2 cells tend to form glioblasts or oligodendrocyte precursor cells (OPCs). From migratory OPCs, in the absence of Notch, Olig2 cells further differentiate into pre-oligodendrocytes and mature into myelinating oligodendrocytes. In the presence of Notch, differentiation of Olig2 cells towards astrocytic lineages is favoured. Schematic based on (Briscoe and Novitch, 2008; Marshall, 2005; Traiffort et al., 2016).

1.3. Myelin

The myelin sheath is the extension of cell membrane of glial cells wrapping around axons. These glial cells are called oligodendrocytes in the central nervous system (CNS) and Schwann cells in the peripheral nervous system (Sherman and Brophy, 2005) (Figure 1.5). A

single axonal segment of myelin is called an internode, and consecutive internodes are flanked on both sides by Nodes of Ranvier (Ranvier, 1871, as cited by (Hartline, 2008)), which are short unmyelinated gaps along the length of the axon where voltage-gated sodium channels are clustered and saltatory action potential is propagated (Czopka and Lyons, 2011; Sherman and Brophy, 2005). In between the internodes of myelin segments near the nodes of Ranvier, myelin lamellae end in little expanded loops containing cytoplasm called the paranodal loops (Baumann and Pham-Dinh, 2001). Myelin sheath can be disrupted in various demyelinating diseases like Multiple Sclerosis (Franklin and Ffrench-Constant, 2008) or Charcot-Marie-Tooth disease (Patzkó and Shy, 2011) and often leads to other neurodegenerative diseases involving axonal transport defects and axonal degeneration (Edgar and Nave, 2009; Roy et al., 2009; De Vos and Hafezparast, 2017; De Vos et al., 2008).

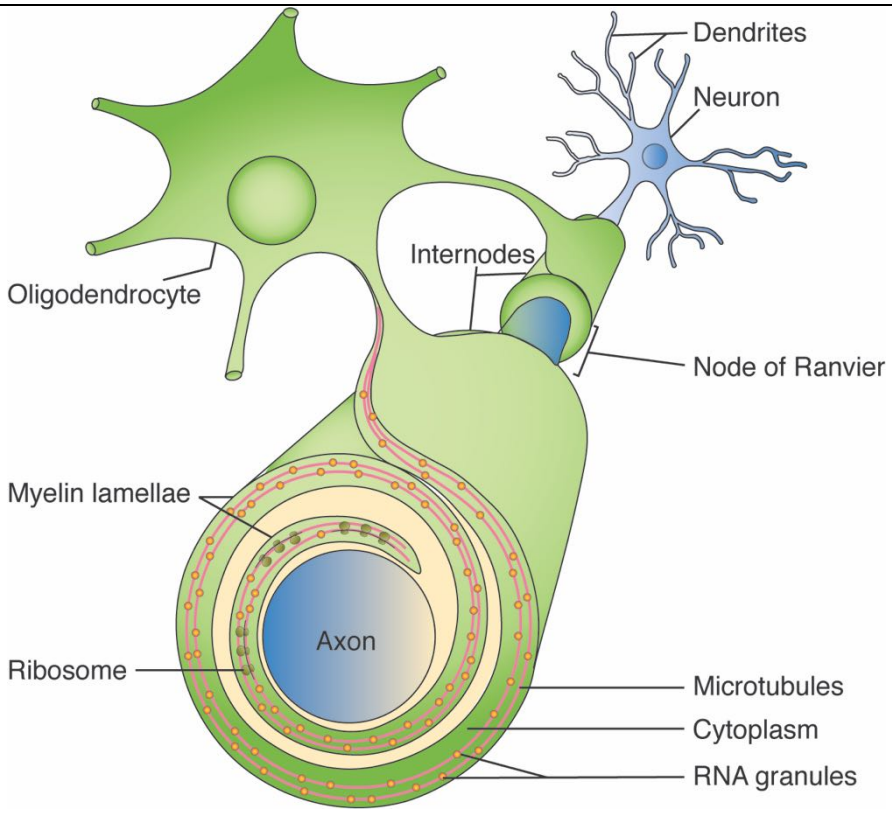

Figure 1.5: Oligodendrocyte ensheathing an axon. An oligodendrocyte extends its cell membrane and surrounds neighbouring axons to form myelin sheaths. Schematic based on (Sherman and Brophy, 2005).

1.3.1. Importance of myelin

Myelin has been described to have three important functions. Chronologically, it was first described as a way to protect axons (Figure 1.6). Robert Remak first reported in 1838 the co-existence of two types of fibres being wrapped by a thin sheath. In 1854, Virchow proposed to name this sheath 'myelin' and wrote: "The medullary sheath serves as an isolating mass, which confines the electricity within the nerve itself and allows its discharge to take place only at the non-medullated extremities of the fibers" (as cited by (Zalc, 2016)). Later in 1878, Louis Ranvier wrote: "Electrical wires immersed in a conductive medium need to be protected from this medium by a non-conductive sheath" (as cited by (Zalc, 2016)).

The second major function is the realisation of high signal conduction speed. In an unmyelinated axon, the electrical impulse entering the axon through an open sodium gated channel, spreads to charge the adjacent regions ahead of the travelling impulse. Whereas, in a myelinated axon of a vertebrate or shrimp, the electric impulse entering at an active node, charges the adjacent internodal membrane faster, owing to the reduced capacitance due to the myelin sheath (Figure 1.6B). Reduction of capacitance between the interior and the exterior of the nerve fiber enhances the conduction speed. Conduction velocity can be accelerated by increasing the diameter of the axon and/or wrapping the axon with myelin sheath (Rushton, 1951). Invertebrate non-myelinated axons propagate action potentials (APs) at around 1 m/s for an axon of about 10 μm in diameter, which is sufficient for small sized animals between 0.1 – 30 cm. In vertebrates, the entire CNS in confined to the skull and vertebral system that are rigid structures imposing a physical constraint to prevent increase in axon diameter. Acquisition of myelin sheath allows to maintain the axon diameter below 10-15 μm and still attain an AP conduction speed of around 50 m/s allowing vertebrates to increase in size (Zalc, 2016).

The third function for myelin is to provide lactate support. Oligodendrocytes have been shown to provide lactate support to the axons through monocarboxylate transporter, likely to

occur at the paranodal loops of myelin wraps (Fünfschilling et al., 2012; Lee et al., 2012; Morrison et al., 2013).

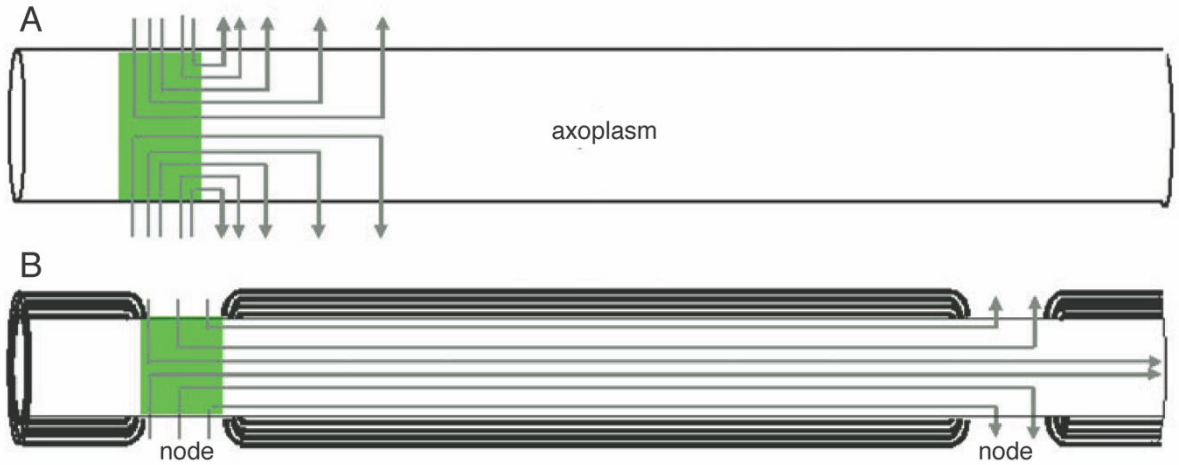

Figure 1.6: Axonal conduction in unmyelinated versus myelinated fibres. (A) In an unmyelinated nerve, current entering the axon through open sodium channels in an active zone (in green), spreads to charge immediately adjacent non-active membrane to initiate an impulse at the new site from which current further spreads in turn. (B) In a vertebrate myelinated axon, current entering through sodium channels at an active node, charges adjacent internodal membrane more rapidly owing to the reduced capacitance afforded by the sheath. Electrotonic charging of the small capacitance of the next nodal membrane is also rapid, leading to a conduction speed an order of magnitude higher than that in a non-myelinated axon of the same outside diameter. Figure adapted from (Hartline, 2008).

1.3.2. Myelin structure and composition

Myelin is a poorly hydrated structure containing only 40 % water in contrast to gray matter (80 %). Myelin is a peculiar membrane with its dry weight consisting of 70 % lipids and only 30 % of proteins (Figure 1.7), which is the reverse of the ratio in other cell membranes.

Its thickness, low water content, and richness in lipids favour the insulating properties of the myelin sheath, allowing low capacitance and therefore rapid nerve conduction / AP velocity (Quarles et al., 2006).

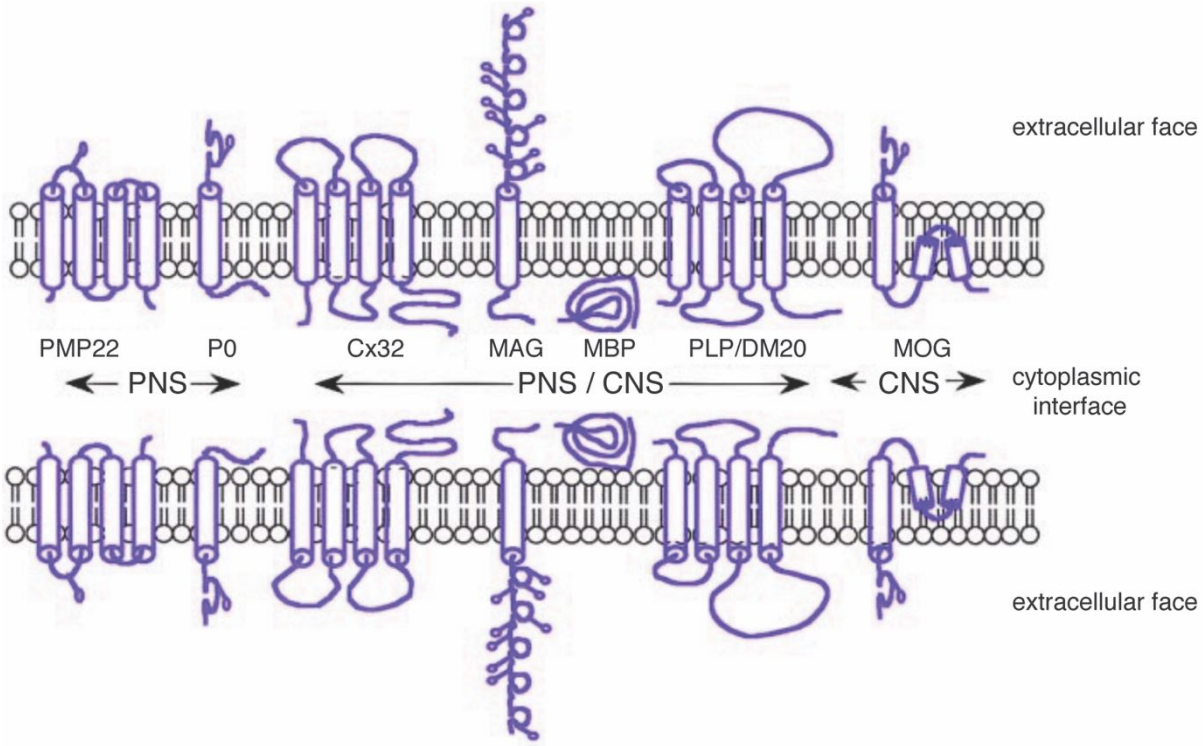

Figure 1.7: Structure of mammalian compact myelin. Structure of myelin showing the lipid bilayer and different myelin proteins in CNS and PNS myelin. Figure adapted from (Baumann and Pham-Dinh, 2001).

1.3.2.1. Myelin composition – proteins

Since the myelin sheath in the CNS is composed of around 30 % protein, proteins still play a vital role in the formation of myelin (Bai et al., 2011). Myelin basic protein (MBP) is a cell adhesion protein and studies show that there is 40 % peptide homology in zebrafish Mbp compared to mammals (mouse) and it is present in both CNS and PNS of zebrafish and mammals. MBP constitutes about 30 % of the total myelin proteins. MBP has been found to be associated and interacting with the transmembrane myelin protein PLP1 in mammals (Edwards et al., 1989). Studies using the 'shiverer' mutant mouse have shown indirect and direct proofs that MBP is essential in the compaction of myelin, as the major dense line is absent in the myelin of these mice (Campagnoni and Macklin, 1988; Privat et al., 1979; Roach et al., 1985).

Proteolipid proteins (PLPs) were first discovered as they could be extracted by organic solvent mixtures as these are lipid-protein complexes and hence also acquiring the name of proteolipids (Folch and Lees, 1951). These constitute about 50 % of the total myelin proteins. A second isoform of PLP, called the DM20 constitutes about 10-20 % of the PLP in mammalian adults. DM20 in zebrafish is found to be in close association with the PLP1 gene of mammals (Schweitzer et al., 2006). Spontaneous mutations in PLP gene including the 'jimpy' mouse and other animal models serve as well used models for human dysmyelinating diseases (Boison and Stoffel, 1994; Boison et al., 1995). Lacking PLP/DM-20, myelination still happens with compaction but condensation of the intraperiodic lines, suggesting that PLP forms a stabilizing membrane after compaction (Boison et al., 1995; Duncan et al., 1987; Klugmann et al., 1997). Furthermore focal axonal swellings following axonal degeneration has been associated with the absence of PLP/DM20 (Griffiths et al., 1998; Rosenfeld and Freidrich, 1983).

Interestingly from an evolutionary point of view, P0 is a major myelin protein both in the PNS and CNS in fish whereas from amphibians onwards, and also in mammals P0 is only found in the PNS, and as mentioned before MBP and PLP become the major CNS protein constituents here (Zalc, 2016). 2',3'-Cyclic-nucleotide 3'-phosphodiesterase (CNPase), which hydrolyses artificial substrates, 2',3'-cyclic nucleotides into their 2'-derivatives represents 4 % of the total myelin proteins in mammals. Although the role for this exact enzymatic activity is unclear, mice overexpressing CNPase showed perturbed myelin and aberrant oligodendrocyte expansion (Gravel et al., 1996). Many glycoproteins like myelin associated glycoprotein (MAG), myelin/oligodendrocyte glycoprotein (MOG), oligodendrocyte/myelin glycoprotein (oMGp) (Quarles, 1997) and other proteins some of which have enzyme activities do represent minor components of myelin (Baumann and Pham-Dinh, 2001).

1.3.2.2. Myelin composition – lipids

Myelin phospholipids comprise 40 % of total myelin lipids. Ethanolamine phosphoglycerides in the form of plasmalogen, account for one third of the phospholipids. Diphosphoinositides and triphosphoinositides represent 1-1.5 % and 4-6 % of phospholipids respectively (Baumann and Pham-Dinh, 2001; Quarles et al., 2006). One of the major characteristics of myelin lipids is the high concentration and unique expression of glycosphingolipids, in particular galactocerebrosides, i.e., galactosylceramides (GalC) and their sulphated derivates, sulfatides, i.e., sulfogalactosylceramides (Zalc et al., 1981). GalC represents 20 % of the lipid dry weight of mature myelin. During development, the GalC content of the brain is proportional to the amount of its myelination (Norton and Poduslo, 1973). Other minor galactolipids in myelin do include fatty esters of cerebrosides like acylgalactosylceramides and galactosyldiglycerides (Schmidt-Schultz and Althaus, 1994; Theret et al., 1988). Sialosylgalactosylceramide, a sialylated derivative of galactocerebroside, the ganglioside GM4, and ganglioside GM1 are further minor components of myelin (Cochran et al., 1982; Kotani et al., 1993).

1.4. Zebrafish as a model organism to study myelin

As myelinated axon with Nodes of Ranvier is a vertebrate-specific adaptation, and invertebrate model organisms like Caenorhabditis elegans or Drosophila melanogaster do not possess myelinated axons (Zalc, 2016). Zebrafish is one of the simplest models for studying the functionality of genes for myelination (for review, see Czopka, 2016; Preston and Macklin, 2015). In contrast to mice or humans, excellent regeneration capabilities of adult and differentiated nervous tissue is a unique ability of zebrafish (Becker and Becker, 2008) which further helps in studying the process of re-myelination after axonal regeneration.

Subsequent to two successive genome duplications, roughly 340 million years ago, a third genome duplication termed teleost specific genome duplication occurred following divergence from non-teleost ray-finned fish (Amores et al., 2011; Glasauer and Neuhauss,

2014; Meyer, 1998; Meyer and Schartl, 1999; Meyer and Van De Peer, 2005; Postlethwait et al., 2000; Shimeld and Holland, 2000). Zebrafish (Danio rerio) belong to the family Cyprinidae and Class Actinopterygii under the Phylum Chordata. Zebrafish have most of the genes conserved across species (Figure 1.8). Approximately 71 % of human genes have a zebrafish orthologue and reciprocally 69 % of zebrafish genes have a human orthologue (Howe et al., 2013). Following the pioneering work of George Streisinger in the early 1980s, zebrafish has emerged as a robust vertebrate model system (Streisinger et al., 1981).

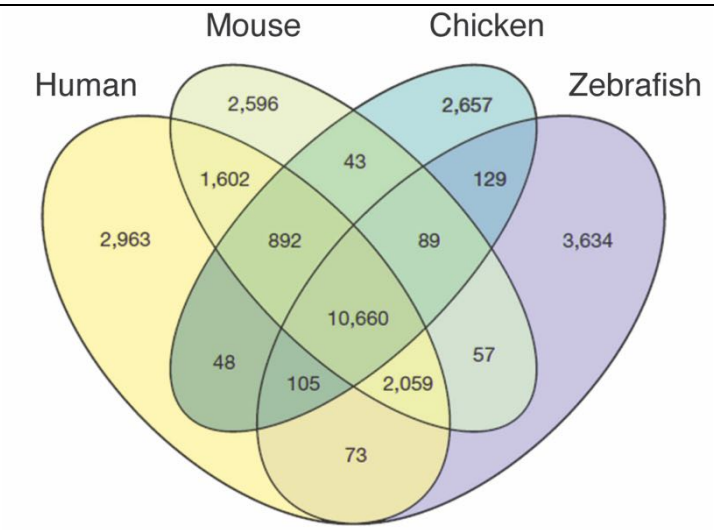

Figure 1.8: Orthology relationships of zebrafish, chicken, mouse, human genome. Orthologue genes shared between the zebrafish, human, mouse and chicken genomes. Figure adapted from (Howe et al., 2013).

Zebrafish are cost efficient in terms of maintenance, time efficient as they breed almost every day. They are almost translucent during their developmental stages making them ideal candidates for *in vivo* imaging. Due to their small size, large number of offspring from a single mating and complete ex-utero development, zebrafish larvae can be highly useful for high throughput drug testing (Giacomotto and Ségalat, 2010; Lessman, 2011; Miscevic et al., 2012; Weinstein, 2010). Knocking down translation of a specific protein can be easily done with Morpholino injections into the one to four cell stage of their embryos (Bill et al., 2009).

Zebrafish have emerged as a powerful model for studying myelination and remyelination in vivo (Brösamle and Halpern, 2002; Czopka, 2016; Czopka and Lyons, 2011; Kirby et al.,

2006b; Preston and Macklin, 2015). It is known that the production of myelin sheath in human starts at 25th week of foetal development (Hasegawa et al., 1992). In mice, myelination is found to start at about P6 (Foran & Peterson, 1992). In zebrafish, it starts at 3 days post fertilization (dpf) (Brösamle & Halpern, 2002; Kirby et al., 2006). So, myelination happens within the first week of development, compared e.g. with only the first month in rodents, thus making zebrafish again a time efficient model. The molecular mechanisms driving myelination is highly conserved across species (Raphael and Talbot, 2011). Transcription factors such as Olig1, Olig2, Nkx2.2, Sox10 regulating oligodendrocyte lineage in mammals are also functioning similarly in zebrafish (Monk and Talbot, 2009). Further, signalling pathways like Notch (Kim et al., 2008; Park, 2005), Shh (Schebesta and Serluca, 2009), Wnt (Azim and Butt, 2011), ErbB (Lyons et al., 2005), EGF (Pruvot et al., 2014) that drive oligodendrocyte lineage progression act comparably between fish and mammals.

Myelin proteins like Mbp (Nawaz et al., 2013), Plp1 (Schweitzer et al., 2006), P0 (Bai et al., 2011) have conserved homologs in zebrafish. The co-expression of these myelin proteins MBP, PLP1/P0/DM20 starts from two days preceding the appearance of mature oligodendrocytes, suggesting a definite role for them in myelination in zebrafish as well (Brösamle and Halpern, 2002). Lipid composition and myelin periodicity are also conserved across fish and mammalian species (Avila et al., 2007). Nevertheless, additional myelin proteins specific to fish myelin like Zwilling-A/B (Schaefer and Brösamle, 2009) and ClaudinK (Münzel et al., 2012) have been identified in zebrafish. It is not yet known if these proteins are replaced by other myelin proteins in mammals. Another major myelin protein in zebrafish, which is not found in rodents, is 36K (Jeserich, 1983; Jeserich and Waehneldt, 1986).

1.5. 36K – a major CNS protein in zebrafish

36K was first discovered in trouts (Jeserich, 1983) (Figure 1.9A). It was found to be expressed only in the trout central nervous system (CNS) myelin and not in the PNS and neither in the CNS nor PNS of rodents (Jeserich and Waehneldt, 1986) (Figure 1.9B). In

humans, expression of transcripts of FLJ13639, an orthologue to 36K has been shown in cortex and white matter (Morris et al., 2004), but no evidence at protein level (Figure 1.9C). 36K belongs to the short chain dehydrogenase family. This is a family of oxidoreductases that requires NAD(P) to catalyse oxidation or reduction. The coenzyme binding domain TGXXXGXG is conserved domain across species (Morris et al., 2004).

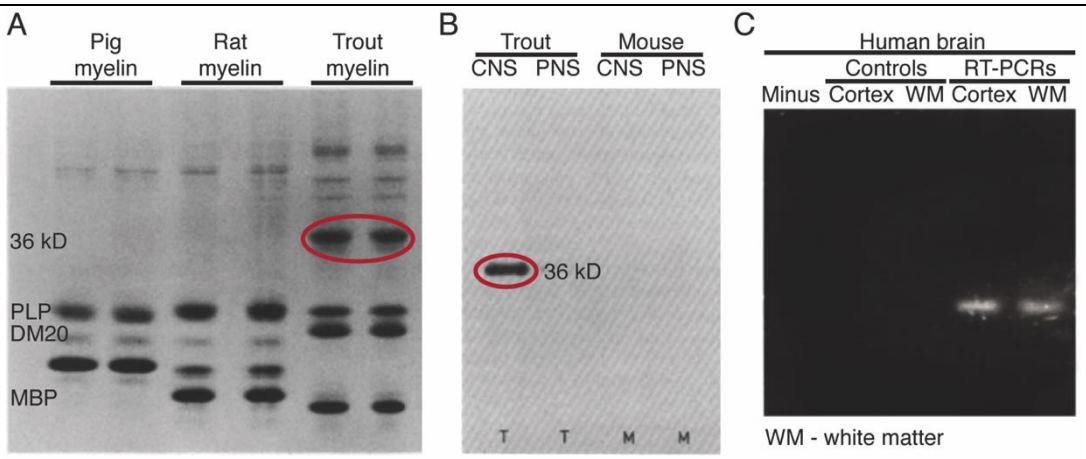

Figure 1.9: 36K is present in fish CNS. (A) Polyacrylamide gel showing CNS myelin proteins from pig, rat and trout. 36 kD band observed in trout myelin. Figure adapted from (Jeserich, 1983). (B) Immunoblot with rabbit anti-36K showing 36K only in trout CNS. Figure adapted from (Jeserich and Waehneldt, 1986). (C) Confirmation of human 36K (FLJ13639) mRNA expression in human brain cortex and white matter by reverse transcription polymerase chain reaction (RT PCR). Figure adapted from (Morris et al., 2004).

Expression of 36K has been shown in zebrafish by wholemount in situ hybridisation (WISH) to start from 3 dpf and to increase between 4-5 dpf (Figure 1.10A). 36K is present in both the myelin membrane and the cytoplasm as well as in compact myelin of the zebrafish CNS (Figure 1.10B-D). Proteomic studies have identified 36K to be one of the most abundant proteins in zebrafish brain (Gebriel et al., 2014). Despite its abundance, the function of 36K in CNS myelin remains unknown.

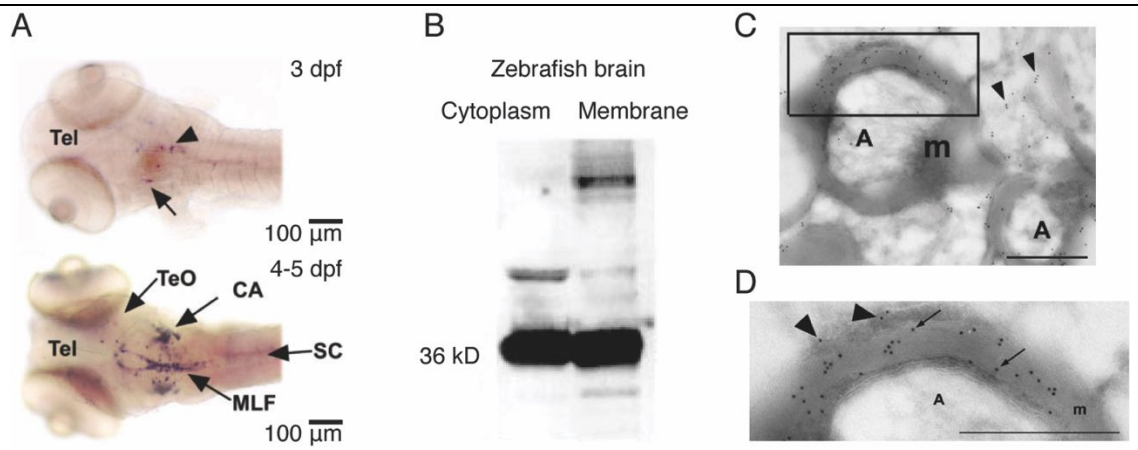

Figure 1.10: Expression of 36K in zebrafish. (A) mRNA expression of 36K in zebrafish starts around 3 dpf and increases between 4-5 dpf as shown by WISH. (B) 36K is present in both myelin cytoplasm and membrane. (C, D) Electron microscopic images showing immunogold labelling of 36K in zebrafish brain. Arrowheads depict 36K expression in non-compact myelin. Arrows depict 36K expression in compact myelin. A-axon, m-myelin. (D) is a magnification from (C). Figures adapted from (Morris et al., 2004).

1.6. Aims of this study

In contrast to mammals, zebrafish can successfully regenerate and remyelinate CNS axons following injury. In addition to the major conserved myelin proteins like Mbp and Plp1, 36K is one of the major CNS myelin proteins in zebrafish. 36K is only a hypothetical protein in humans, and not present in the myelin of rodents. 36K is found in oligodendrocyte cell bodies, cell membrane and compact myelin and even though it is one of the main proteins in zebrafish brain the function of 36K still remains unknown. Understanding the function of 36K would lead to better comprehension of vertebrate CNS myelin in general, and therefore possibly also leading to opportunities to improve therapies for myelin regeneration.

One could speculate that there could be a similar function for 36K like for Mbp, as it is a highly basic protein like Mbp and is present in similar cellular regions like Mbp as well. Alternatively or additionally, there could be an enzymatic role for 36K in CNS myelin as 36K is a short chain dehydrogenase.

In order to investigate the function of 36K, translation blocking Morpholino knockdowns have been performed in zebrafish and the following questions have been addressed:

Does 36K knockdown cause a functional phenotype?

Behaviour experiments have been performed to address this question. Unprovoked behaviour test and stimulated response tests have been performed.

Does 36K knockdown cause a myelin phenotype?

Transgenic lines like *Tg(mbp:EGFP-CAAX)*, *Tg(mbp:EGFP)* and *Tg(claudinK:EGFP)* have been deployed to visualise internodal myelin and myelinating oligodendrocytes *in vivo.* Transmission electron microscopy has also been performed to analyse compact myelin.

Does 36K knockdown alter oligodendrocyte precursor cells (OPCs)?

Tg(olig2:GFP) has been used to study oligodendrocyte precursor cells (OPCs).

How does 36K regulate OPC numbers?

From a mRNA microarray analysis, various pathways influencing spinal cord progenitors were assessed and an upregulation in Notch pathway was found in 36K knockdown. To confirm this, an indirect Notch inhibitor has been used to rescue the phenotypes.

Are lipids altered in 36K knockdown zebrafish larvae?

Since Notch signalling interacts within the lipid cell membrane and some short chain dehydrogenase (SDRs) have been found to be involved in lipid metabolism, thin layer chromatography and mass spectrometry have been performed in 36K knockdown zebrafish larvae to analyse a possible function of 36K SDR on lipid metabolism – and by doing so indirectly on Notch signalling as well.

2. Materials

2.1. Chemicals

Chemicals	Company/Sources	Identification number
(4-(2-hydroxyethyl)-1-piperazineethanesulfonic acid) (HEPES) $C_8H_{18}N_2O_4S$	VWR	441487M
10x Tris/Glycine/SDS	Biorad	1610772
4–20 % Mini-PROTEAN® TGX™ Gel, 10 well, 50 µl from Bio-Rad	Biorad	456-1094
4x Laemmli Buffer	Biorad	161-0747
6x DNA Loading buffer	Fisher Scientific	R0611
Agarose LE	Biozym Scientific GmbH	840004
Ampicillin Sodium	Sigma	A0166
Ampuwa Water	Ampuwa	09016871/100
Calcium Nitrate tetrahydrate $Ca(NO_3)_2.4H_2O$	Calroth	153192865
cOmplete™, Mini, EDTA-free Protease Inhibitor Cocktail	Sigma Aldrich	04693159001ROChE
Cutsmart buffer	NEB	#B7204S
Dimethyl Sulfoxide (DMSO) $(CH_3)_2SO$	Sigma	D8418
dNTPs 100mM Solutions	Thermofisher	R0182
Dulbecco's Phosphate-Buffered Saline (DPBS)	Gibco by Life Technologies	14190-094
DyNAmo Flash Probe qPCR kit	Thermofisher	F455L
Ethidium Bromide 1 %	Sigma Aldrich	46067
Ethyl 3-aminobenzoate methane sulfonate (MS222) $C_{10}H_{15}NO_5S$	Fluka	A5040
GeneRuler 1 kb DNA ladder 250 to 10000 bp	Fisher Scientific GmbH	SM0311
GeneRuler 100 bp plus DNA ladder	Fisher Scientific GmbH	SM0321

GeneRuler Ultra Low range DNA ladder	Fisher Scientific GmbH	SM1211
Glycerine 99 %	PanReac AppliChem	A3092
Green GC Phusion Buffer	NEB	F539L
I-Sce-I Enzyme	NEB	R0694S
Immun-Blot PVDF Membrane, Pre-cut, 7 x 8.4 cm	Biorad	1620174
Instant Ocean Sea Salt	Instant Ocean	SS15-10
iScript Reverse Transcription Supermix for RT-qPCR	Biorad	1708841
Isopropanol C_3H_8O	Calroth	6752.4
Kanamycin Sulphate	AppliChem	A4789
Low melting point agarose	Sigma	A2576
Magnesium Sulphate heptahydrate $MgSO_4.7H_2O$	Merck	1.05886.1000
Methanol CH_3OH	AppliChem	131091.161
Methylene blue $C_{16}H_{18}ClN_3S$	Merck Darmstadt	6040
Milk powder	PanReac AppliChem	A0830.1000
Mineral Oil	Sigma	M5904
Mowiol	Sigma	81381
N-[N-(3,5-Difluorophenacetyl)-L-alanyl]-S-phenylglycine t-butyl ester (DAPT) $C_{23}H_{26}F_2N_2O_4$	Selleckchem	S2215
N-Phenylthiourea (PTU) $C_6H_5NHCSNH_2$	Sigma	P7629
Normal Goat Serum	Sigma Aldrich	G9023
Phenol Red	Sigma	P0290
Phusion Polymerase	NEB	M0530
Potassium Chloride KCl	Fluka Chemika	351861/1
Proteinase K	PanReac AppliChem	A3830,0100
RIPA Lysis and Extraction Buffer	Thermofisher	89900
Sodium Chloride NaCl	AppliChem	A2942,1000
Super Signal West Femto Maximum Sensitivity Substrate	ThermoFisher	34095
Trichloromethane $CHCl_3$	Sigma Aldrich	288306
Trichostatin A (TSA) $C_{17}H_{22}N_2O_3$	Sigma	T8552

Tris-HCl	Calroth	9090.3
Tritron X-100	Sigma	X100
Tween 20	Sigma	P9416

2.2. Recombinant DNA

Plasmids	Company/Sources	Identification number
Plasmid 36K cDNA	Source BioScience	IRBOp991A0379D
Plasmid 36k cDNA MO1 binding site mutated	Mutation in MO1 binding site: atgagcttataccggaacagtgcat	Cloned from plasmid 36K cDNA
Plasmid human DHRS12 cDNA	Source BioScience	IRAUp969E0658D

2.3. Commercial Assays

Commercial Assays/Kits	Company/Sources	Identification number
Nucleospin Tissue	Machenery Nagel	740952.50
TRIzol RNA Isolation	Invitrogen	15596018
Pierce™ BCA Protein Assay Kit	ThermoFisher	23225
Nucleospin RNA clean up kit	Machenery Nagel	740948.50
Nucleospin Gel, PCR Clean-up kit	Machenery Nagel	740609.250
Rapid DNA Ligation Kit	Fisher Scientific	K1422
Nucleobond Xtra Midi	Machenery Nagel	740410.50
Nucleobond Xtra Midi EF	Machenery Nagel	740420.50
Quikchange Lightning Mutagenesis Kit	Agilent	210518
mMESSAGE mMACHINE™ SP6 Transcription Kit	ThermoFisher	AM1340
Poly(A) Tailing Kit	ThermoFisher	AM1350

Qubit RNA HS Assay Kit	Life Technologies	Q32852

2.4. Antibodies

2.4.1. Primary antibodies

Antibodies	Host species	Type	Company/Source	Identification number
36K (EDQKFMSVMEDLAKGFQPH)	Rabbit	Polyclonal	Perbio Science Deutschland	Custom designed
Egfp	Mouse	Monoclonal	Takara Bio Clontech	632380
Pcna	Mouse	Monoclonal	Sigma	P8825
Cleaved caspase 3	Rabbit	Polyclonal	Cell Signalling Technologies	9661
Beta actin - Peroxidase	Mouse	Monoclonal	Sigma Aldrich	A3854
Gfap	Mouse	Monoclonal	Merck Millipore	MAB360
App	Rabbit	Polyclonal	Merck Millipore	171610
Sv2	Mouse	Monoclonal	DSHB	AB_2315387

2.4.2. Secondary antibodies

Antibodies	Host species	Type	Company/Source	Identification number
Goat Anti-Rabbit IgG (H+L)	Goat	Polyclonal	Jackson Immunoresearch Europe	111-035-144
Goat Anti-Mouse IgG (H+L)	Goat	Polyclonal	Jackson Immunoresearch Europe	115-035-146

Goat Anti-Rabbit IgG (H+L), Alexa Fluor 546	Goat	Polyclonal	Invitrogen	A-11010
Goat Anti-Mouse IgG (H+L), Alexa Fluor 488	Goat	Polyclonal	Invitrogen	A-11001
Goat Anti-Mouse IgG (H+L), Alexa Fluor 594	Goat	Polyclonal	Invitrogen	R37121

2.5. Oligonucleotides

Names	Sequence
36K MO1	ATGCTGAGTTCCGGTACAGAGACAT
MO2	GTGGCCCCTCGACGGTACTTTTAAC
36K Forward Primer for RT PCR / q-rt-PCR	CACAGCTCAATGAAGGAG
36K Reverse Primer for RT PCR / q-rt-PCR	CCATCTTCCGATCCTGATA
36K Probe for q-rt-PCR	CACCAGAGCAAGGAGCAGATACA
Ef1a Forward Primer for RT PCR / q-rt-PCR	GGAGTGATCTCTCAATCTTG
Ef1a Reverse Primer for RT PCR / q-rt-PCR	CTTCCTTCTCGAACTTCTC
Ef1a Probe for q-rt-PCR	TCTCTTGTCGATTCCACCGCA
Beta actin Forward Primer for RT PCR / q-rt-PCR	GCCAACAGAGAGAAGATG
Beta actin Reverse Primer for RT PCR / q-rt-PCR	CATCTATGAGGGTTACGC
Beta actin Probe for q-rt-PCR	ATTGTGATGGACTCTGGTGATGGTG
Mbpa Forward Primer for RT PCR / q-rt-PCR	CTGGGCAGAAAGAAGAAG
Mbpa Reverse Primer for RT PCR / q-rt-PCR	GATGACCACGAAATGAAC
Mbpa Probe for q-rt-PCR	CTCCTCCGAAGAACCTGCTGAT
Plp1b Forward Primer for RT PCR / q-rt-PCR	CAGGAATCACCCTTCTTG
Plp1b Reverse Primer for RT PCR / q-rt-PCR	GAATCCGTTGCTAGGTTC
Plp1b Probe for q-rt-PCR	CCACCACCTACAACTACGCTATTCTG
Her 4.1 Forward Primer for RT PCR / q-rt-PCR	ATCAGCAGCAGAGAAACTC
Her 4.1 Reverse Primer for RT PCR / q-rt-PCR	GAGCCAGAAGAGTCTTGA
Deltaa Forward Primer for RT PCR / q-rt-PCR	GCTACACCTGTTCCTGTC

Deltaa Reverse Primer for RT PCR / q-rt-PCR	GCATGTCATGGCACTAAG
Notch1a Forward Primer for RT PCR / q-rt-PCR	GGCACCTGCATTAATGAG
Notch1a Reverse Primer for RT PCR / q-rt-PCR	CACGTCTGACCTGTGAAG

2.6. Equipment

Equipment	Company/Sources	Identification number
Reverse Osmosis Mobile Filtration System		MobilRO16
CFX96 Real Time System	Biorad	
CHEMOSTAR ECL & Fluorescence Imager	Intas	
Transblot Turbo Transfer System	Biorad	1704150
Fluorescent microscope	Nikon	AZ100
Two photon light sheet microscope	Custom built	(Manuscript in preparation)
Two-photon point scanning microscope	LaVision	Trimscope II
EnSight™ multimode plate reader	Perkin Elmer	

2.7. Other miscellaneous used materials

Materials	Company/Sources	Identification number
6 well plates	TPP Techno Plastic Products	92406
12 well plates	TPP Techno Plastic Products	92412
Eppendorf® LoBind microcentrifuge tubes	Sigma	Z666548 SIGMA
Eppendorf® LoBind microcentrifuge tubes	Sigma	Z666556 SIGMA
Falcon Tubes 50 mL	Greiner Bio-One	227263

Falcon Tubes 15 mL	Greiner Bio-One	188272
FEP tubes	Bola	S 1815-04
Homogenising: 2 ml Tubes + 1.4 mm Ceramic beads	Bio-Budget Technologies	70-3-19-627
Macro Vis Cuvette	Eppendorf	30079345
Microcentrifuge tubes 1.5 ml	Starlabs	E1415-1500
Microcentrifuge tubes 2 ml	Starlabs	E1420-2000
Microloader 20 µl	Eppendorf AG	5.242.956.003
Mounting slides	Paul Marienfeld Germany	1000200
Pasteur Plast Pipette	Ratio lab GmbH	2600111
PCR tubes	Starlabs	B1402-5500
Petri dish	TPP Techno Plastic Products	93040
Petri dish	TPP Techno Plastic Products	93100
Precellys Ceramic Kit 1.4 mm	PEQLAB Biotechnologie GmbH	91-PCS-CK14
Pipette tips 10 µl, graduated Filter Tip (Sterile)	Starlabs	S1121-3810
Pipette tips 10/20 µl XL, graduated Filter Tip (Sterile)	Starlabs	S1120-3810
Pipette tips 20 µl, Bevelled Filter Tip (Sterile)	Starlabs	S1120-1810
Pipette tips 100 µl, Bevelled Filter Tip (Sterile)	Starlabs	S1120-1840
Pipette tips 200 µl, Graduated Filter Tip (Sterile)	Starlabs	S1180-8810
Pipette tips 1000 µl XL, Graduated Filter Tip (Sterile)	Starlabs	S1122-1830
Pipette tips 10 µl, graduated Tip	Starlabs	S1111-3800
Pipette tips 10/20 µl XL, graduated Tip	Starlabs	S1110-3800
Pipette tips 200 µl, Tip	Starlabs	S1111-0800
Pipette tips 200 µl, Bevelled Tip	Starlabs	S1111-1800
Pipette tips 1000 µl, graduated	Starlabs	S1111-6800

Tip		
Pipette tips 1000 µl, blue graduated Tip	Starlabs	S1111-6800
RNAstable tubes	Biozym	M93221-001
UVette	Eppendorf	30106300

2.8. Buffers – Recipes

For 2.5 litres of 3x Danieau:

2.9M NaCl	150 mL
60mM Ca(NO3)2 × 4 H2O	75 mL
40 mM MgSO4	75 mL
70mM KCl	75 mL
0,5M Hepes	75 mL
dH_2O	2050 mL

For 10 Litres of 0.3x Danieau:

3x Danieau	1 L
dH_2O	9 L

For 1 litre 0.3x Danieau + methylene blue:

500x methylene blue	2 mL
0.3x Danieau	998 mL

For 1 litre 30 % Danieau + PTU:

50x PTU	20 mL
0.3x Danieau	980 mL

TBS 10x (concentrated TBS):

Trizma HCl	24.23 g
NaCl	80.06 g
dH_2O	800 ml

pH to 7.6 is adjusted with pure HCl.

For 1 litre of TBST:

10x TBS	100 mL
dH_2O	900 mL
Tween20	500µL

For 500 mL of 10X PBS:

NaCl	40.0	g
KCl	1.0	g
1M PO_4 Buffer	100.0	mL (see below)
dH_2O	400	mL

1M PO_4 Buffer (pH 7.3, 100mL)

1M Na_2HPO_4	80 mL	(1M Na_2HPO_4: Na_2HPO_4: 14.2 g, dH_2O: 100 mL)
1M NaH_2PO_4	20 mL	(1M NaH_2PO_4: $NaH_2PO_4.H_2O$: 13.8 g, dH_2O: 100 mL)

pH is adjusted to 7.3

For 200 mL of 4 %PFA:

PFA	8.0	g
dH_2O	180	mL

At 60°C 1N NaOH is added in drops until pH 7.2.

When the solution is clear, it is allowed to cool and then 20mL 10X PBS is added.

2.9. Experimental Organisms

Experimental Models: Cell Lines		
CHO-K1 cells	DSMZ - Deutsche Sammlung von Mikroorganismen und Zellkulturen GmbH	ACC 110

Experimental Models: Organisms/Strains	
Zebrafish: TU wildtype fishline	EZRC, KIT

Zebrafish: TL wildtype fishline	EZRC, KIT	
Zebrafish: AB wildtype fishline	EZRC, KIT	
Zebrafish: Brass wildtype fishline	EZRC, KIT	
Zebrafish: Tg*(olig2:GFP)*	(Shin et al., 2003)	Obtained from Becker lab, Edinburgh
Zebrafish: Tg(*claudinK:EGFP)*	(Münzel et al., 2012)	Obtained from Becker lab, Edinburgh
Zebrafish: TgBAC*(gfap:gfap-GFP)*	(Chen et al., 2009)	Ordered from EZRC, KIT
Zebrafish: Tg*(mbp:EGFP-caax)*	(Almeida et al., 2011)	Obtained from Lyons lab, Edinburgh
Zebrafish: *Tg(mbp:GFP)*	(Almeida et al., 2011)	Obtained from Lyons lab, Edinburgh
Zebrafish: Tg*(-8.4ngn1:GFP)*	(Blader et al., 2003)	Ordered from EZRC, KIT

2.10. Software and Algorithms

Software	Identifiers/Versions
CFX Manager™	Biorad 1845000
qBase+	Biogazelle NV
QuikChange® Primer Design Program	Agilent Technologies
OligoArchitectTM Online	SIGMA-ALDRICH®; by PREMIER Biosoft.
Serial Cloner	Serial Basics Version 2.6.1
Fiji is just ImageJ	ImageJ Version 1.51n
Intas software	
Nikon software	Nikon Instruments Europe B.V.
LabVIEW	National Instruments 2014
GraphPad Prism	Prism Version 6.0e
Adobe Illustrator	Adobe Version 22.0.1

3. Methods

3.1. Animal maintenance and cell culture

3.1.1. Zebrafish housing and maintenance

Adult zebrafish were maintained according to actual husbandry license §11. All experiments were carried out according to national and institutional law, following ARRIVE guidelines. Zebrafish were kept at 28°C with a light/dark cycle of 14/10 hours according to standard protocols as described in Westerfield, 2000. Embryos were kept at 28°C in an incubator in 0.3x Danieau's buffer. 0.3x Danieau's buffer was supplemented with 0.00001 % methylene blue solution until 24 hpf. From 24 hpf, 0.3x Danieau's buffer was supplemented with 0.003 % phenylthiourea (PTU) to prevent pigmentation when used for imaging.

3.1.2. CHO cell culture and transfection

CHO cell culture and transfection was performed by PD Dr. Matthias Eckhardt, Institute of Biochemistry and Molecular Biology, University Clinics, University of Bonn, Germany. Dulbecco's Modified Eagle Medium is nutrient Mixture F-12 (1:1) with 5 % foetal calf serum and 2 mM glutamine was used to grow CHO-K1 cells. 18 hours before transfection cells were seeded in 6-well-plates so as to reach 70-80 % confluency at the time of transfection. Lipofectamine LTX was used to perform transfection according to manufacturer's instruction. Briefly, for one 35 mm well, 2.5 µg DNA (2.25 µg 36K or DHRS12 expression plasmid and 0.25 µg pEGFP-C2 or, as control, only 2.5 µg pEGFP-C2) was mixed with 2.5 µl PLUS reagent and 8 µl of Lipofectamine LTX in 200 µl OptiMEM medium, incubated for 10 min at room temperature and added to the cells. Cells were harvested after 48 hours.

3.2. Fish treatments

3.2.1. Morpholino injections

Antisense oligonucleotide Morpholinos (MOs) were designed to block the translation of 36K with Genetools, LLC (Philomath, USA). MOs were dissolved and stored at a stock concentration on 2 mM in Ampuwa water. Following a series of dilution experiments, a working concentration of 0.15 mM (MO mix: MO at 0.15mM diluted with phenol red, 0.5x Cutsmart buffer, Ampuwa water) was used for 36K MO1 and MO2. Control Morpholino was used at a working concentration of 0.25 mM to avoid any differences due to injection or developmental differences. MO mix were incubated at 65°C for 5 minutes before being loaded into a micropipette. A glass capillary pulled into a micropipette was used as the injection needle. It was filled with the MO mix. A volume of 1.8 nL (~2 ng of MO1 or MO2, ~3.7 ng of control MO) was injected into the yolk of the embryos while they were between one cell and four cell stages.

For rescuing the effect of MO1, the injected zebrafish 36k mRNA (72 pg in 1.8 nL) was mutated so that the MO1 could not bind to it anymore. Plasmid containing 36K cDNA from Source Bio was mutated using Agilent Quikchange Lightning Mutagenesis kit. Plasmid with mutated MO sites was transcribed using mMESSAGE mMACHINE™ SP6 Transcription Kit to generate the rescue mRNA.

3.2.2. TSA treatment (bath immersion treatment)

TrichostatinA (TSA), a histone deacetylase inhibitor has been shown to prevent oligodendrocyte differentiation and migration (Takada and Appel, 2010). Embryos were bath-immersed in 100 ng/mL TSA in 0.3x Danieau from 36 hpf until stage of analysis as described in (Takada and Appel, 2010). As TSA was dissolved in methanol, controls were kept in 0.00001 % methanol in 0.3x Danieau.

3.2.3. DAPT treatment (bath immersion treatment)

N-[N-(3,5-difluorophenacetyl)-l-alanyl]-S-phenylglycine t-butyl ester (DAPT), a gamma secretase inhibitor has been shown to inhibit Notch (Geling, 2002). A dilution series titration assay has shown that DAPT at 5 µg/mL can rescue upregulated Notch phenotypes in developing zebrafish larvae (Salta et al., 2014). So embryos were raised from 24 hpf until stage of analysis in 5 µg/mL DAPT in 0.3x Danieau as described in (Salta et al., 2014). Controls were raised in 0.1 % DMSO in 0.3x Danieau.

3.3. Experiments

3.3.1. Imaging

For length measurement, images were taken using a Nikon AZ100 multi-zoom microscope. The larvae were kept in a small Petri dish (35 x 10 mm) and bright field images were taken using 0.5x objective with 1x magnification. At least four larvae were in focus in every image.

For all other in-vivo fluorescent images, a custom-built two-photon light sheet microscope (manuscript in preparation) was used unless otherwise mentioned. Principle of light sheet fluorescent microscopy (LSFM) is depicted in Figure 3.1.

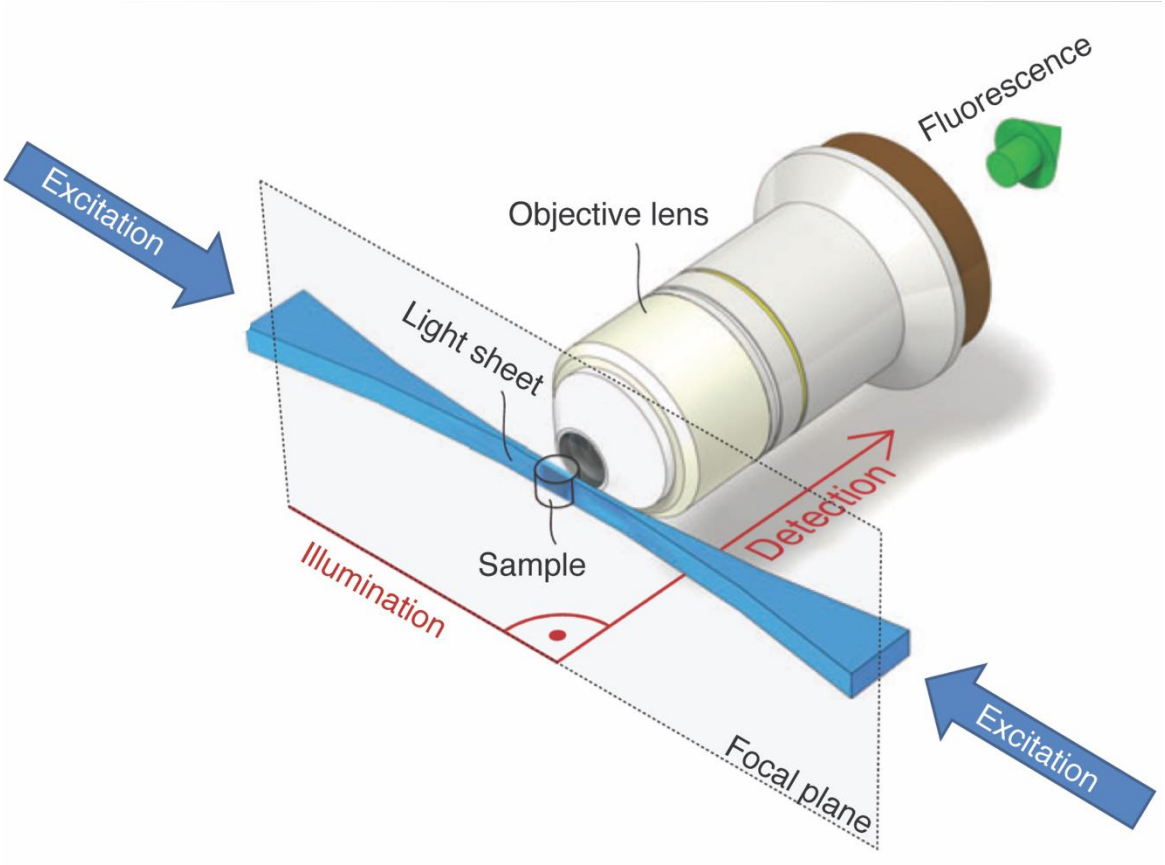

Figure 3.1: Principle of light sheet fluorescent microscope. Illumination axis is orthogonal to the detection axis. Our multidirectional confocal scanned 2-photon light sheet microscope illuminates the sample by the generation of a light sheet from two opposing directions. This effectively increases the illuminated field of view and reduces stripe artefacts which are known for LSFM images (Ahrens and Keller, 2013). The setup utilizes the low scattering of infrared light, which is invisible to the fish, and aims at acquiring high resolution images all through thick specimen like a zebrafish larva. Orthogonal detection through a rolling shutter high-speed camera combined to using low scattering infrared light results in better contrast, a higher imaging depth, faster image acquisition, less photo-damage. Image modified from (Huisken and Stainier, 2009).

Embryos were anaesthetized in 1:5000 MS222 and each embryo was mounted inside a Fluorinated Ethylene Propylene (FEP) tube which has an inner diameter of 1 mm and outer diameter of 1.6 mm in 1.25 % low melting point agarose in 0.3x Danieau. Both the FEP tube and the agarose gel have a refractive index of 1.33 to match the refractive index of water. Data acquisition is with a custom written software implemented in LabVIEW, which controls all the electro-mechanical parts of the setup. For imaging green fluorescent protein (GFP),

InSight DeepSee tunable TiSa laser from Spectraphysics was used to excite the samples at 930 nm. Illumination is in the form of a light sheet and is generated by scanning mirrors. Nikon 40x NA 0.8 water dipping objectives are used for both excitation and detection. Detection is perpendicular to the illumination. A PIFOC system moves the detection objective. A high blocking infrared filter is used which is transparent for the emission light but blocks the excitation light that might be reflected into the detection objective. A 700 nm short pass filter is used for detection of GFP. Fluorescence is detected by Orca Flash 4.0 V2 Digital CMOS camera by Hamamatsu. Images of 2048 x 2048 pixels yield a resolution of 0.1625 µm/pixel in x and y axes and a resolution of ~1 µm/pixel in z axis.

Images showing anti-Sv2 staining were taken with a LaVision Trimscope two-photon point scanning microscope. Embryos were mounted in a drop of 1.25 % low melting point agarose in 1x PBS. Images were acquired using a 20x water immersion objective lens (NA 1.0, W Plan-Apochromat, Zeiss). InSight DeepSee laser from Spectra-Physics was used to excite the sample at 1041 nm. Images were acquired as z-stacks with a resolution of 0.16 µm/pixel.

3.3.2. Electron microscopy

For transmission electron microscopy, larvae were immersion fixed in glutaraldehyde fixative: 25 % Glutaraldehyde + 4 % PFA + 3 % Sucrose in 0.07 Molar Cacodylate buffer (pH 7.38 and osmotic concentration of 797 mOsm). Further processing and electron microscopy were performed by AG Hartmann, Neuroanatomy, Institute of Anatomy, University of Bonn, Germany.

3.3.3. Behaviour experiments

For behaviour experiments, larvae from different experimental groups were arranged in 12 well plates with one larva per well. In each plate, the number of embryos from each experimental group was the same, so as to avoid any differences due to different recording time or stimulus. For example, when there were four groups – uninjected, control MO, MO1, MO1+RNA, each 12-well plate had three larvae from each group with one larva per well. The

larvae were allowed to acclimatize in the well plates for about two to three hours before recording. The camera was fixed at the top of the well plates. Two well plates were recorded simultaneously. All recordings were done with the same lighting and temperature conditions and in the afternoons between 14:00-16:00.

Two types of behaviour experiments were used for this study. Unprovoked behaviour test is similar to open field swim test, a commonly used test in rodents (Hall, 1934). For this assay, the swim behaviour of the larvae was recorded for ten minutes. The recordings were analysed from second to ninth minute. During the measurement, the experimenter started the recording and then left the room so as to avoid any possible external influence on the behaviour.

For stimulated behaviour test, which is similar to forced swim test, a marble was dropped next to the plates and the larvae swam in response to the marble drop. The marble used weighed ~20 g and was dropped from a height of 9.5 cm along a slanted board 15^{o} angle always at a fixed distance from the well plates with the larvae. The vibration caused by the marble drop stimulated escape response in the larvae. The first swim episode following the marble drop was analysed. Two trials for each larva was tested and the average values were taken so as to exclude the problem of one trial being over representative of the value.

3.3.4. Reverse transcription polymerase chain reaction (RT PCR) and quantitative Real Time PCR (q-rt-PCR)

Thirty larvae were collected and total RNA was extracted using TRIzol RNA Isolation according to manufacturer's instruction. The larvae were homogenized using Precellys tubes (5000 – 1x10-005). RNA pellet was suspended in 20 µL RNAse free water. Total RNA was measured using Qubit RNA HA Assay Kit according to manufacturer's instructions and stored at -80°C. 1 µg total RNA was reverse transcribed using iScript Reverse Transcription Supermix for RT-qPCR. q-rt-PCR was performed using DyNAmo Flash Probe qPCR kit with CFX96 Real-Time System. For q-rt-PCR, following 7 minutes (min) at 95°C 40 amplification cycles were carried out: 5 seconds (s) at 95°C, 30 seconds at 60°C. RT PCR was performed

using NEB Phusion. After 30 s of initial denaturation at 95°C, 30 amplification cycles were carried out: 5 s at 95°C, 10 seconds at 60°C, 2 seconds at 72°C followed by 10 minutes of final extension at 72°C. All primers and probes used are listed in the Materials section (Chapter 2.5.).

For miR-132 qPCR, 100 ng total RNA was transcribed using Exiqon miRCURY LNA Universal RT microRNA PCR kit according to manufacturer's instructions. cDNA was diluted 1:20. iTaq Universal SYBR Green Supermix was used for qPCR in the following composition: 1µL primer mix, 1µl water, 5µL master mix, 3µL 1:20 cDNA. Following 10 minutes of initial denaturation at 95°C, 40 amplification cycles were carried out: 10 s at 95°C, 1 minute at 60°C with a ramp rate 1.6°C/s.

3.3.5. Western blot

Fifty larvae were homogenized in 90 µL RIPA Lysis and extraction Buffer with 1x cOmplete Mini EDTA-free Protease Inhibitor. Samples were incubated in RIPA with protease inhibitor for half hour at 4°C, then homogenized using pellet pestle, centrifuged (13000 rpm) at 4°C for 20 minutes. Supernatant was measured using Pierce BCA Protein Assay Kit according to manufacturer's instructions. 4–20 % Mini-PROTEAN® TGX™ Gel, 10 well, 50 µl (Biorad) was used. 50 µg of larvae protein diluted in 1x Laemmli buffer was loaded unless otherwise mentioned. For adult organs, 20 µg of protein was loaded. Gels were run at 100-150 V for 45-60 minutes in Tris/Glycine/SDS buffer. Proteins were then transferred onto PVDF membrane (Biorad), which had been fixed in 100 % methanol and distilled water for 15 s each. Transfer was using Biorad Trans Turbo blot (2.5 Amperes, up to 25 Volts for 3 minutes). After blotting, membranes were blocked in (1x TBS with 0.1 % Tween20 and 5 % milk powder) for two hours and then incubated in primary antibody overnight (anti-36K 1:2000, anti-Beta actin 1:10000) with blocking buffer overnight. For anti-App Western blot, membranes were incubated in boiling PBS for 5 minutes before blocking for two hours in 10 % foetal bovine serum (FBS) containing TBS and then in primary antibody solution (anti-App 1:2000). The membrane was washed in TBST (1x TBS with 0.1 % Tween-20), incubated with

HRP-labelled secondary antibody in blocking buffer at room temperature for 1 h and washed in TBST again. The membrane was then developed in Femto substrate (Thermofisher) and imaged using Intas Imager varying from 5 seconds to ten minutes of exposure.

3.3.6. Immunohistochemistry

CHO cells staining: Cells seeded and attached (overnight after seeding) on glass coverslips were obtained from PD Dr. Matthias Eckhardt. Cells were washed with PBS prewarmed to 37°C. Following removal of PBS, 24 hours after transfection, cells were fixed for 10 minutes with 4 % paraformaldehyde (PFA) and then washed again with PBS. Cells were incubated in 50 mM NH_4Cl in PBS for 20 minutes followed by 2 time (2x) wash with PBS. 30 minutes incubation in 1 % BSA in PBS was used for blocking non-specific binding sites. Cells were then incubated in primary antibody (anti-36K 1:1000 / anti-EGFP 1:2000 / no primary antibody) in 0.2 % gelatine in PBS for 120 minutes. Following antibody removal, they were washed 3x 5 minutes every time with PBS. They were incubated in secondary antibody (Alexa Fluor 546 for anti- 36K 1:4000 / Alexa Fluor 488 for anti-EGFP 1:4000) in 0.2 % gelatine in PBS for 90 minutes. Cells were then rinsed with PBS, followed by 2 x 5 minutes wash with PBS. DAPI at 1:2000 was added to stain nuclei following which they were briefly washed in water. They were then mounted on glass coverslips with Mowiol and stored at 4°C until they were imaged.

Larval wholemount for anti-SV2 staining: Zebrafish larvae were anesthetized with MS222 (1:1000), washed in PBS followed by immersion in 4 % paraformaldehyde (PFA) in PBS overnight. For wholemount larval staining, larvae were then washed with PBS 10 min 3 times (3x). Following this, they were dehydrated through a series of 25 %, 50 %, 75 %, 100 % Methanol in PBS for 10 min at each dilution. Embryos in 100 % methanol were stored at -20°C and rehydrated through a series wash of methanol/PBST 100 %, 75 %, 50 %, 25 % for 5 min at each step. Embryos were then washed in PBST 5 min 3x followed by Tris buffer (150 mM Tris-HCl pH 9.0) wash 5 min. Embryos were then equilibrated in Tris buffer at 70°C for 15 min, and then washed 2x 5 min in PBST. They were permeabilized in 5 µg/mL

ProteinaseK in PBS for 50 min, fixed again in 4 % PFA for 20 min and then washed in PBST 2x 5 min. They were blocked in 10 % normal goat serum (NGS) / 2 % Bovine serum albumin (BSA) / PBST at 4°C for 4 hours. They were then incubated in primary antibody solution 2 % NGS / 2 % BSA/PBST with anti-Sv2 antibody (1:250) at 4°C for 72 hours. Anti-Sv2 was deposited to the DSHB by Buckley, K.M. (DSHB Hybridoma Product Sv2). They were then washed 4x 1 hour followed by 2x 30 min with PBST at room temperature (RT) before incubation with secondary antibody goat anti-mouse IgG (H+L) Alexa Fluor 594 (1:1000) for 48 hours. They were then washed 6x 15 min in PBST, 5x 5 min in PBST. Following this, they were post-fixed in 4 % PFA for 20 mins RT and then washed with PBST 5 min 5x. Stained larvae were then mounted in agarose for imaging or stored in glycerol.

Adult and larval paraffin sections: (Larvae were fixed and then sent to Dr Anna Japp, Neuropathology following fixation for paraffin sections staining). Zebrafish larvae or adults were anesthetized by immersing in MS222 (1:1000), washed in PBS followed by immersion in 4 % Formalin in PBS overnight and stored at 4°C. They were then embedded in paraffin. Sections were counter stained with haematoxylin. They were stained with respective antibodies (anti-36K (custom made with Perbio Science Deutschland) 1:500, anti-Pcna (Abcam) 1:1000, anti-Cleaved caspase 3 (Cell signaling Technologies) 1:200, anti-Gfap 1:500 (Merck)) using Ventana Benchmark XT Automated IHC/slide staining system.. Slides were scanned using Mirax slide scanner by Zeiss. Images were prepared using virtual slide viewer software Panoramic viewer.

3.3.7. Microarray analysis

For microarray analysis, total RNA was extracted from thirty larvae. They were homogenized using Precellys tubes (5000 – 1x10-005). RNA extraction was using TRIzol RNA Isolation (Invitrogen 15596018) according to manufacturer's instruction. The samples were then column purified using Nucleospin RNA clean up kit. RNA integrity was checked using absorbance at 230 and 260 nm, and A260/280 ratio using Qubit Fluorometer and Eppendorf Bio spectrophotometer. 1ug of RNA from each sample was left to dry in RNAstable tubes

overnight in the laminar flow hood according to manufacturer's instructions and then shipped to Oaklabs GmbH (Hennigsdorf, Germany) for ArrayXS Zebrafish, where the expression levels of 60023 genes were measured. Samples from control MO and MO1 groups at 3 dpf from six independent experiments (independent days of injections) were analysed. All microarrays were in 8x60K format, 8 subarrays/slide. The arrays were imaged using a SureScan Microarray Scanner. Detailed protocol is available from Oaklabs (http://www.Oak-labs.com/).

3.3.8. Lipid extraction and thin layer chromatography / Analysis of sphingolipids

Lipid extraction were performed in collaboration with PD Dr. Matthias Eckhardt, Institute of Biochemistry and Molecular Biology, University Clinics, University of Bonn, Germany. Detailed methods are as described in (Nagarajan et al., in submission, 2018). 100 fish larvae were collected at 5 dpf and given to PD Dr. Matthias Eckhardt for lipid extractions and thin layer chromatography.

3.3.9. Mass spectrometry

Lipid extraction and mass spectrometry were performed in collaboration with PD Dr. Matthias Eckhardt, Institute of Biochemistry and Molecular Biology, University Clinics, University of Bonn, Germany and PD Dr. Roger Sandhoff, Lipid Pathobiochemistry Group, German Cancer Research Centre, Heidelberg, Germany respectively. Detailed methods are as described in (Nagarajan et al., in submission, 2018). Triplicates of 40 fish larvae were collected at 5 dpf and given to PD Dr. Matthias Eckhardt for lipid extraction. Lipid samples were sent to PD Dr. Roger Sandhoff for liquid chromatography - tandem mass spectrometry (LC/MS-MS).

3.4. Quantification and analysis

3.4.1. qPCR analysis

q-rt-PCR analysis was performed using CFX Manager™ and qBase software. Raw data files were opened with CFX manager, the wells were labelled and the appropriate fluorophores

used were selected. Baseline threshold was set for every probe according to the values acquired from a concentration-based slope analysis. The raw data files with the C_q values were then opened with qBase. The calculated efficiency values for each probe were entered. Beta actin and ef1a were chosen as reference targets. Triplicates were averaged and outliers according to qBase were manually checked before exclusion. All data were normalized to the reference genes and scaled to average unless otherwise specified hence generating calibrated normalized relative quantities (CNRQ) (Hellemans et al., 2007). All error bars shown are standard error of the mean (SEM).

3.4.2. Western blot quantification

Western blot membranes were quantified from the chemiluminescent bands using the Fiji Gel Lane Analysis for intensity and then normalized to beta actin unless otherwise mentioned.

3.4.3. Length measurement

Images were acquired using Nikon AZ100 fluorescent microscope. Images were blinded during analysis. Using Fiji, the length of four to eight larvae were measured from every image.

3.4.4. Behaviour experiments analysis

For analysis, the videos recorded at 30 frames per second (fps) were opened with Fiji and converted to image sequences. For unprovoked behaviour test, image sequences were reduced so that an image every 5 s for eight minutes (96 frames) was saved as a stack. For stimulated behaviour test, 30 frames from the time of marble drop were saved as a stack with the original 30 fps.

By manually tracking (identifying the position of the larva on every frame in each well) using the Fiji MTrackJ plugin (Meijering et al., 2012), the distance of swimming was measured. For

stimulated behaviour test, two trials were analysed and the average value was taken for each larva.

3.4.5. Cell counting

In vivo images acquired with a two-photon light sheet microscope. Bright field images were used to orientate the fluorescent images and to crop two spinal segments (in most cases third and fourth spinal segments, as the images were always taken at the same region above the yolk extension). For dorsally migrated cells, all the cells that were not touching the ventral spinal cord pMN were counted, as indicated by dashed lines in the representative images shown in the figures. The observer was blinded to the experimental groups before analysis/cell counting. The Fiji Cell counter plugin (Author: Kurt De Vos, University of Sheffield) was used for counting cells.

3.4.6. Microarray data analysis

Statistical analysis and quality control of data were performed by OakLabs GmbH (Hennigsdorf, Germany) with the aim of generating a list of differentially expressed probes. Data normalisation was done by using ranked median quantiles as described in (Bolstad et al., 2002). By default, a Welch's t-test (or unequal variances t-test) was used to test whether the signals of a gene in two biological groups of samples have equal means since this is more reliable when the two biological groups have unequal variances and unequal sample sizes. P values were adjusted according to the adaptive Benjamini-Hochberg procedure to decrease the number of 'false negatives' (Benjamini and Hochberg, 1995, 2000). Only probes which had a $|\log_2 \text{fold}| > 0.5$ and a p-value of $< .05$ were considered. Heatmaps were generated using Heatmapper (Babicki et al., 2016). More details on analysis is available from Oaklabs (http://www.Oak-labs.com/).

3.4.7. Statistical Analysis

All error bars shown are standard error of the mean (SEM) unless otherwise specified. All the graphs generated and the statistical analyses were performed using GraphPad Prism version 6.0. All the experiments were repeated at least three times (at least N=3) unless otherwise mentioned. N represents the total independent number of experiments. n represents the total number of larvae used or analysed.

Column statistics were performed to test if the values come from Gaussian distribution with D'Agostino & Pearson omnibus normality test. For two groups of data, if the values were normally distributed, two tailed t-test was used. If not, Mann-Whitney U test was used as it is a non-parametric test and would not assume Gaussian distribution. In case of three or more groups, if the values were normally distributed, one-way analysis of variance ANOVA was used followed by Bonferroni's multiple comparison post-hoc test. If the values were not normally distributed, Kruskal-Wallis ANOVA with Dunn's multiple comparison post-hoc test was used. For grouped analyses, two-way ANOVA followed by Tukey's multiple comparison post-hoc test was used. Mean with SEM is indicated as variability in all the graphs unless otherwise mentioned. Asterisks in the graphs show: ns when $P > 0.05$, * when $P \leq 0.05$, ** when $P \leq 0.01$, *** when $P \leq 0.001$ and **** when $P \leq 0.0001$.

4. Results

36K is a major component of fish CNS myelin protein (Jeserich, 1983; Morris et al., 2004). Proteomic studies have found 36K to be one of the most abundantly identified proteins in zebrafish brain (Gebriel et al., 2014). Despite the abundance as described in (Chapter 1.5) the function of 36K in CNS myelin remains unknown. In this study, following characterisation of 36K expression in zebrafish, knockdown experiments with translation blocking Morpholinos were performed in zebrafish to address the function of 36K. The phenotypes following Morpholino injections were analysed.

Note: Most of the figures in this Chapter (4 – Results) have been submitted for publication (Nagarajan et al., 2018, in submission/review). This citation has not been mentioned every time. All experiments were performed by the author of this thesis unless otherwise mentioned. When the experiments were performed by or with major help of anyone other than the author of this thesis or if the figures were taken or adapted from other sources, it is explicitly mentioned in the figure legend.

4.1. Characterisation of 36K expression

It is necessary to understand the localisation of 36K at different stages during development in zebrafish to investigate its function. So, *36k* mRNA and 36K protein were characterised.

4.1.1. Characterisation of 36k mRNA expression

In order to confirm presence of *36k* RNA expression, RT PCRs were performed from different organs of adult zebrafish (Figure 4.1A). This showed strong expression mainly in spinal cord, brain and eyes, in comparison to other non-CNS tissues. RT PCRs were also done during zebrafish development to identify whether there is *36k* expression (Figure 4.1B). To quantify *36k* expression during development, qPCR was performed from 1 dpf to 10 dpf

and relative expression was found to increase from 3 dpf and reach a stable high plateau of expression from ~7 dpf onwards (Figure 4.1C).

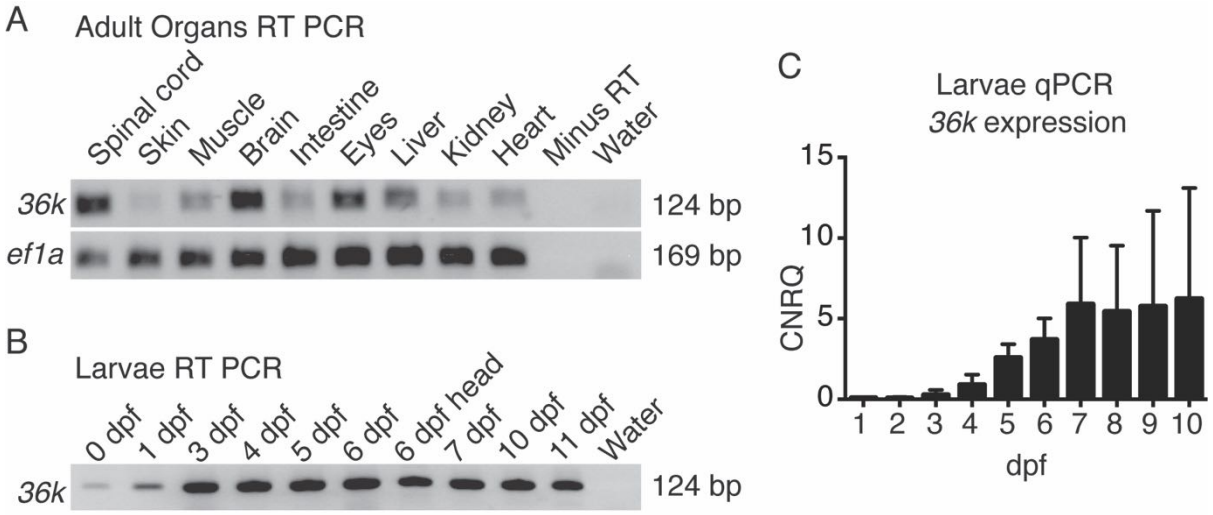

Figure 4.1: *36k* gene expression increased from 3 dpf during development and was primarily in the CNS of adult zebrafish. (A) RT PCR showing expression of *36k* in different organs of adult zebrafish, with *ef1a* as control. (B) RT PCR showing *36k* expression in larvae during development. (C) qPCR of *36k* expression during development normalized to β-actin and ef1a showing calibrated normalized relative quantities (CNRQ). *36k* expression was found to increase after 3 dpf and reach a plateau by 7 dpf. Error bars show SEM.

4.1.2. Characterisation of 36K *antibodies and* 36K *protein expression*

As part of characterising 36K protein expression, we raised custom made rabbit antibodies against zebrafish 36K C-terminus peptide sequence together with Perbio Science Deutschland (Bonn, Germany). With the aim of characterising these antibodies, a vector plasmid construct containing a CMV promoter driving 36K cDNA expression was transfected into chinese Hamster ovary (CHO) cells together with PD Dr. Matthias Eckhardt, Institute of Biochemistry and Molecular Biology, University of Bonn. These cells were immunostained with our custom-made antibodies. Expression was observed only in the 36K transfected cells and not in the controls, suggesting antibody specificity (Figure 4.2A-D). Further, expression of 36K was found to be present in the entire cytoplasm and cell membrane (Figure 4.2C-D). In western blot, 36K expression was only seen in 36K transfected cells whereas β-actin as loading control and EGFP as transfection control, were expressed in all lanes (Figure 4.2E).

Western blot was performed from developing zebrafish larvae at 3 dpf, 5 dpf and 10 dpf for testing 36K protein expression using these antibodies. From 3 dpf, mRNA expression was found to increase as shown by qPCR (Figure 4.1C). At 3 dpf, 36K protein was not detectable by western blot. At 5 dpf and 10 dpf, an increasing protein band was observed at 36 kilo Dalton (kD) in whole larvae lysate (Figure 4.3A). In adult zebrafish, 36K was found to be present in brain, spinal cord and retina but not in any other organs tested by western blot (Figure 4.3B). When adult zebrafish paraffin sections were immunostained, 36K expression was specifically found in CNS white matter (Figure 4.3C).

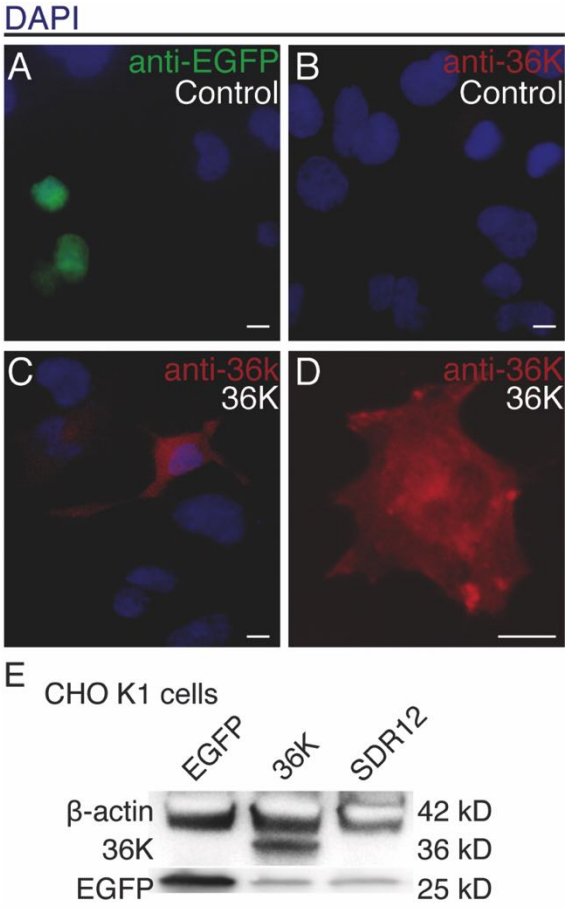

Figure 4.2: Custom made anti-36K antibodies specifically stained 36K overexpressed in CHO cells. (A) Anti-EGFP (green) stained CHO cells transfected with control plasmid. (B, C, D) Anti-36K (red) stained CHO cells transfected with (B) control plasmid (C, D) plasmid containing 36K cDNA. (D) Enlarged view of a 36K transfected cell stained with anti-36K antibodies. Nuclear DAPI staining is shown in blue. Scale bars: 10 µm. (E) Western blot showing 36K expression only in 36K transfected cells with β-actin as loading control and EGFP as transfection control. Fixed cells for staining and samples for preparing western blot protein lysates following CHO cell culture and transfection were obtained from PD Dr. Matthias Eckhardt.

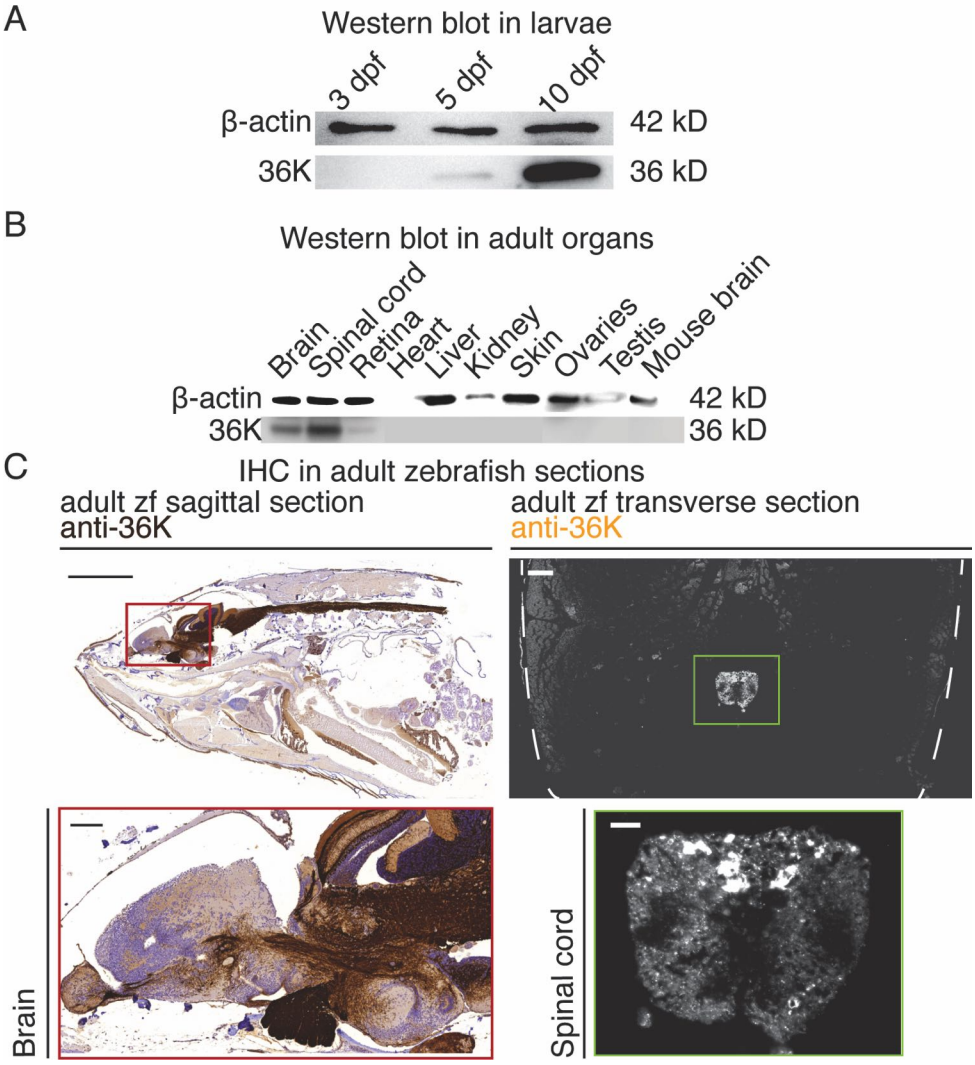

Figure 4.3: 36K protein expression in larvae increased after 3 dpf and was mainly found in adult zebrafish CNS. (A) Western blot of 36K at different developmental stages with β-actin as loading control. (B) Western blot of 36K with adult zebrafish organs and also mouse brain with β-actin as loading control showing expression only in zebrafish CNS tissues (brain, spinal cord, retina). (C) Anti-36K staining in sagittal paraffin section from adult zebrafish showing specific expression in brain and spinal cord white matter. Sections were counter stained with haematoxylin. Scale bar: 2000 µm. (Red inlay) Enlarged view. Scale bar: 200 µm. Adult paraffin sagittal section staining was performed by Dr. Anna Japp, Institute of Neuropathology, Universitätsklinikum Bonn. Anti-36K fluorescent staining in transverse paraffin section from adult zebrafish showing specific expression in spinal cord white matter. Dashed lines depict fish skin. Scale bar: 200 µm. (Green inlay) Enlarged view. Scale bar: 40 µm. Adult paraffin transverse section fluorescent staining was performed by AG Hartmann, Neuroanatomy, Institute of Anatomy, University of Bonn.

4.2. 36K protein expression was efficiently knocked down by 36K Morpholino

Translation blocking Morpholinos were designed together with Genetools, LLC (Philomath, USA) so as to investigate the function of 36K. In eukaryotic gene expression pre-mRNA is transcribed in the nucleus (Figure 4.4A), introns are spliced out, and the mature mRNA is then exported to cytoplasm (Brown, 1981). The small subunit of ribosome binds to one end of the mRNA and other eukaryotic initiation factors forming the initiation complex, which then scans along the mRNA until a start codon is reached. Then the large subunit of the ribosome attaches to the small subunit and protein translation begins. Translation blocking Morpholinos are antisense oligonucleotides that bind to the 5' untranslated region or the start codon of the mature mRNA and interfere with the progression of ribosomal initiation complex from the 5' cap to the start codon, hence preventing translation of protein from the targeted mRNA transcript (Figure 4.4B).

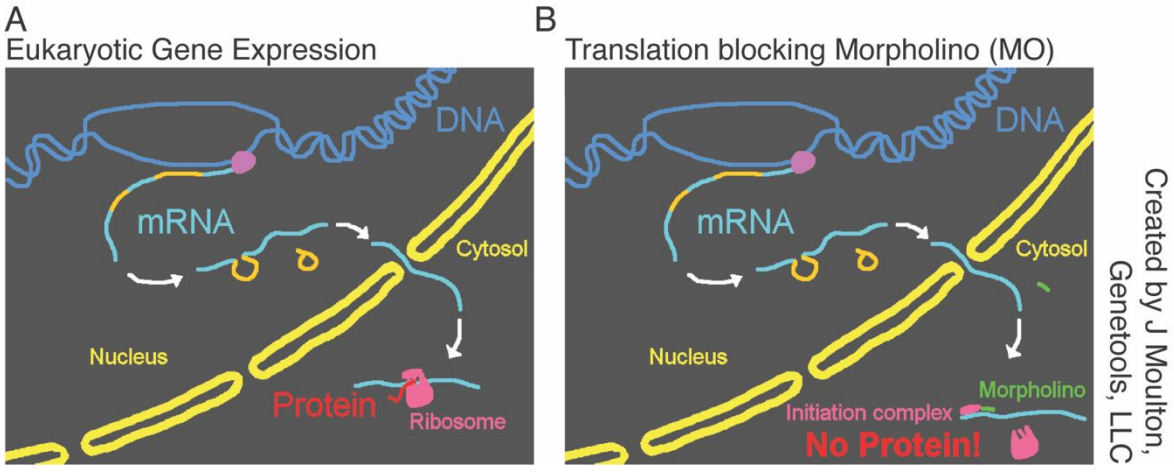

Figure 4.4: Translation blocking Morpholino interferes with the ribosomal initiation complex hence knocking down protein expression. (A) Schematic showing eukaryotic gene expression. (B) Translation blocking Morpholino (in green) blocks gene expression by interfering with ribosomal initiation complex. Images originally created by Jon D Moulton, Genetools, LLC.

4.2.1. 36K *Morpholino knocked down* 36K *expression specifically and efficiently*

Zebrafish larvae were injected with either control Morpholino (control MO), 36K translation blocking Morpholino (MO1), or MO1 together with rescue mRNA (MO1+RNA). Control MO had no target and hence no biological activity. Rescue mRNA was zebrafish *36k* mRNA, in which the MO1 binding site was mutated so that MO1 could not bind to it anymore although the peptide sequence remained unaltered. With 36K translation blocking Morpholino (MO1), ~81.8 % knockdown was observed at 4 dpf in injected larvae in comparison to control MO injected larvae as shown by Western blot (Figure 4.5A-B), suggesting the specificity of the Morpholino MO1. 36K expression level in the MO1 group could be rescued when co-injected with 36K mRNA.

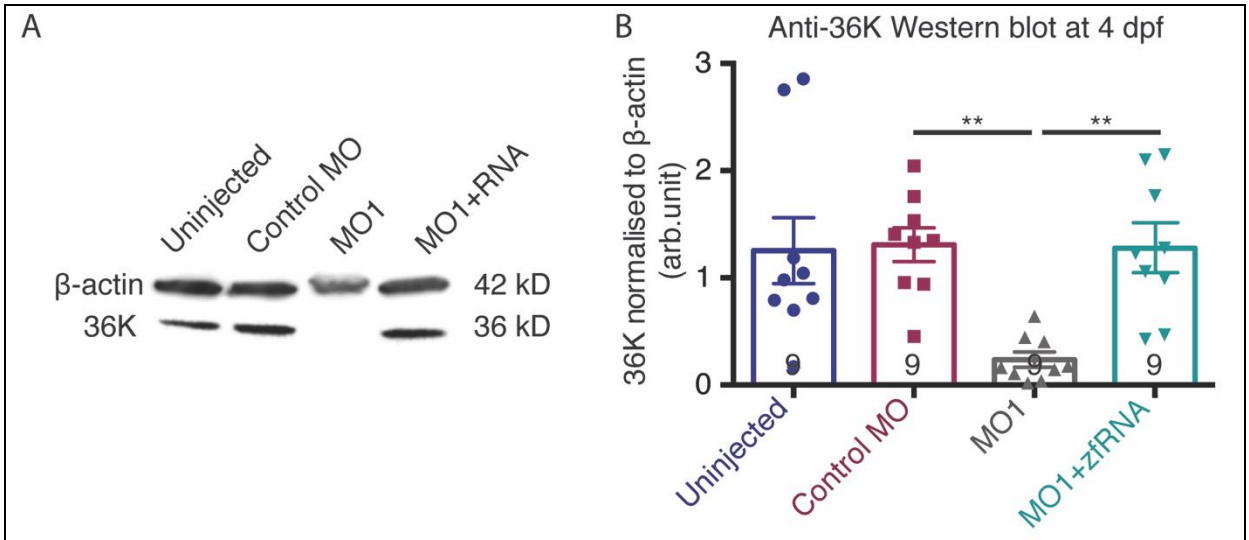

Figure 4.5: 36K Morpholino specifically knocked down 36K protein expression. (A) Representative anti-36K western blot showing 36K knockdown and rescue. (B) Quantification of different anti-36K western blots normalised to β-actin. N=9. One-way analysis of variance ANOVA P value 0.0016 followed by Tukey's multiple comparisons test for control MO vs MO1 (**) and MO1 vs MO1+zfRNA (**).

In the direction of further confirming 36K MO knockdown and for more precise localisation of expression of 36K knockdown, an immunostaining with anti-36K was performed on paraffin sections together with Dr. Anna Japp, Institute of Neuropathology, Universitätsklinikum Bonn.

Control MO larvae had more 36K expression in hindbrain (Figure 4.6A-B) and also spinal cord region (Figure 4.6A, C) at 4 dpf in comparison to MO1 injected larvae. 36K expression was observed in the membrane and in cell bodies in these immunostained paraffin sections. In addition to the CNS tissues, occasional and variable expression was observed in skin and muscle both in the control MO as well as MO1 groups.

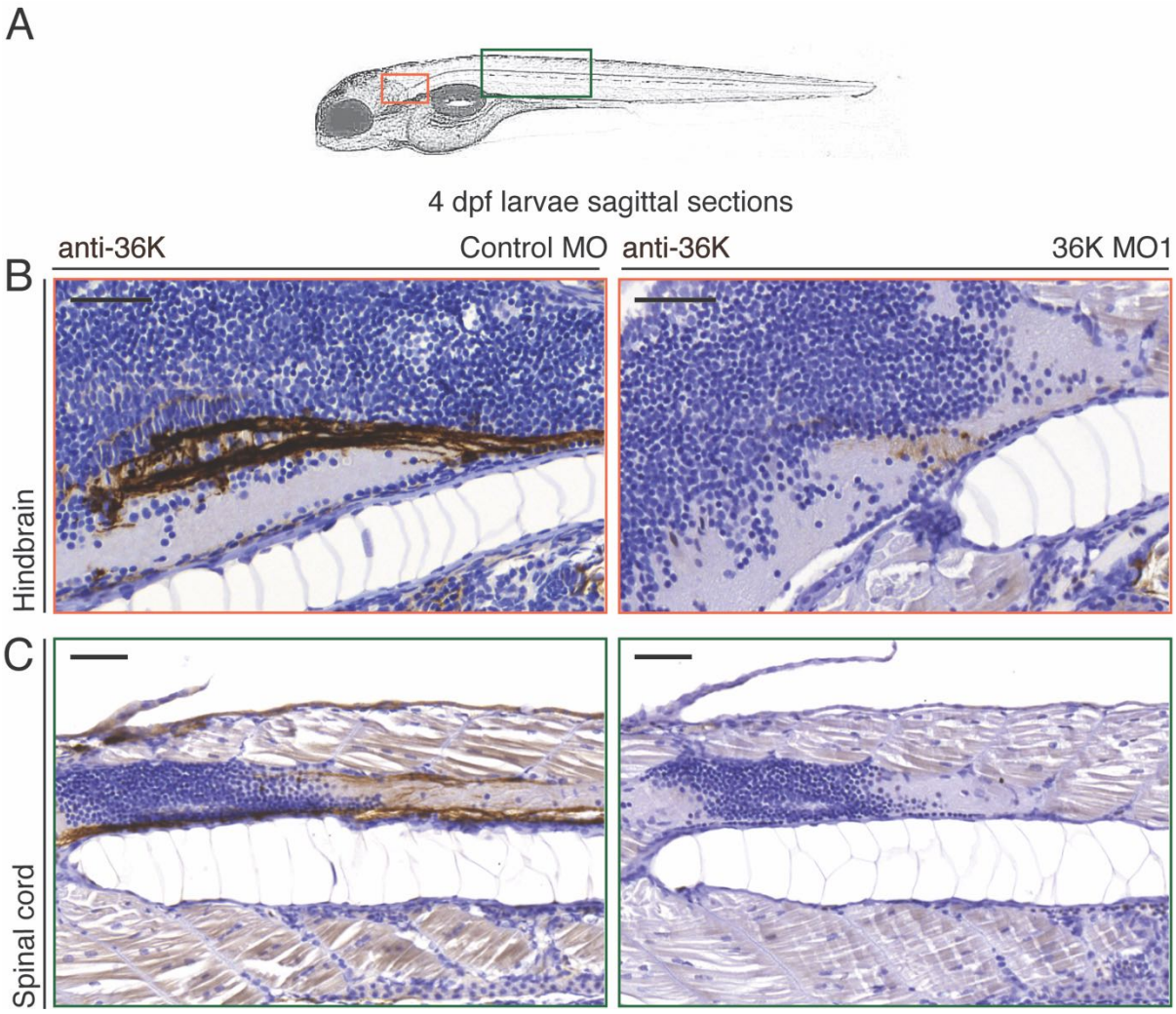

Figure 4.6: 36K knockdown larvae showed reduced 36K expression in hindbrain and spinal cord regions. Representative images showing sagittal paraffin sections of 4 dpf larvae labelled with anti-36K (brown) and nuclei counter stained with Haematoxylin. (A) A zebrafish larva overview sketch showing the regions presented in B and C. (B) Anti-36K immunostaining showing 36K expression in control MO (left) and MO1 (right) in the hindbrain region. Scale bars: 50 µm. (C) 36K expression was observed in the ventral and also in the dorsal spinal cord in control MO (left) whereas it was almost completely absent in the MO1 larvae (right). Scale bars: 50 µm. Immunostaining done by Dr. Anna Japp.

4.2.2. 36K knock down resulted in a shorter body length

In the MO1 injected larvae, 8 % reduction in body length was observed (Figure 4.7A-C). This reduction in body length was rescuable in the MO1+RNA group (Figure 4.7B) confirming the specificity of the MO1 Morpholino. However, when MO1 was co-injected with the human homologue of 36K, the short chain dehydrogenase 12 (SDR12), no rescue was observed (Figure 4.7C). A second translation blocking Morpholino (MO2) targeting 36K had a similar body length phenotype (Figure 4.7B). This further confirmed the specificity of our observations for the phenotype of 36K knockdown. Cardiac oedema and slower yolk consumption were also observed in some MO1 larvae (e.g. Figure 4.7A).

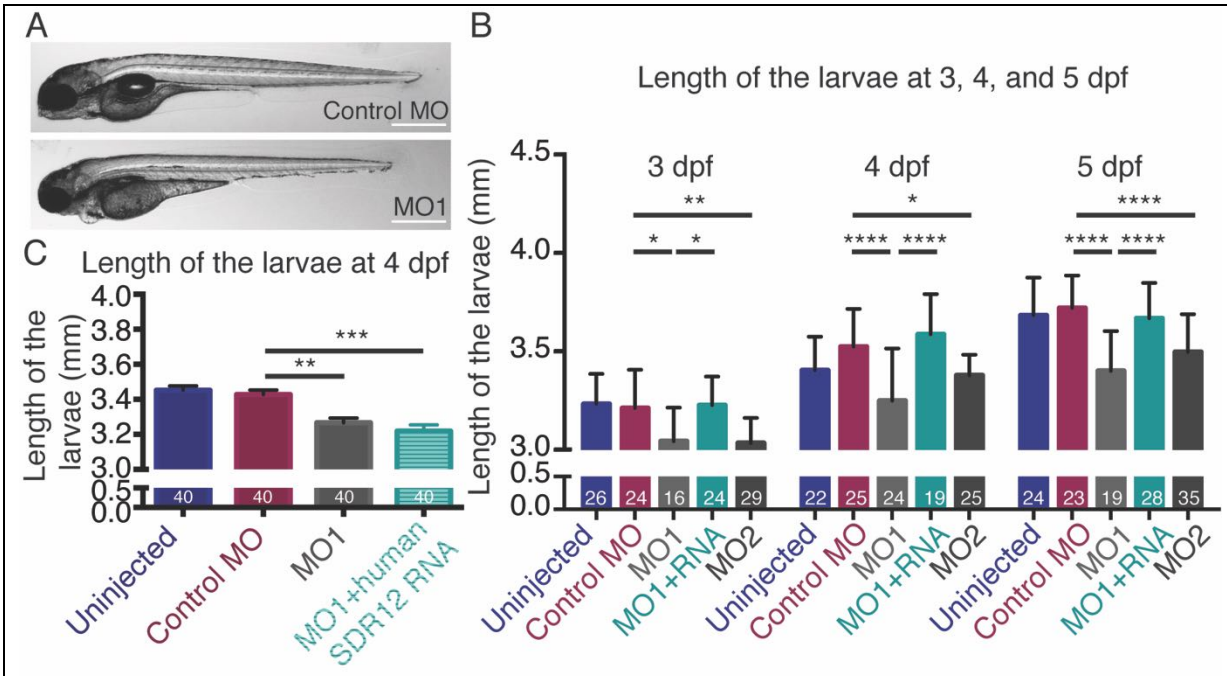

Figure 4.7: 36K knockdown larvae had a reduction in body length. (A) Lateral view of control MO (upper) and MO1 (lower) larvae at 4 dpf. Scale bar: 500 µm. (B) Graph showing length of the larvae from different groups at 3, 4 and 5 dpf. Sample sizes: N = 3. n shown in each bar. 2way ANOVA P ≤ 0.0001 followed by Tukey's multiple comparisons test for control MO vs MO1, control MO vs MO2, MO1 vs MO1+RNA. Control vs MO1+RNA was not significant at all three time-points P > 0.05. (C) Graph showing length of the larvae from different groups at 4 dpf. Sample sizes: N = 3. n = 40 for all groups. Kruskal-Wallis ANOVA P ≤ 0.0001 followed by Dunn's multiple comparisons test for control MO vs MO1 (**) and control MO vs MO1+human SDR12 RNA (***).

4.3. Knockdown of 36K resulted in a behavioural phenotype

With the aim of testing whether there is a functional phenotype following 36K knockdown, two types of behaviour experiments were performed: unprovoked swim test and stimulated swim test.

4.3.1. 36K knock down larvae exhibited a reduction in the distance of swimming

Unprovoked swim test is comparable to open field test, a well-known behaviour test in rodents (Stanford, 2007). In this test, fish were let to swim unprovoked for eight minutes in a twelve well plate with one larva in each well (Figure 4.8A). Distance of swimming was then measured (Figure 4.8B). Larvae in MO1 injected group were found to swim 60 % less than the controls. This phenotype was rescued in MO1+RNA group in which MO1 was co-injected with 36K mRNA. MO1 larvae had smaller bouts of swimming in comparison to the controls (Figure 4.8C).

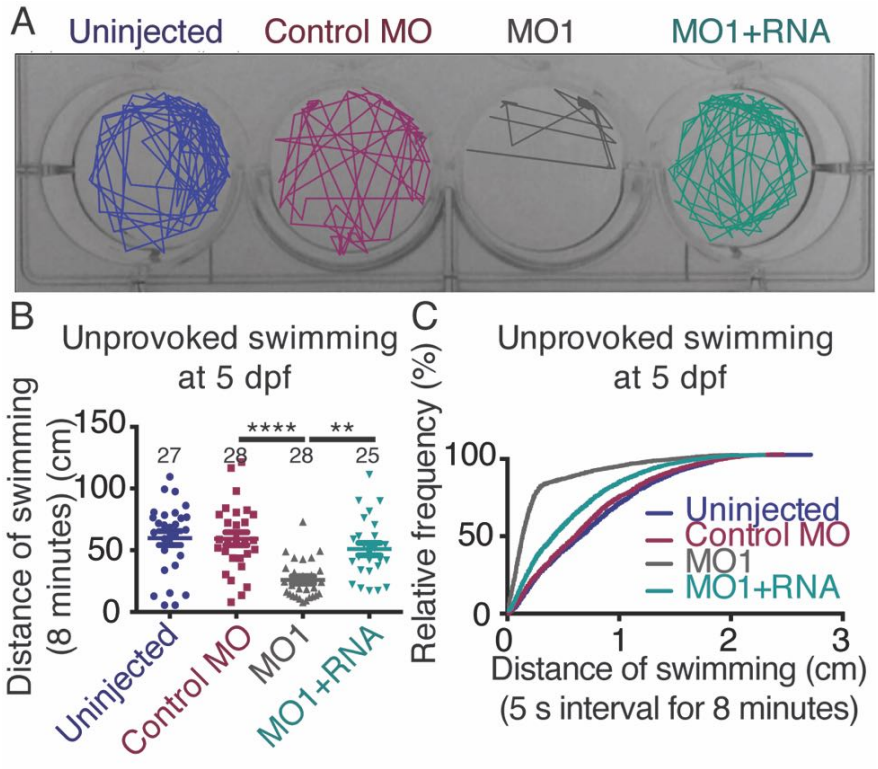

Figure 4.8: 36K knockdown larvae swam less than controls. (A) Manually tracked representative swim tracks of 5 dpf larvae from different groups after 8 minutes of swimming. (B) Graph showing distance of swimming of different groups of 5 dpf larvae in 8 minutes with straight tracks sampled every 5 s. N = 3. n shown in each bar. Kruskal-Wallis ANOVA $P \leq 0.0001$ followed by Dunn's multiple comparisons test for control MO vs MO1 (****), MO1 vs MO1+RNA (**). (C) Cumulative distribution showing relative frequency vs distance of swimming with a sampling time of 5 s clearly showing smaller bouts of swimming in MO1 larvae in average.

4.3.2. 36K knockdown fish responded less in stimulated behaviour tests

Further, in an attempt to test if neural conduction is affected, stimulated behaviour tests were performed. Mauthner axons are the largest calibre axons in zebrafish and they are the first axons to be myelinated (Almeida et al., 2011). These axons are responsible for triggering the motor output for the escape response in zebrafish (Fetcho et al., 2008). In this stimulated behaviour test, the larvae started swimming (escaped) as a response to a marble drop. From MO1 group, 30 % fewer fish responded to the marble drop (Figure 4.9A). But when they

responded, they swam similar distance like the controls (Figure 4.9B). This suggests that there could be impairment in neuronal conduction, as fewer fish respond to a stimulus.

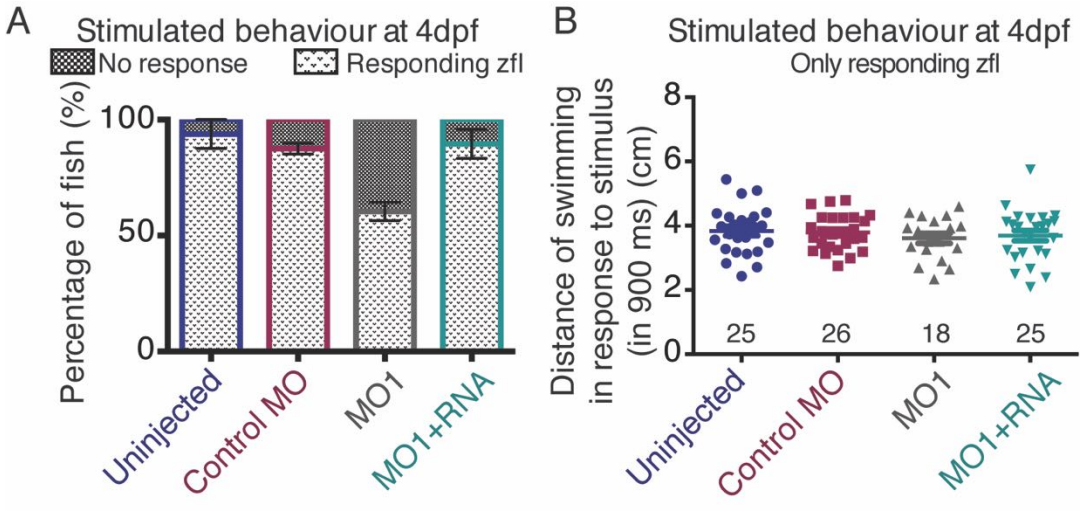

Figure 4.9: Fewer 36K knockdown larvae responded to stimulus. (A) Graph showing percentage of fish that responded to stimulus. N = 4. 2-way ANOVA $P \leq 0.0001$ followed by Tukey's multiple comparisons test for Control MO vs MO1 (**), MO1 vs MO1+RNA (**). (B) Graph showing distance of swimming in response to stimulus excluding fish that did not respond. N = 4. n shown in each bar. Kruskal-Wallis ANOVA $P > 0.05$ not significant.

4.4. Knockdown of 36K resulted in reduced myelin gene expression

Since 36K MO1 larvae respond less in cases of behaviour than controls, to investigate neuronal conduction, effects on myelin were assessed. As Mauthner axons, which trigger the escape response, are the first to be myelinated, and escape response was impaired in 36K knockdown larvae, it was hypothesised that differences in response might be due to myelination problems in the 36K MO knockdown larvae.

4.4.1. 36K knockdown larvae had reduced Mbp expression

Tg(mbp:EGFP-caax) (Almeida et al., 2011) larvae zebrafish were used to visualise internodal myelin *in vivo*. In 36K MO1 knockdown larvae, disrupted Mbp+ myelin was observed in comparison to control MO group when observed with 2-photon light sheet microscope

(Figure 4.10A, A'). In *Tg(mbp:EGFP)* (Almeida et al., 2011), significantly fewer mbp+ cells were observed in both dorsal and ventral spinal cord (Figure 4.11A, A', B-C).

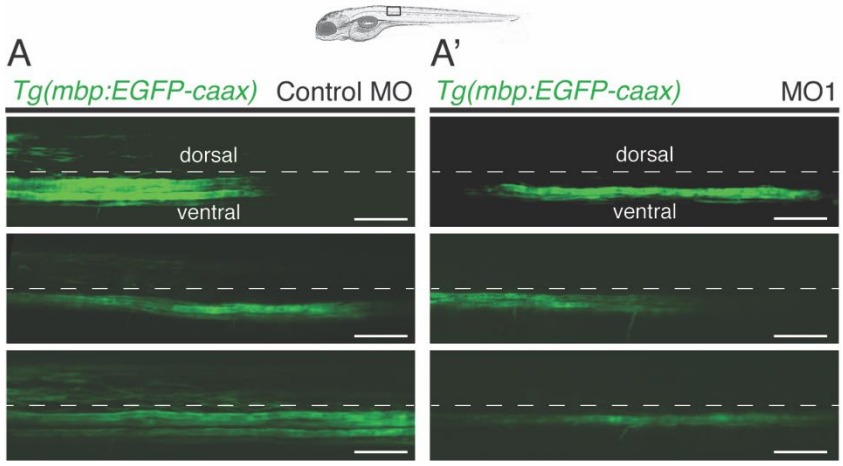

Figure 4.10: 36K knockdown larvae had less Mbp+ expression in the membranes. (A and A') Representative images of maximum intensity z-projections from N=3 depicting lateral view of spinal cord in 4 dpf *Tg(mbp:EGFP-caax)* fish injected with control MO (A) and MO1 (A'). Images were acquired under the same conditions as z-stacks of 100 µm using a 2-photon light sheet microscope. Scale bar: 40 µm.

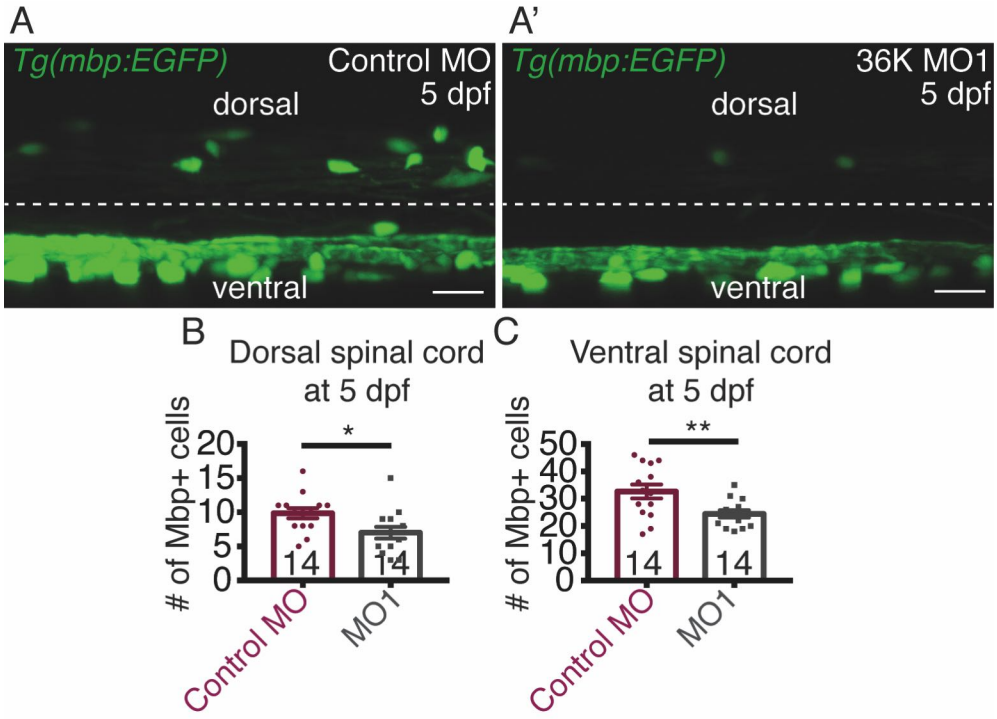

Figure 4.11: 36K knockdown larvae had fewer mbp+ cells. (A, A') Representative lateral view of maximum intensity z-projections acquired from 100 µm stacks using a 2-photon light sheet microscope depicting two spinal segments above the yolk extension at 5 dpf in *Tg(mbp:EGFP)* larvae zebrafish injected with control MO (A) and MO1 (A'). Scale bars: 20 µm. (B, C) Fewer mbp+ cells in two spinal segments were observed in MO1 larvae (B) in the dorsal spinal cord (C) in the ventral spinal cord. Mean number of cells in control MO: in dorsal spinal cord ~= 10, in ventral spinal cord ~= 33. Mean number of cells in MO1: in dorsal spinal cord ~= 7, in ventral spinal cord ~= 24. N = 4. n shown in each bar. For (B), unpaired t-test P value 0.0182 * for control MO vs MO1. For (C), unpaired t-test P value 0.0087 ** for control MO vs MO1.

4.4.2. 36K knockdown larvae had reduced expression of mature myelin genes

Since defects in spinal cord myelination were observed through 2-photon light sheet microscopy, myelin gene expression was evaluated through q-rt-PCR. *mbpa* and *plp1b* were found to be downregulated in 36K knockdown larvae in comparison to control MO group (Figure 4.12A-B).

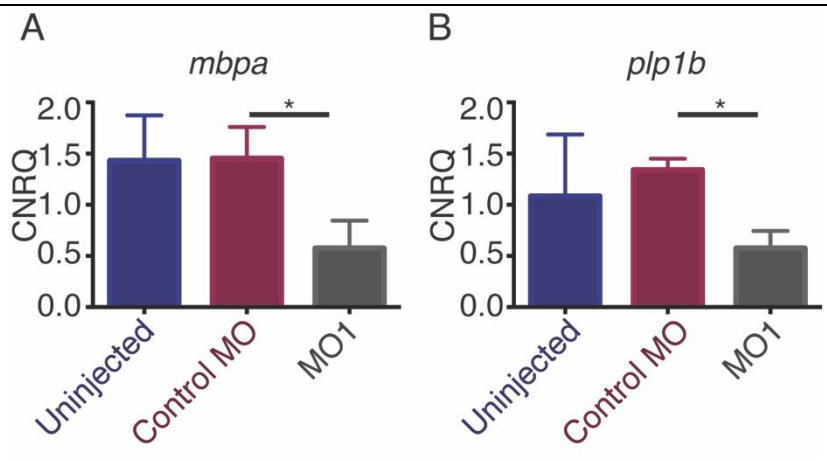

Figure 4.12: 36K knockdown larvae had less mature myelin genes. (A and B) q-rt-PCR data showing CNRQ of (A) *mbpa* and (B) *plp1b* normalized to *β-actin* and *ef1a*. N = 5. Kruskal-Wallis ANOVA P ≤ 0.05 followed by Dunn's multiple comparisons test for control MO vs MO1 (*) for both *mbpa* and *plp1b*.

A microarray analysis was performed together with OakLabs GmbH (Hennigsdorf, Germany) to compare the expression of genes between control MO and 36K knockdown larvae. From this analysis (Figure 4.13), downregulation of *mbpa* and *plp1b* could be observed further confirming our qPCR results (Figure 4.12A-B). *ClaudinK*, which is a marker for myelinating oligodendrocytes (Münzel et al., 2012) was also found to be downregulated. *plp1a*, which is expressed in undifferentiated oligodendrocytes was the only myelin related gene to be upregulated in the Morpholino larvae. All other commonly known and tested for myelin markers were found to be downregulated (Figure 4.13).

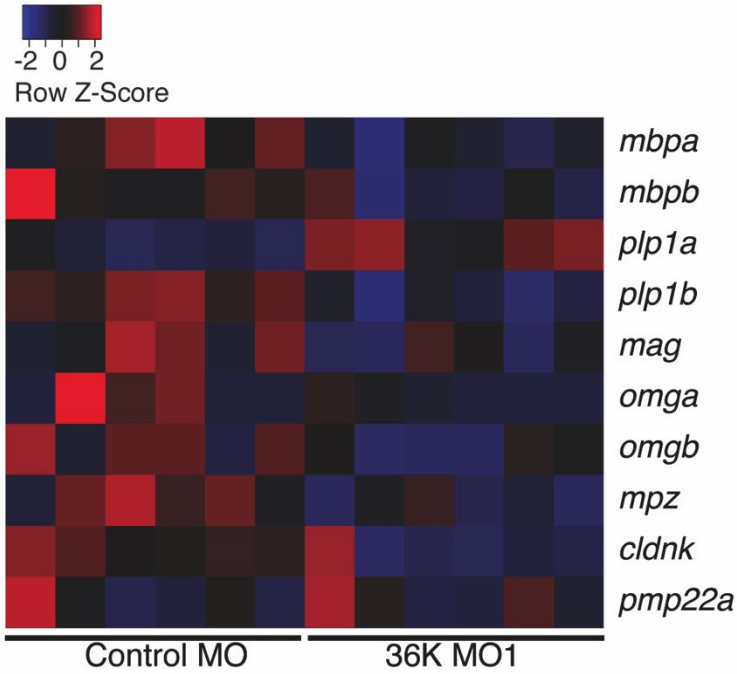

Figure 4.13: Expression of myelin related genes in 36K knockdown larvae. Heatmap generated from microarray analysis data depicting expression of myelin related genes in control MO (left) and MO1 (right) injected zebrafish larvae.

4.4.3. Electron microscopy suggested myelin compaction defects in 36K knockdown larvae

The effects on compaction of myelin were analysed with electron micrographs at 5 dpf between MO1 and control MO groups. We observed unusual cytoplasmic vacuolated structures in between the myelin lamellae in the MO1 group (Figure 4.14A, A').

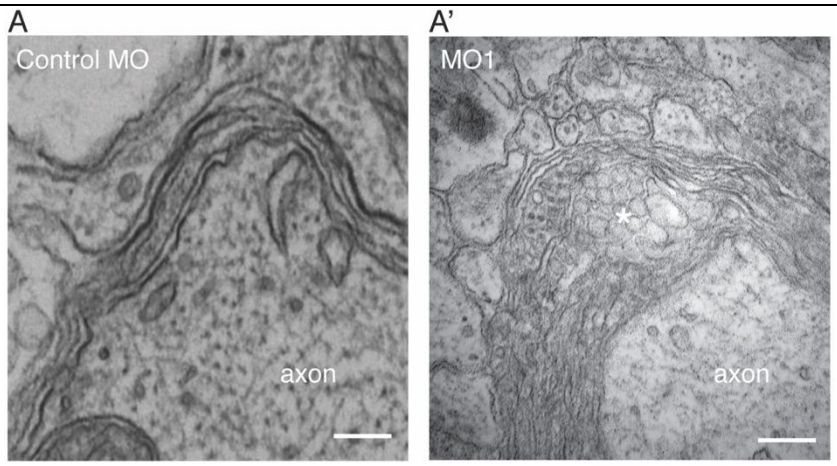

Figure 4.14: 36K knockdown larvae might have compaction defects. Electron micrographs showing myelin around axons in control MO (A) and MO1 (A'). Scale bar: 0.3 µm. TEM done by Prof. Dieter Hartmann.

4.4.4. 36K knockdown larvae had fewer myelinating oligodendrocytes

Since myelin was found to be disrupted, to visualise myelinating oligodendrocytes, *Tg(claudinK:EGFP)* (Münzel et al., 2012) zebrafish larvae were used. ClaudinK is shown to be specifically expressed in myelinating and remyelinating cells in zebrafish (Münzel et al., 2012). Fewer ClaudinK+ cells were observed in 36K knockdown larvae in both the ventral and the dorsal spinal cord region in comparison to control MO larvae (Figure 4.15A, A', B-C).

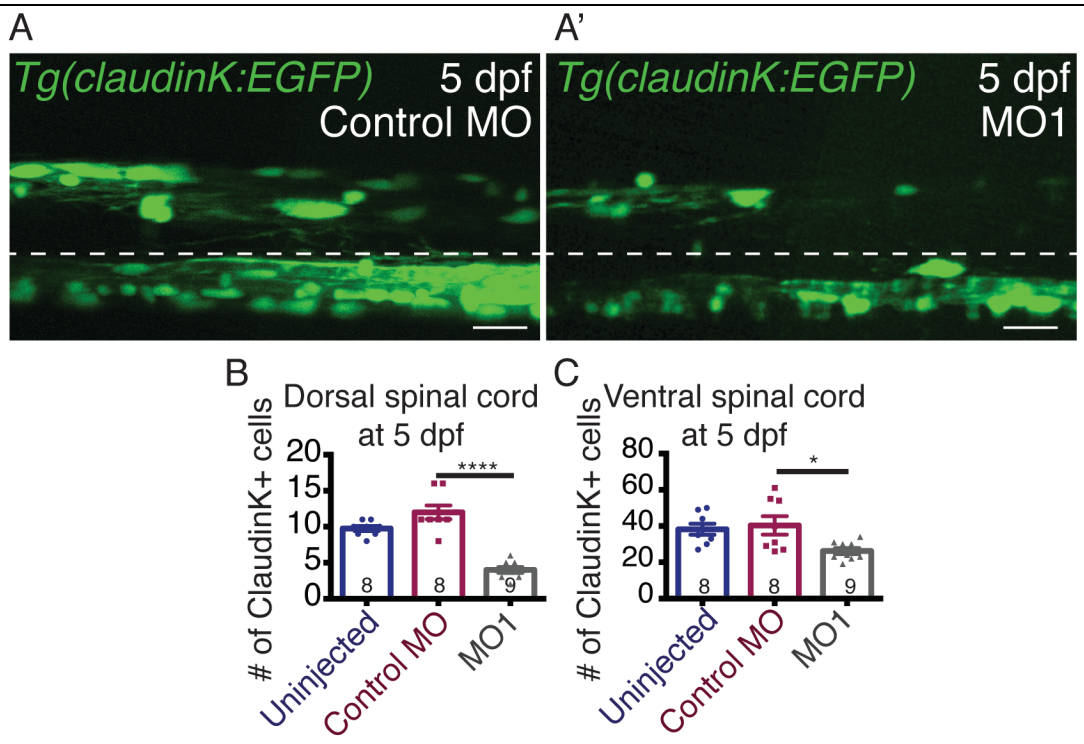

Figure 4.15: 36K knockdown larvae had fewer myelinating oligodendrocytes. (A, A') Representative lateral view of maximum intensity z-projections acquired from 100 µm stacks using a 2-photon light sheet microscope depicting two spinal segments above the yolk extension at 5 dpf in *Tg(claudinK:EGFP)* larvae injected with control MO (A) and MO1 (A'). Scale bars: 20 µm. (B, C) Number of ClaudinK positive cells within two spinal segments (B) in the dorsal spinal cord (C) in the ventral spinal cord. Mean number of ClaudinK positive cells in two spinal segments: in uninjected larvae in dorsal spinal cord ~= 10, in ventral spinal cord ~= 38; in control MO in dorsal spinal cord ~= 12, in ventral spinal cord ~= 40; in MO1 group in dorsal spinal cord ~= 4, in ventral spinal cord ~= 26. N = 3. n shown in each bar. For (B), one-way analysis of variance ANOVA $P \leq 0.0001$ followed by Tukey's multiple comparisons test for control MO vs MO1 (****). For (C), one-way analysis of variance ANOVA $P \leq 0.05$ followed by Tukey's multiple comparisons test for control MO vs MO1 (*).

4.5. 36K knockdown altered dorsally migrated OPCs and oligodendrocytes

As there were fewer myelinating oligodendrocytes in 36K knockdown larvae, and the myelinating oligodendrocytes arise from oligodendrocyte precursor cells (OPCs), *Tg(olig2:GFP)* (Shin et al., 2003) larvae zebrafish were used to examine whether the number of OPCs are altered in 36K knockdown larvae. During vertebrate spinal cord development, ventral neural progenitors pMN give rise to motor neurons and later to oligodendrocyte precursor cells (OPCs). Olig2 is expressed from early OPC stage through migration, differentiation, and myelination in both fish and mammals (Park et al., 2002; Zhou and Anderson, 2002; Chapter 1.2). OPCs are highly dynamic and have a net dorsal movement (Kirby et al., 2006) as depicted in the schematic diagram (Figure 4.16) (Ravanelli and Appel, 2015).

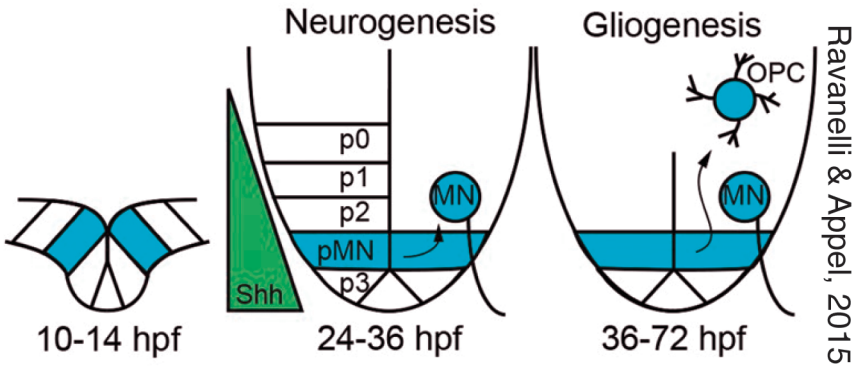

Figure 4.16: OPCs migrate to the dorsal spinal cord. Schematic showing a transverse section of the zebrafish neural tube, with ventral domains p0-p3 patterned along the Sonic hedgehog (Shh) signalling gradient. pMN domain depicted in green has progenitors defined by the expression of transcription factor olig2. pMN progenitors give rise to motor neurons (MN) until 36 hpf and then to oligodendrocyte precursor cells (OPCs) from 36 hpf which then migrate to dorsal region during differentiation. Schematic adapted from (Ravanelli and Appel, 2015).

4.5.1. 36K knockdown larvae had fewer dorsally migrated OPCs

At 3 dpf, when myelination starts in zebrafish (Brösamle and Halpern, 2002), fewer olig2+ OPCs were observed in dorsal spinal cord in MO1 larvae in comparison to the control MO group (Figure 4.17A, A', B). Further, this reduction in dorsal spinal cord OPC numbers could

be rescued when MO1 was co-injected with 36K mRNA (MO1+RNA). However, in the ventral spinal cord, no difference was observed in olig2+ OPC numbers between control MO and 36K knockdown larvae (Figure 4.17C). Fewer dorsally migrated olig2+ OPCs in MO1 injected larvae were also confirmed using a high throughput automated protocol using the EnSight© multimode plate reader (Figure 4.17D). This could also be observed in larvae injected with second translation blocking Morpholino (MO2), further confirming the specificity of the observations (Figure 4.17E). To confirm that fewer OPC numbers was not only due to a developmental delay, dorsal olig2+ OPCs were analysed again at 5 dpf. Fewer olig2+ OPCs were observed also at 5 dpf in 36K knockdown larvae in comparison to control MO (Figure 4.18A, A', B), which again could be rescued in MO1+RNA injected larvae.

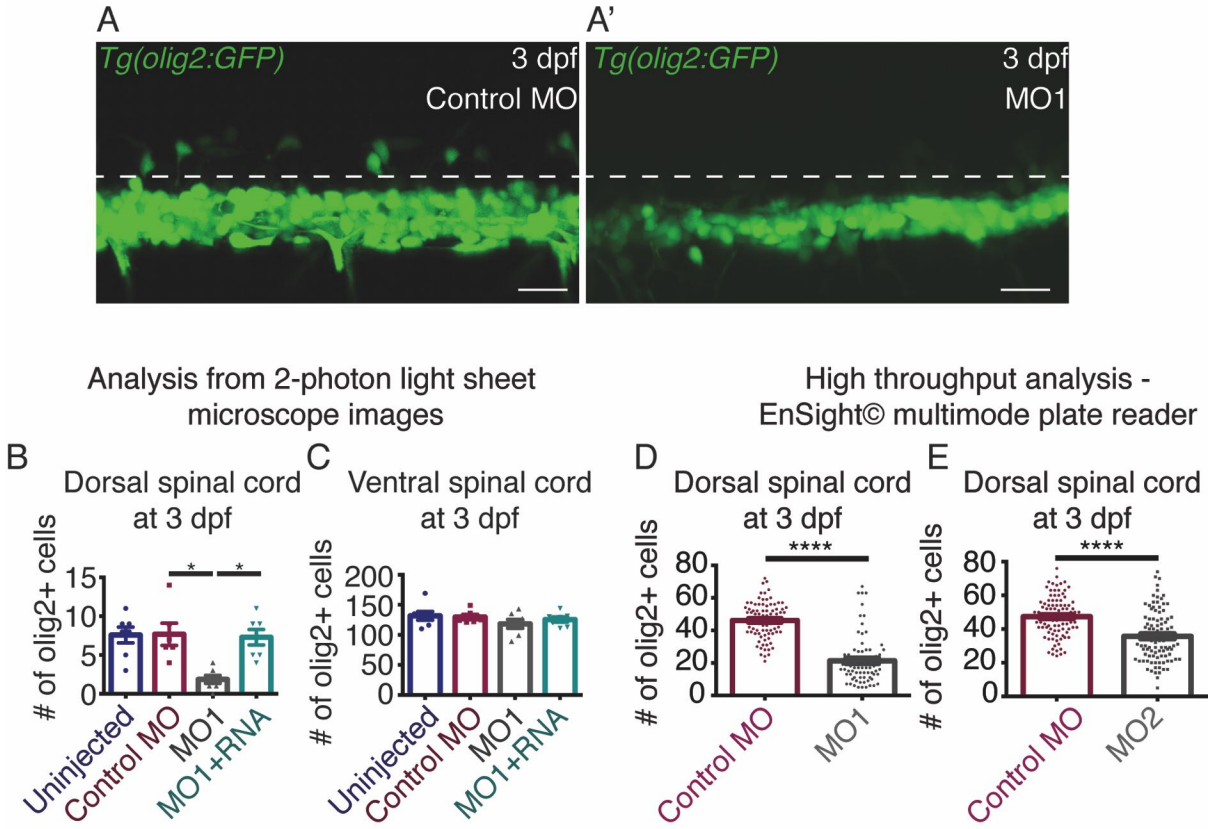

Figure 4.17: 36K knockdown larvae had fewer dorsally migrated OPCs at 3 dpf. (A, A') Representative lateral view of maximum intensity z-projections acquired from 100 µm stacks using a 2-photon light sheet microscope depicting two spinal segments above the yolk extension at 3 dpf in *Tg(olig2:GFP) larvae zebrafish* injected with control MO (A) and MO1 (A'). Scale bars: 20 µm. (B, C) Number of olig2+ cells in two spinal segments (B) in the dorsal spinal cord (C) in the ventral spinal cord. Mean number of olig2 positive cells in two spinal segments: in uninjected larvae in dorsal spinal cord ~= 7, in ventral spinal cord ~= 130; in control MO in dorsal spinal cord ~= 7, in ventral spinal cord ~= 130; in MO1 in dorsal spinal cord ~= 2, in ventral spinal cord ~= 120; in MO1+RNA in dorsal spinal cord ~= 7, in ventral spinal cord ~= 125. N = 3. n shown in each bar. For (B), Kruskal-Wallis ANOVA P ≤ 0.01 followed by Dunn's multiple comparisons test for control MO vs MO1 (*), MO1 vs MO1+RNA (*). For (C), Kruskal-Wallis ANOVA P > 0.05 not significant. (D, E) Fewer dorsally migrated olig2+ cells were observed in MO1 injected larvae (D) and MO2 injected larvae (E) at 3 dpf in the entire spinal cord quantified using high throughput EnSight© multimode plate reader. For (D), N=2. n=89 in Control MO, n=77 in MO1. Mann Whitney two tailed test p-value ≤ 0.0001 (****). For (E), N=3. n=102 in Control MO, n=102 in MO2. Mann Whitney two tailed test p-value ≤ 0.0001 (****). Measurements by EnSight© multimode plate reader were performed with the help of Enrico Mingardo, Felix Häberlein.

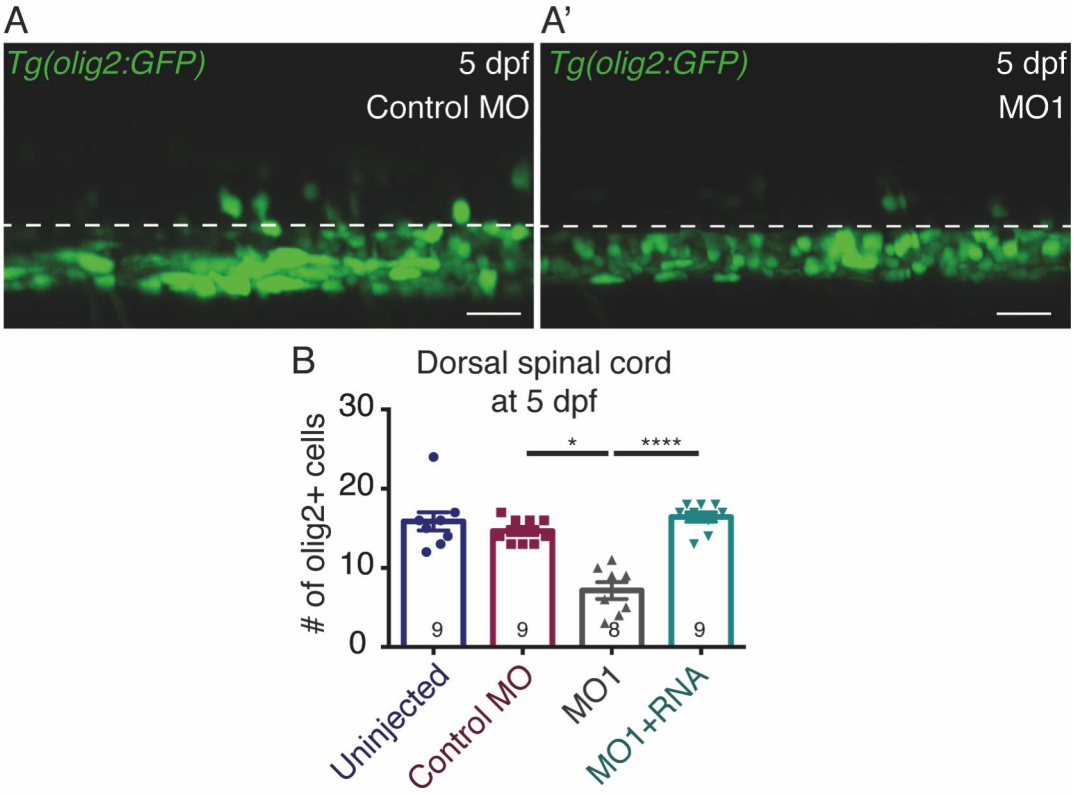

Figure 4.18: 36K knockdown larvae had fewer dorsally migrated OPCs at 5 dpf. (A, A') Representative lateral view of maximum intensity z-projections acquired from 100 µm stacks using a 2-photon light sheet microscope depicting two spinal segments above the yolk extension at 5 dpf in *Tg(olig2:GFP)* injected larvae zebrafish with control MO (A) and MO1 (A'). Scale bars: 20 µm. (B) Number of olig2 positive cells in two spinal segments in the dorsal spinal cord. Mean number of olig2 positive cells in two spinal segments in dorsal spinal cord: in uninjected larvae ~= 15; in control MO ~= 15; in MO1 ~= 7; in MO1+RNA in dorsal spinal cord ~= 16. N = 3. n shown in each bar. Kruskal-Wallis ANOVA $P \leq 0.0001$ followed by Dunn's multiple comparisons test for control MO vs MO1 (*), control MO vs MO1+RNA (****).

4.5.2. 36K knockdown larvae had an increase in proliferating cells but no change in apoptotic cells

The reduction in the number of dorsally migrated OPCs could be either due to less proliferation, or less differentiation, and/or more cell apoptosis. From microarray analysis data performed together with Oaklabs GmbH (Hennigsdorf, Germany), proliferative markers like proliferating cell nuclear antigen (*pcna*) (Herce et al., 2014; Maga and Hübscher, 2003) (Figure 4.19A) and nucleolar protein interacting with forehead-associated domain of marker Ki-67 (*nifk*) (Takagi et al., 2001) (Figure 4.19B) were found to be increased in the 36K

knockdown group in comparison to control MO group. Elevated Pcna expression was further confirmed by immunostaining of larvae paraffin sections (Figure 4.20A, A').

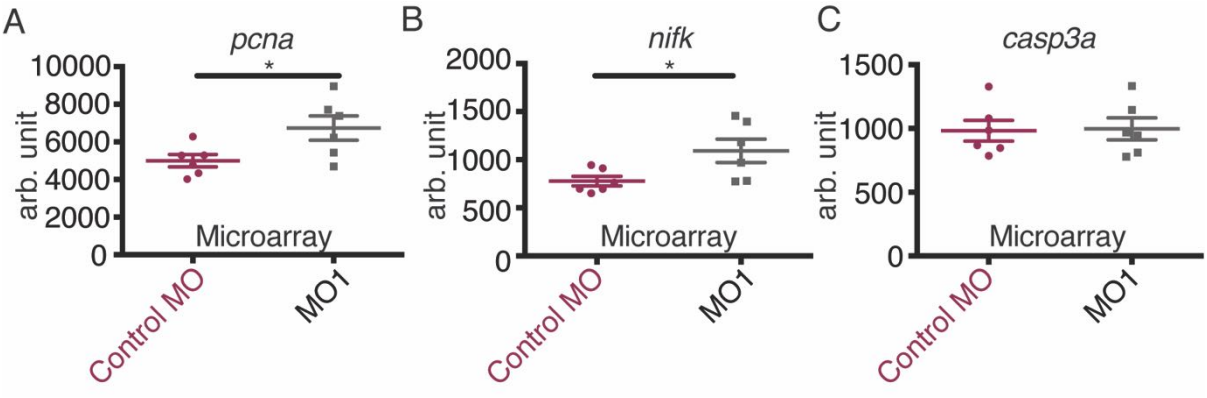

Figure 4.19: 36K knockdown larvae showed increased cell proliferation but no change in apoptosis. (A) – (C) Graphs showing the expression of (A) *pcna*, (B) *nifk*, (C) the apoptosis marker *casp3a* in control MO and MO1 at 3 dpf from microarray analysis. N=6. Unpaired two tailed t test with Welch's correction. P Value 0.0450 (*) for *pcna* (A), P Value 0.0493 (*) for *nifk* (B) and P Value of 0.9045 (not significant) for *casp3a* (C).

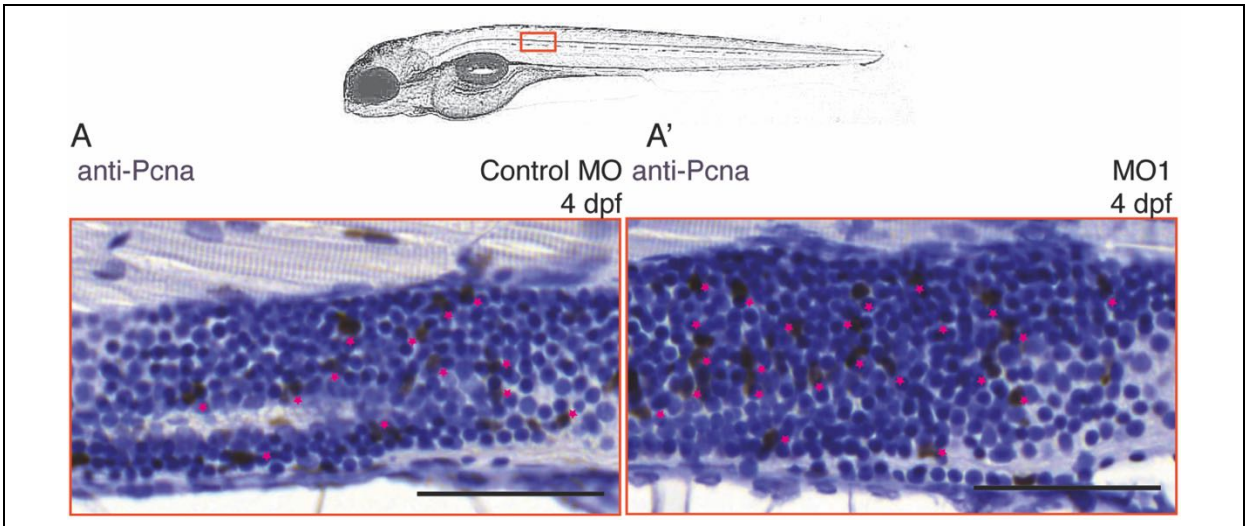

Figure 4.20: Anti-Pcna staining suggested increased proliferation in spinal cord in 36K knockdown larvae. (A, A') Representative images of sagittal views of paraffin sections of 4 dpf larvae injected with control MO (A) and MO1 (A') showing cells labelled with anti-Pcna marked with pink asterisks and nuclei counter stained with Haematoxylin. Scale bars: 50 µm. Immunostaining done by Dr. Anna Japp.

For apoptosis, no difference was found in *caspase 3* (*casp3a*) (Ghavami et al., 2009) between control MO and MO1 injected larvae zebrafish from the microarray data (Figure 4.19C) which could be further confirmed by immunostaining of paraffin sections with anti-Cleaved caspase 3 (Figure 4.21A, A', B, B').

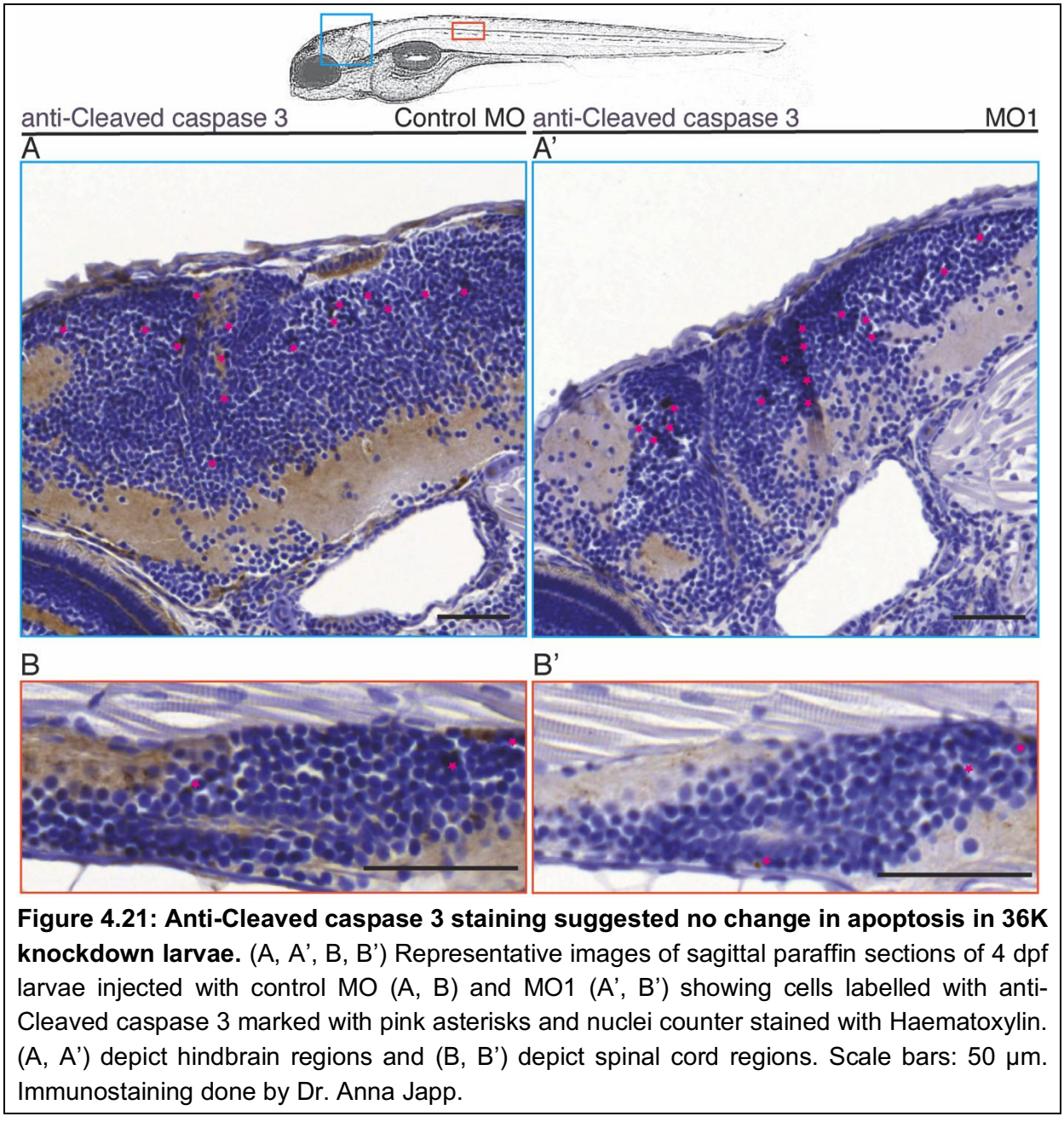

Figure 4.21: Anti-Cleaved caspase 3 staining suggested no change in apoptosis in 36K knockdown larvae. (A, A', B, B') Representative images of sagittal paraffin sections of 4 dpf larvae injected with control MO (A, B) and MO1 (A', B') showing cells labelled with anti-Cleaved caspase 3 marked with pink asterisks and nuclei counter stained with Haematoxylin. (A, A') depict hindbrain regions and (B, B') depict spinal cord regions. Scale bars: 50 µm. Immunostaining done by Dr. Anna Japp.

Taken together these experiments showed more proliferation and no change in apoptosis in 36K knockdown larvae, hence suggesting that the reduced amount of dorsally migrated olig2+ cells in 36K MO knockdown larvae might be due to less or altered migration and/or

differentiation of precursor cells and not due to less proliferation or enhanced apoptosis. The increased progenitors might be differentiating into other cell types apart from oligodendrocytes. The possible cell fate of these cells is later addressed in Chapter 4.6.3..

4.5.3. In the absence of dorsally migrated OPCs, no 36K was detectable in developing larvae

With the aim of studying 36K expression when there are no differentiated oligodendrocytes, zebrafish larvae were treated with TrichostatinA (TSA), a histone deacetylase (HDAC) inhibitor shown to inhibit the differentiation of OPCs to oligodendrocytes completely (Takada and Appel, 2010). The treatment was from 36 hpf onwards, which is subsequent to neurogenesis (Ravanelli and Appel, 2015) and until 4 dpf. In TSA treated larvae, there were no dorsally migrated olig2+ OPCs detectable (Figure 4.22A, A'). Interestingly, also no 36K expression was observed at 4 dpf in TSA treated larvae as shown by Western blot (Figure 4.22B), suggesting that there is no measurable level of 36K expression when there are no differentiated oligodendrocytes.

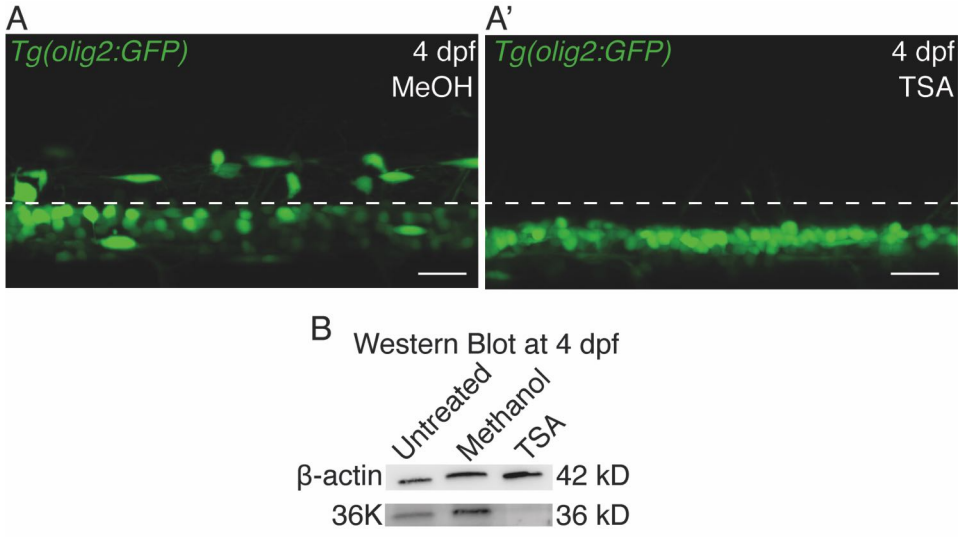

Figure 4.22: Following TSA treatment, no 36K was detectable in developing larvae by Western blot. (A, A') Representative lateral view of maximum intensity z-projections acquired from 100 µm stacks using a 2-photon light sheet microscope depicting two spinal segments above the yolk extension at 4 dpf in *Tg(olig2:GFP)* zebrafish larvae treated with MeOH as control (A) and TSA (A'). Scale bars: 20 µm. (B) Western blot of 36K showing untreated, Methanol control and TSA treated larvae at 4 dpf with β-actin as loading control.

4.6. 36K knockdown larvae showed Notch upregulation

In order to understand how 36K regulates dorsal spinal cord olig2+ OPC numbers, expression levels of genes involved in different pathways during neurogenesis and gliogenesis, were analysed in the MO1 and control MO groups from our microarray analysis data. Several pathways have been previously described to be involved in neurogenesis and gliogenesis during the development of spinal cord (Briscoe and Novitch, 2008). Sonic hedgehog (Shh) pathway has been shown to have a featured role in dorsoventral patterning (Fuccillo et al., 2006). Fibroblast growth factor (FGF), Retinoic acid (RA) have been shown to be involved in posterior fates of neural ectoderm (Kudoh et al., 2002). Notch signalling has been found to promote gliogenesis while suppressing oligodendrocyte differentiation and also shown to have a role in proliferation and apoptosis (Artavanis-Tsakonas, 1999; Fortini et al., 1993; Grandbarbe, 2003; Kim et al., 2008). Bone morphogenetic protein (BMP) signalling is a regulator of development and patterning of the dorsal-ventral axis (Bond et al., 2012). Wnt signalling has been shown to play a role in ventral patterning (Yu et al., 2008).

4.6.1. 36K knockdown larvae had upregulated Notch targets

Since the generation of neuronal subtypes in the ventral spinal cord is dependent on a gradient of Shh/Gli signalling, expression levels of genes in this pathway *gli3, gli2a, gli2b, shha, smoothened (smo), patched1 (ptch1)* were analysed within the mRNA microarray data. *fgf3 and spry4 (sprouty* (Drosophila) homolog 4 [Source:ZFIN;Acc:ZDB-GENE-010803-2]), a downstream gene of FGF pathway was assessed for FGF signalling (Kudoh et al., 2002). Retinoic acid receptor subunits *rarab, rxrgb* and downstream gene *cyp26a1* (cytochrome P450, subfamily XXVIA, polypeptide 1 [Source:ZFIN;Acc:ZDB-GENE-990415-44]) for RA pathway, *bmp1a* and *bmp1b* for BMP signalling, *wnt11 inducible signalling pathway protein 1a* (*wisp1a*) and *nephronophthisis 4* (*nphp4*), a positive regulator of Wnt for Wnt pathway,

were examined. All these genes were not found to be regulated in MO1 in comparison to control MO injected larvae (Table 4.1).

However, within the Notch signalling pathway, Notch targets were found to be upregulated. These are tabulated in Table 4.2. hairy-related 4 (her4) is a target of Notch (Takke et al., 1999) and was found to be upregulated in 36K knockdown (Table 4.2, Figure 4.23A). Deltaa and Deltab, major ligands that bind to Notch in addition to jagged1a (Louvi and Artavanis-Tsakonas, 2006; Tallafuss et al., 2010) were found to be upregulated (Table 4.2, Figure 4.23A).

Ensemble ID	Gene Symbol	Mean control MO	Mean MO1	P value	log_2fold changes
Shh/Gli signalling related genes:					
ENSDART00000058992	Gli3	221.375	219.448	0.881	-0.017
ENSDART00000024555	Gli2a	670.343	778.123	0.115	0.216
ENSDART00000017912	Gli2b	86.535	94.571	0.023	0.130
ENSDART00000149395	Shha	936.319	1278.794	0.053	0.441
ENSDART00000005985	Smo	475.229	564.748	0.435	0.211
ENSDART00000148258	Ptch1	124.429	141.708	0.354	0.168
Fgf signalling related genes:					
ENSDART00000110754	Fgf3	96.622	106.808	0.374	0.136
ENSDART00000099528	Spry4	1088.316	1156.488	0.353	0.082
RA related genes:					
ENSDART00000044677	Rarab	328.214	354.400	0.475	0.115
ENSDART00000002554	Rxrgb	233.809	239.104	0.734	0.035
ENSDART00000041728	Cyp26a1	459.563	433.215	0.982	-0.010
BMP genes:					
ENSDART00000059795	bmp1b	10.902	13.196	0.244	0.272
ENSDART00000127875	bmp1a	1352.688	1471.382	0.132	0.123

Wnt signalling related genes:

ENSDART00000076506	Wisp1a	51.452	48.246	0.507	-0.102
ENSDART00000131805	Nphp4	3658.630	3030.034	0.459	-0.266

Table 4.1: Expression of genes related to Shh/Gli, Fgf, RA, BMP, Wnt signalling pathways from microarray analysis data. Genes that are significantly regulated and also have $|\log_2 fold| > 0.5$ have been considered for analysis. No significant difference was observed in genes related to Shh/Gli, Fgf, RA, BMP and Wnt signalling pathways. Mean control MO and mean MO1 depict average arbitrary values from N=6 from the microarray analysis data. The P value was calculated from unpaired two tailed t test with Welch's correction.

Ensemble ID	Gene Symbol	Mean control MO	Mean_MO1	P value	$\log_2$fold changes
Notch targets:					
ENSDART00000079274	Her4.1	349.793	575.647	0.043	0.703
ENSDART00000104206	Her4.2	801.375	1120.265	0.002	0.477
ENSDART00000104209	Her4.3	858.675	1181.913	0.002	0.455
ENSDART00000079265	Her4.4	803.526	1127.739	0.002	0.482
ENSDART00000078936	Her9	1917.884	2890.147	0.083	0.524
ENSDART00000101578	Her8.2	166.769	216.254	0.058	0.360
Notch:					
ENSDART00000129224	Notch1a	96.473	136.358	0.003	0.509
ENSDART00000050855	Notch1b	97.501	141.354	0.015	0.553
ENSDART00000123104	Notch2	566.469	579.641	0.884	0.033
ENSDART00000073930	Notch3	222.319	288.665	0.000	0.379
Ligands binding to Notch:					
ENSDART00000137172	Jagged1a	153.049	228.353	0.012	0.567
ENSDART00000019323	Jagged1b	144.947	151.152	0.643	0.059
ENSDART00000126339	Deltaa	878.966	1744.445	0.002	0.952

ENSDART00000019259	Deltab	470.997	900.189	0.001	0.917

Table 4.2: Expression of genes related to the Notch signalling pathway from microarray analysis data. Notch targets and Delta, ligands binding to Notch are upregulated in MO1. Mean control MO and Mean MO1 depict average from arbitrary values from N=6 from the microarray analysis data. P value is calculated from unpaired two tailed t test with Welch's correction. Genes that are significantly upregulated and also have $|\log_2 fold| > 0.5$ have been shaded in green.

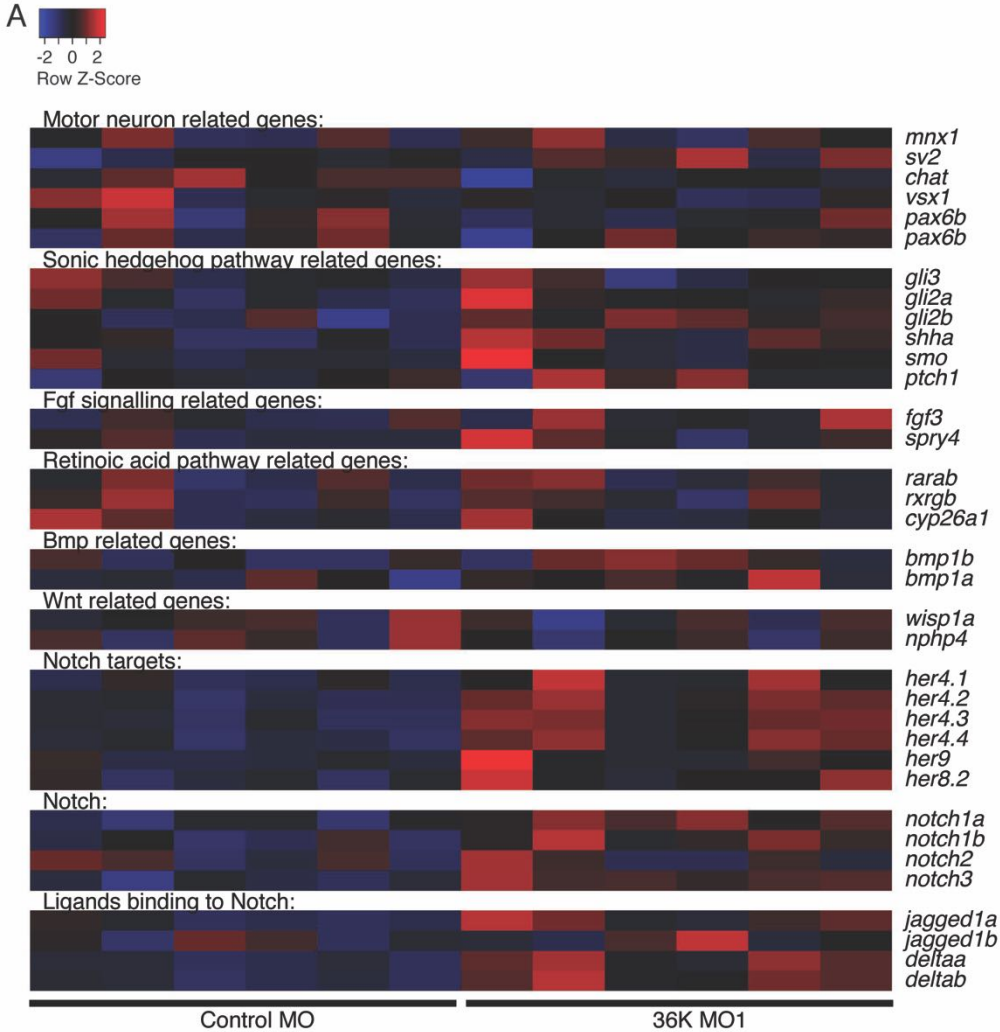

Figure 4.23: Microarray analysis showing an activated Notch. (A) Heatmap generated from microarray analysis data showing expression of genes related to spinal cord progenitors. Significant upregulation was clearly observed in the *notch* targets and ligands binding to notch.

To confirm these microarray analysis data, semi-quantitative RT-PCR experiments were performed for her4.1 (ZFIN ZDB-GENE-980526-521), deltaa (ZFIN ZDB-GENE-980526-29), and notch (ZFIN ZDB-GENE-990415-173) genes (Figure 4.24A). RT-PCR showed upregulation in her 4.1 (Figure 4.24B) and deltaa (Figure 4.24C) confirming the microarray expression analysis (Figure 4.23) but no change was observed in notch1a (Figure 4.24D).

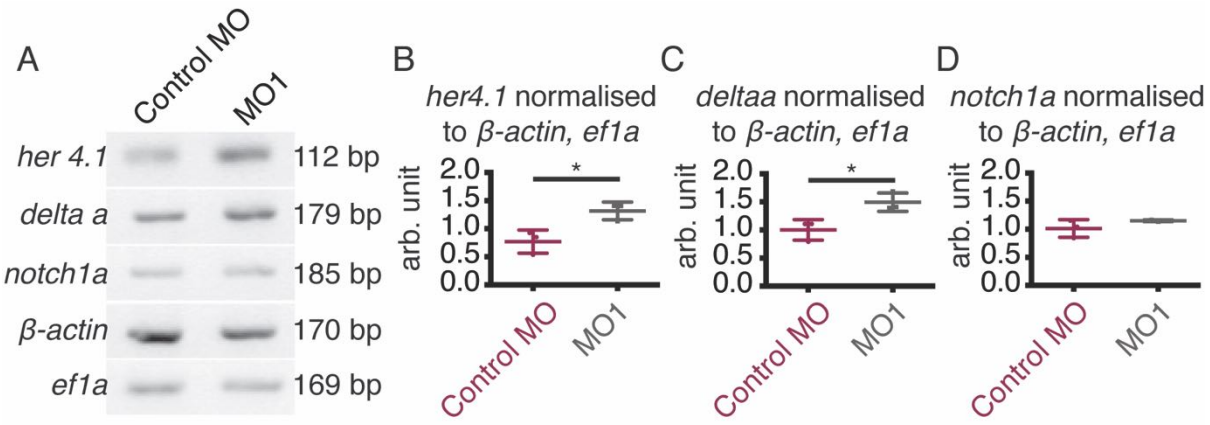

Figure 4.24: RT PCR confirmed upregulated Notch target *her 4.1* and *deltaa* in 36K knockdown larvae. (A) Semi quantitative RT PCR in control MO and MO1 larvae at 3 dpf for her 4.1, deltaa, notch1a with β-actin and ef1a as reference genes. (B, C, D) Graphs showing expressions of (B) her 4.1, (C) deltaa and (D) notch1a normalised to β-actin and ef1a. N = 3. Unpaired two tailed t test with equal SD. P Value 0.0219 * for her4.1 (A), P Value 0.0253 * for deltaa (B), P Value 0.2069 for notch1a (C).

4.6.2. Notch activation influences migration and differentiation of spinal cord progenitors

Notch is known to influence migration and differentiation of both neuronal and glial cells (Figure 4.25). Notch is involved in progenitor maintenance and in the decision making between neuronal and glial lineages. Notch signal inhibits differentiation of neurons from neuronal progenitors. While Notch promotes differentiation of glial progenitors into astrocytes, it inhibits oligodendrocyte differentiation from glial lineages (Louvi and Artavanis-Tsakonas, 2006).

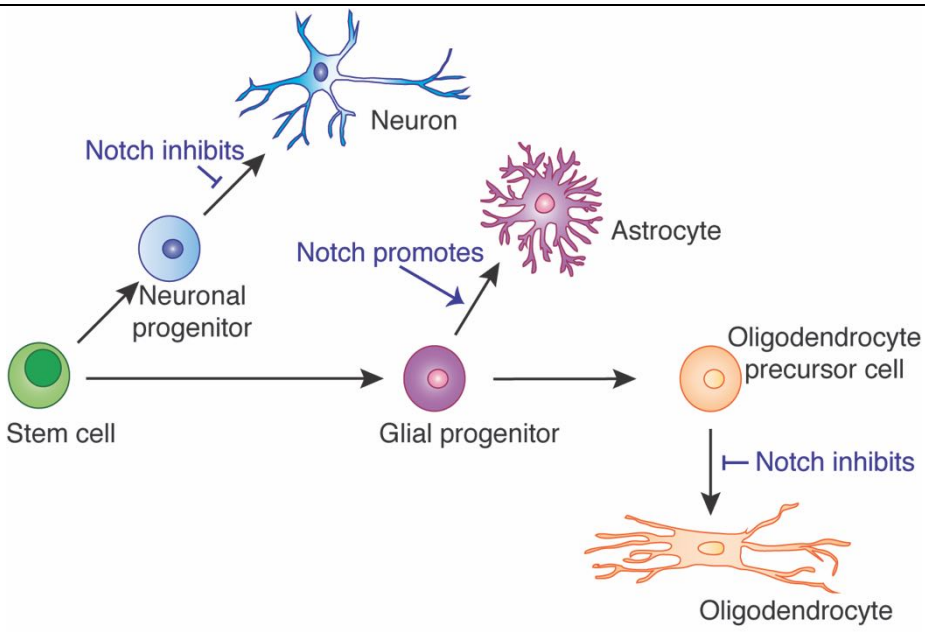

Figure 4.25: Notch signal activation and cell fate decisions. Schematic showing the influence of Notch on neuronal and glial progenitors, the two major lineages of cells generated in the vertebrate nervous system. Neuronal differentiation from neuronal progenitor and oligodendrocyte differentiation from OPC is inhibited by Notch signal. On the other hand, astrocyte differentiation is promoted by Notch signal. Schematic based on (Louvi and Artavanis-Tsakonas, 2006).

4.6.3. 36K knockdown larvae showed increased Gfap+ expression

Since Notch signalling is known to regulate glial precursors in the decision to become astrocytes or OPCs (Louvi and Artavanis-Tsakonas, 2006), *TgBAC(gfap:gfap-GFP)* (Chen et al., 2009) larvae zebrafish were used to visualise astrocytes. In these larvae, increased Gfap+ expression was observed in 36K knockdown larvae in comparison to control MO (Figure 4.26A, A', B). Further, anti-Gfap staining confirmed increased Gfap expression in 36K knockdown larvae (Figure 4.27A, A', B, B') in the spinal cord regions. Expression levels of macrophages and microglial genes were analysed from the microarray data and they were not found to be altered (Table 4.3), which further suggested that the increase in Gfap+ cells was not due to reactive gliosis but due to an increase in the number of astrocytes.

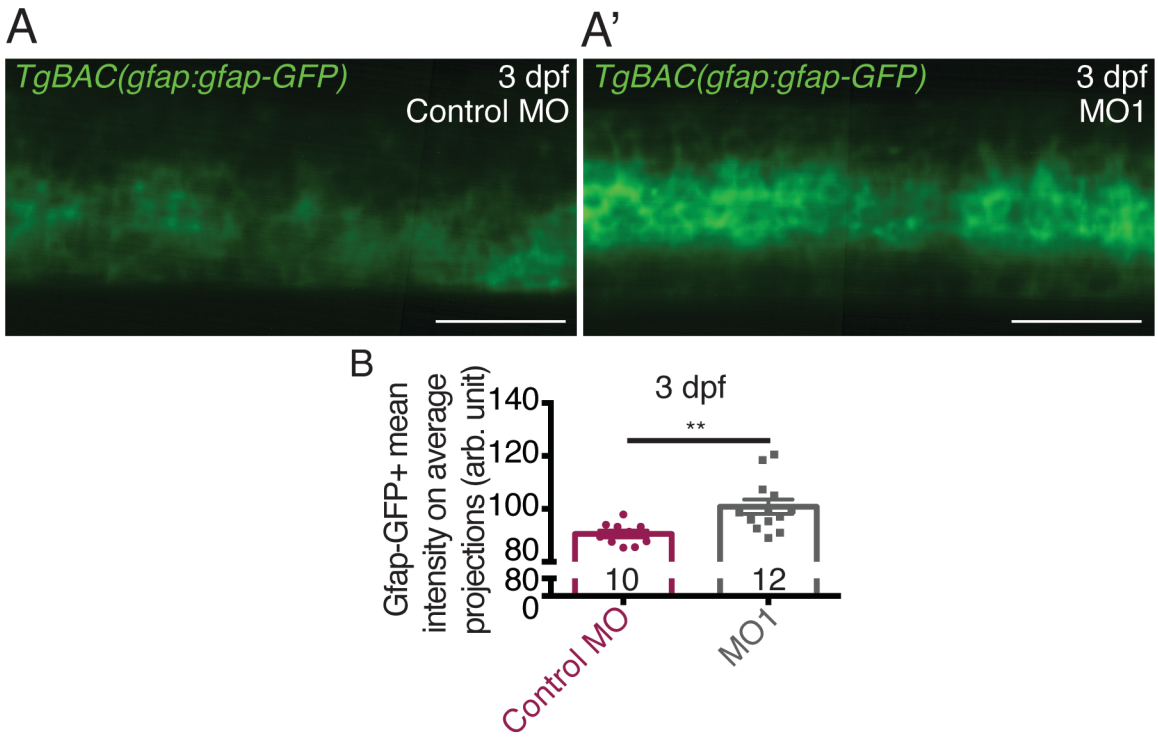

Figure 4.26: 36K knockdown larvae showed increased Gfap+ expression. (A, A') Representative lateral view of maximum intensity z-projections acquired from 100 µm stacks using a 2-photon light sheet microscope depicting two spinal segments above the yolk extension in *TgBAC(gfap:gfap-GFP)* larvae zebrafish at 3 dpf injected with control MO (A) and MO1 (A'). Scale bars: 40 µm. (B) Graph showing mean intensity of average projections from gfap-GFP+ expression in the spinal cord. Sample sizes: N = 4. n shown in each bar. Unpaired two tailed t test with Welch's correction P value 0.0032 (**).

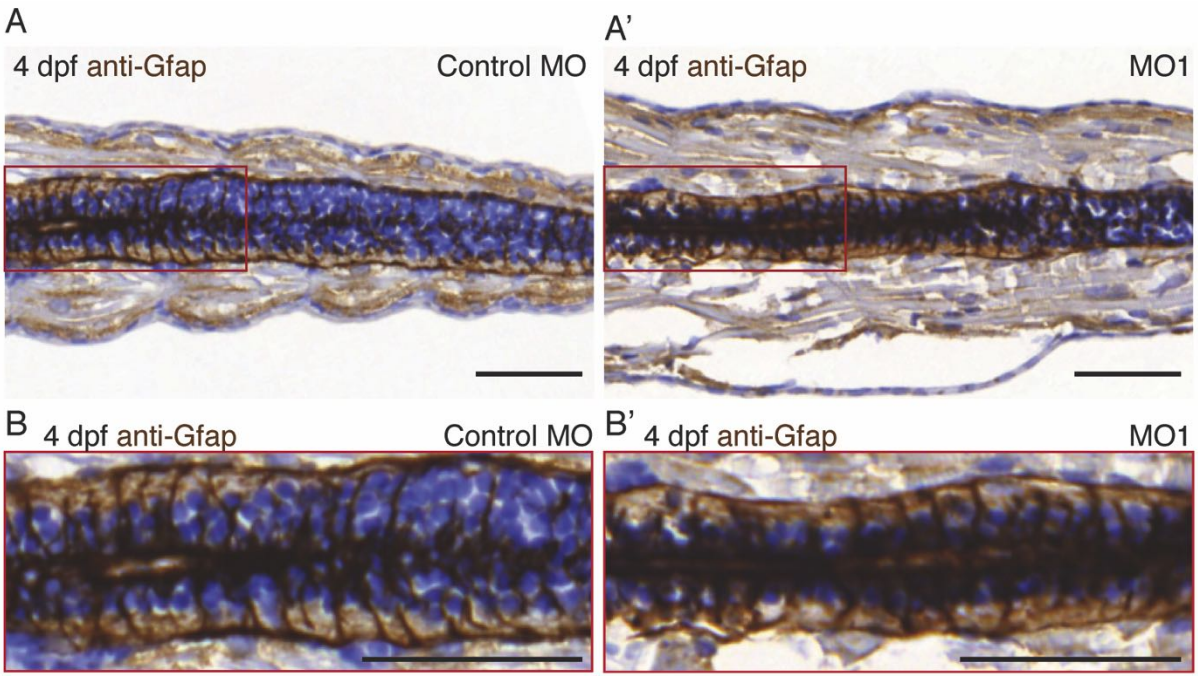

Figure 4.27: 36K knockdown larvae showed increased anti-Gfap expression. (A, A', B, B') Representative images of sagittal paraffin sections depicting spinal cords of 4 dpf larvae injected with control MO (A, B) and MO1 (A', B') showing anti-Gfap immunostaining with nuclei counter stained with Haematoxylin. (B, B') are enlarged images from (A, A' red boxes) respectively. Scale bars: 50 µm. Immunostaining was done by Dr. Anna Japp.

Ensemble ID	Gene Symbol	Mean control MO	Mean_MO1	P value
ENSDART00000131988	mpeg1	9.796	9.448	0.792
ENSDART00000100372	il34	57.788	73.824	0.263
ENSDART00000077545	slc7a7	150.206	151.689	0.993

Table 4.3: Expression of macrophage and microglial related genes from microarray analysis data. Expression levels of macrophage expressed 1 (mpeg1) and the microglia markers interleukin 34 (il34) and solute carrier family 7 (slc7a7) were not elevated in MO1 in comparison to control MO injected larvae.

4.6.4. 36K knockdown larvae had fewer DRG neurons

Dorsal root ganglion (DRG) cells are known to be regulated by Delta-Notch signalling (Cornell and Eisen, 2002). *Tg(-8.4ngn1:GFP)* (Blader et al., 2003) larvae zebrafish were used to observe DRG cells in vivo. In 36K knockdown larvae, fewer ngn1+ DRG cells were found in comparison to control MO at 3 dpf (Figure 4.28A, A', C). With the purpose of confirming that this was not just due to developmental delay, ngn1+ DRG cells were examined again at 5 dpf. Fewer ngn1+ DRG cells were found in MO1 larvae also at 5 dpf suggesting that this shortage is not only due to a delay in development (Figure 4.28B, B', D). However, no changes in axonal innervation were observed (Figure 4.29A, A', A'') when larvae wild type fish, control MO and MO1 injected, were stained with anti-Sv2, a marker for presynaptic terminals (Jonz and Nurse, 2003; Wan et al., 2010). Further no changes in the myelin of the peripheral lateral lines (PLL) could be observed using *Tg(mbp:EGFP)* larvae zebrafish (Figure 4.30). The increase in Gfap+ expression and fewer DRG cells are in context and full agreement with recent literature for Notch upregulation in 36K knockdown larvae (Cornell and Eisen, 2002; Louvi and Artavanis-Tsakonas, 2006).

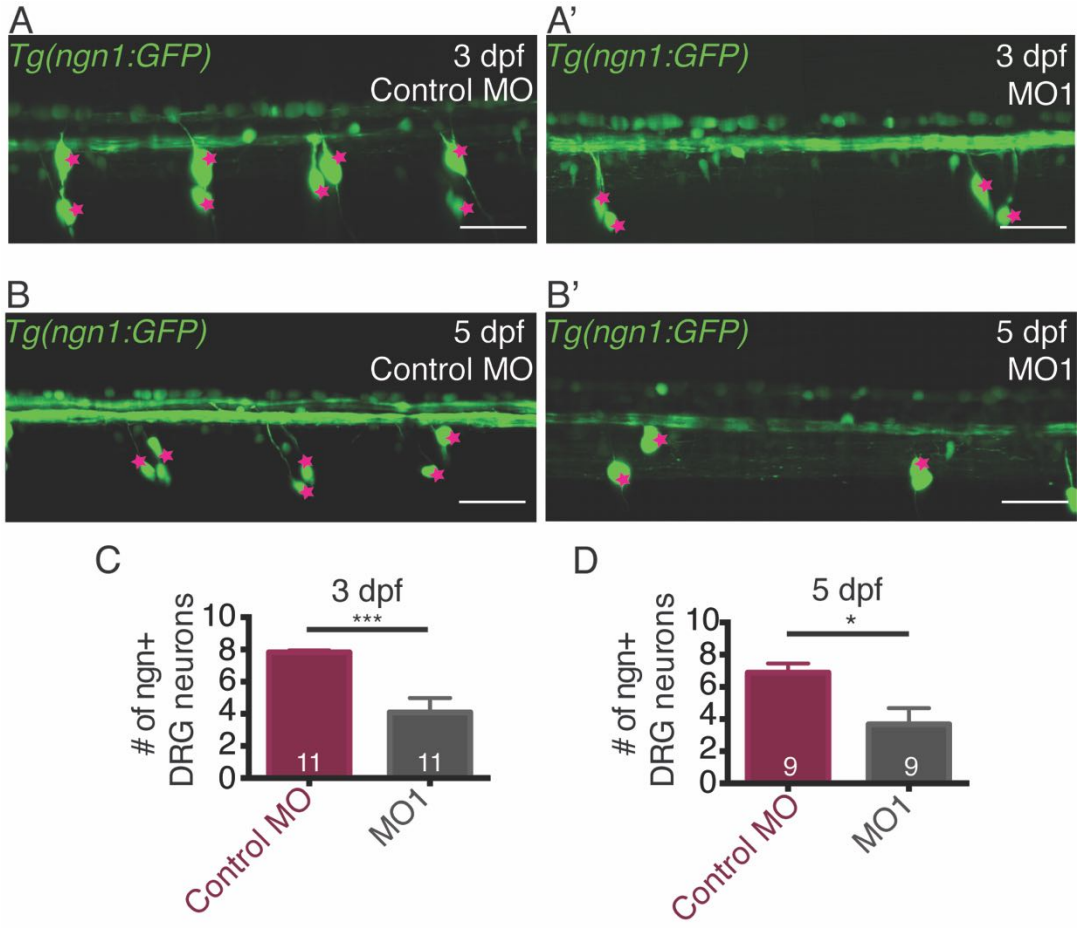

Figure 4.28: 36K knockdown larvae had fewer DRG neurons at 3 dpf and 5 dpf. (A, A', B, B') Representative lateral view images of maximum intensity z-projections acquired from 100 µm stacks using a 2-photon light sheet microscope depicting three-four spinal segments above the yolk extension in *Tg(-8.4ngn1:GFP)* larvae zebrafish at 3 dpf (A, A') and at 5 dpf (B, B') injected with control MO (A, B) and MO1 (A', B'). DRG cells are marked by pink stars. Scale bars: 40 µm. (C, D) Graphs showing number of ngn1+ DRG cells in three-four spinal segments at 3 dpf (C) and at 5 dpf (D). Sample sizes: N = 3. n shown in each bar. For (C), Mann Whitney two tailed test P value 0.0008 (***). For (D), Mann Whitney two tailed test P value 0.02760 (*).

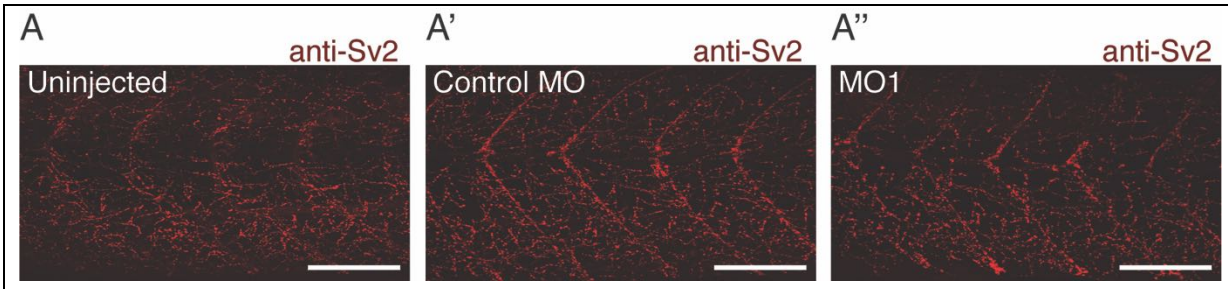

Figure 4.29: 36K knockdown larvae had no change in axonal innervation. (A, A', A'') Representative lateral view of maximum intensity z-projections acquired from 100 µm stacks using a 2-photon point scanning microscope depicting 5 dpf uninjected (A), control MO (A') and MO1 (A'') larvae stained with anti-Sv2 antibodies. Scale bars: 40 µm.

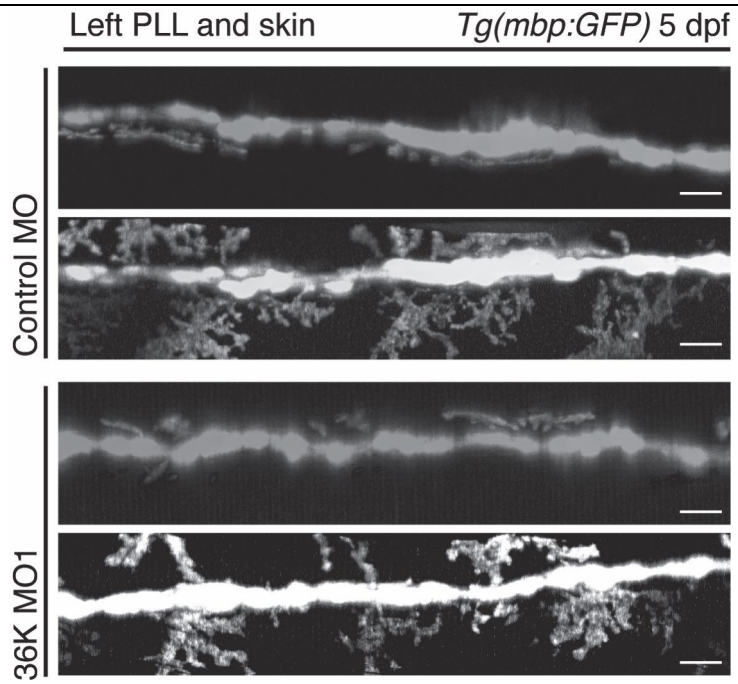

Figure 4.30: 36K knockdown larvae showed no change in peripheral lateral lines. Representative images showing two views of *Tg(mbp:EGFP)* larvae zebrafish at 5 dpf from 3D-projections acquired from 100 µm stacks using a 2-photon light sheet microscope. First upper view depicting peripheral lateral line (PLL) and the second lower view PLL with skin above and below in Control MO (top) and 36K MO1 (bottom) larvae. Scale bars: 20 µm.

4.7. 36K regulates OPC numbers through Notch

Notch is a transmembrane protein, spanning the cell membrane. Notch initially undergoes a Furin protease dependent site 1 (S1) cleavage, which generates the Notch extracellular domain (NECD) non-covalently bound to a transmembrane intracellular fragment (Blaumueller et al., 1997; Kopan et al., 1996; Logeat et al., 1998). Following S1 cleavage, Notch receptors can interact with membrane bound ligands from neighbouring cells. When a ligand binds to Notch, a conformational change is induced and a second ADAM (a disintegrin and metalloprotease) dependent cleavage occurs at Site 2 (S2) in the NECD (Brou et al., 2000; Mumm et al., 2000; van Tetering et al., 2009). Following this cleavage at S2, Notch extracellular truncation targets (NEXT) are then cleaved by presenilin dependent gamma secretase and the Notch intracellular domain (NICD) translocates through the cytoplasm into the nucleus and regulates the expression of transcription factors and downstream genes

(Brou et al., 2000; Louvi and Artavanis-Tsakonas, 2006; Mumm et al., 2000; van Tetering and Vooijs, 2011). In the nucleus, NICD binds with CSL (vertebrate CBF/RBP-κ, Drosophila Su(H), and C. elegans Lag-1) together with co-activator protein Mastermind (MAM), further leading to activation of more/several target genes (Petcherski and Kimble, 2000; Tamura et al., 1995). In the absence of NICD, CSL is associated with co-repressors to repress expression of target genes (Fior and Henrique, 2009; Lubman et al., 2004). Notch activation is depicted in Figure 4.31. Since gamma secretase cleavage is an important step in Notch activation, we used a gamma secretase inhibitor to counteract Notch upregulation in 36K knockdown larvae.

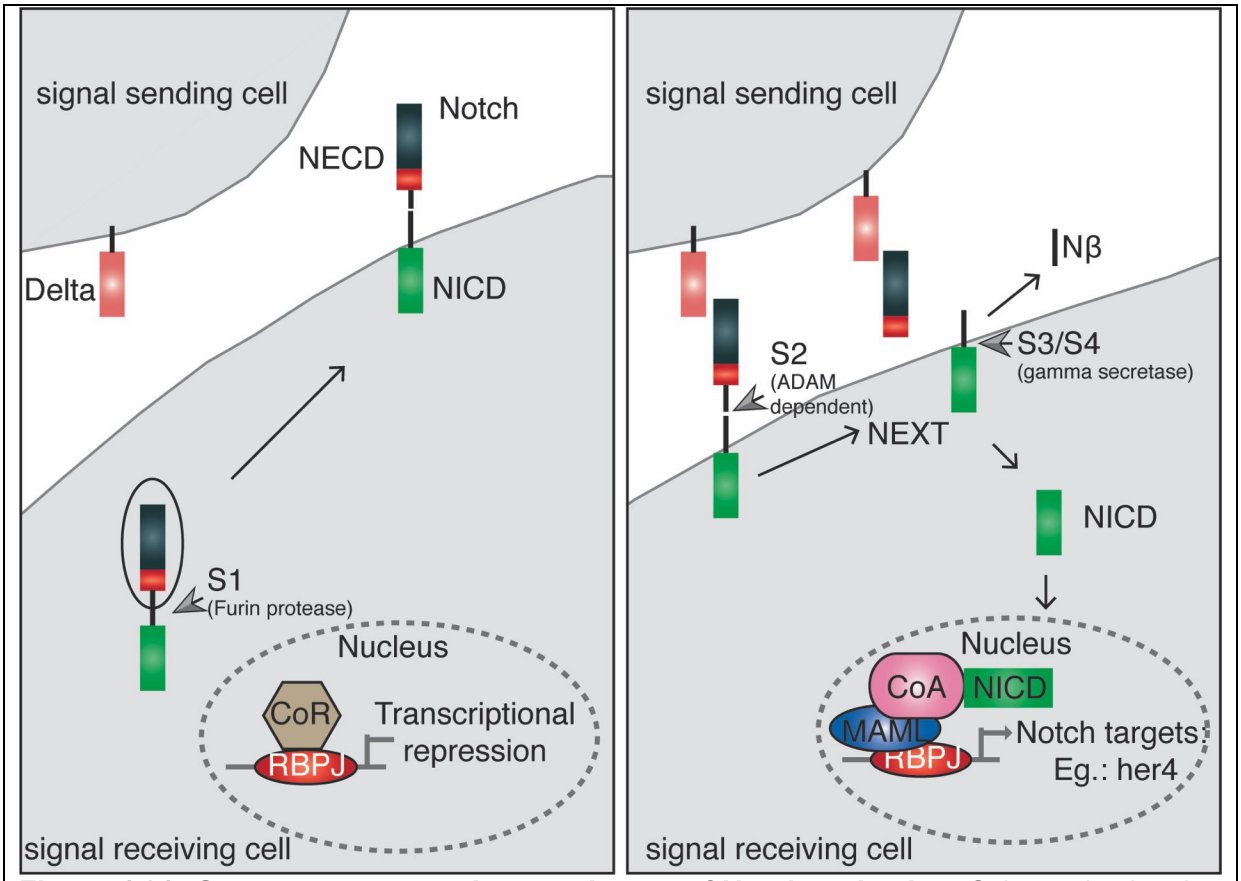

Figure 4.31: Gamma secretase cleavage is part of Notch activation. Schematic showing the steps in activation of Notch. Following S1 site Furin dependent cleavage, ligand can bind to NECD leading to S2 cleavage. Following this, gamma secretase dependent S3/S4 cleavage occurs liberating NICD to translocate into the nucleus further activating the CSL-MAM co-activator complex. In the absence of NICD, CSL binds with co-repressors. Schematic based from (Fior and Henrique, 2009).

4.7.1. DAPT treatment partially rescued length phenotype in 36K knockdown larvae

N-[N-(3,5-difluorophenacetyl)-l-alanyl]-S-phenylglycine t-butyl ester (DAPT), a well-established gamma secretase inhibitor, has been shown to inhibit the cleavage of Notch to form Notch intracellular domain (NICD) and hence impair the activation of Notch pathway (Geling, 2002). With the aim of understanding whether 36K knockdown phenotypes were due to upregulated Notch, MO injected larvae were treated with DAPT. Bath treatment was started from 24 hpf (Figure 4.32A) so that the period of gliogenesis would be covered as explained in Salta et al., 2014. As shown in Figure 4.32B the body length phenotype of MO1 injected zebrafish larvae could be partially rescued with 5 µg/mL DAPT at all ages analysed (Figure 4.32B).

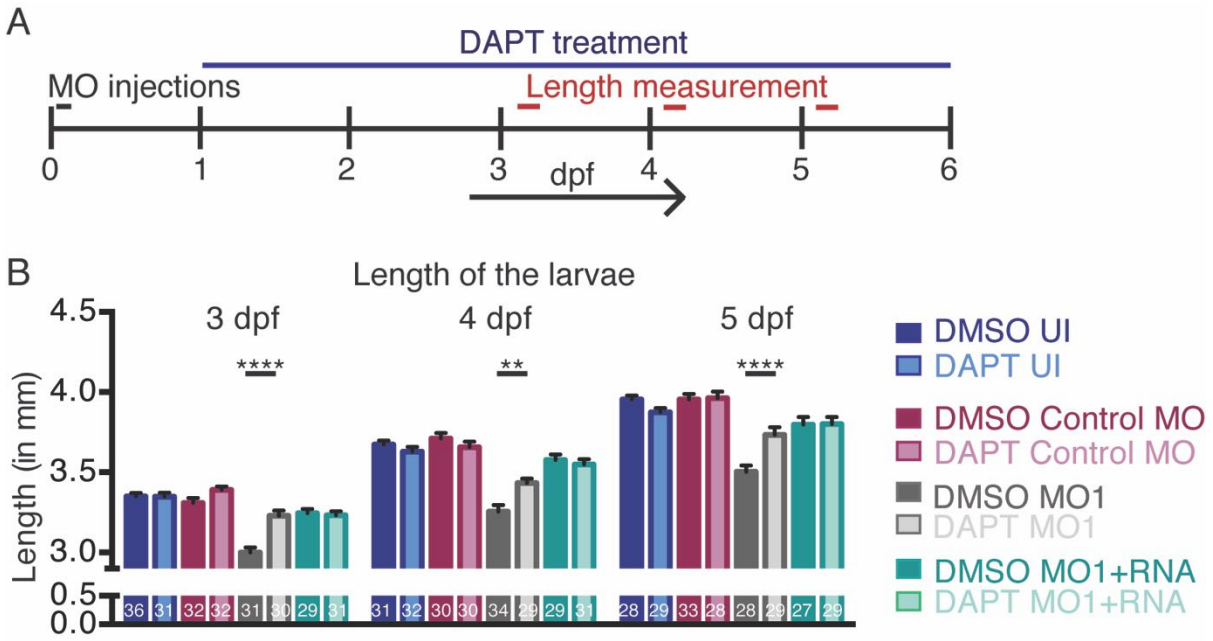

Figure 4.32: Gamma secretase inhibition partially rescued length phenotype in 36K knockdown larvae. (A) Timeline showing MO injections at 0-1 hpf, DAPT treatment from 24 hpf, length measurements at 3, 4, 5 dpf. (B) Graph showing body length of the larvae from different groups at 3, 4 and 5 dpf. Sample sizes: N = 3. n shown in each bar. 2way ANOVA $P \leq 0.0001$ followed by Tukey's multiple comparisons test for DMSO MO1 vs DAPT MO1 at 3 dpf (****), 4 dpf (**), 5 dpf (****).

4.7.2. DAPT treatment rescued dorsally migrated olig2+ OPC numbers in 36K knockdown larvae

Fewer olig2+ OPCs were observed in dorsal spinal cord in 36K knockdown larvae in comparison to control MO group as previously shown (Figure 4.17). To identify whether regulation of dorsally migrated OPC numbers in MO1 larvae was through Notch, dorsally migrated olig2+ OPCs were analysed after DAPT treatment (Figure 4.33A, A', B, B'). Dorsally migrated olig2+ cell numbers were increased in the DAPT treated MO1 group in comparison to DMSO treated MO1 group (Figure 4.33C), suggesting that 36K acts on OPCs through Notch.

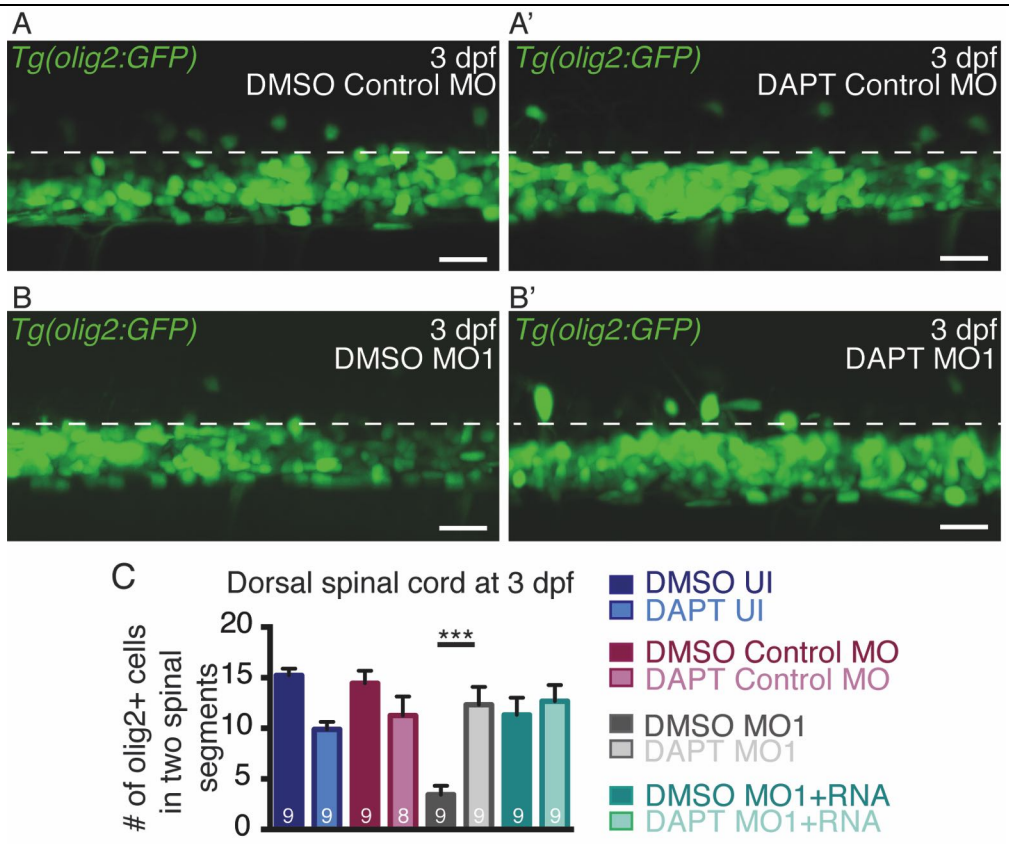

Figure 4.33: DAPT treatment rescued dorsally migrated olig2+ OPC numbers in 36K knockdown larvae. (A, A', B, B') Representative lateral view of maximum intensity z-projections acquired from 100 µm stacks using a 2-photon light sheet microscope depicting two spinal segments above the yolk extension at 3 dpf in *Tg(olig2:GFP)* injected larvae zebrafish with control MO (A, A') and MO1 (B, B'), treated either with DMSO as control (A, B) or DAPT (A', B'). Scale bar: 20 µm. (C) Number of olig2 positive cells in two spinal segments in the dorsal spinal cord. Sample sizes: N = 3. n shown in each bar. One-way analysis of variance ANOVA $P \leq 0.0001$ followed by Tukey's multiple comparisons test for DMSO MO1 vs DAPT MO1 (***).

4.7.3. 36K Morphants might have increased gamma secretase activity

Since gamma secretase inhibitor could rescue the phenotypes in 36K knockdown, we hypothesised that gamma secretase activity is increased in the MO1 fish and hence there is an upregulation of Notch. To examine activity of gamma secretase, cleavage of Amyloid precursor protein (App), a common target of gamma secretase (Krishnaswamy et al., 2009), was evaluated in MO1 larvae by western blot (Figure 4.34A). Anti-App antibody that binds to the C terminus of App was used for this blot so that it could detect App full length (FL), C terminal fragments (CTFs) and also App intracellular domain (AICD). AICD is the part of App cleaved by gamma secretase. App FL was observed as a doublet band at around 98 kD, as previously described in (Song and Pimplikar, 2012). C terminal fragments were observed at around 25 kD and AICD between 9-16 kD. App AICD was found to be increased in MO1 larvae in comparison to control MO larvae (Figure 4.34B).

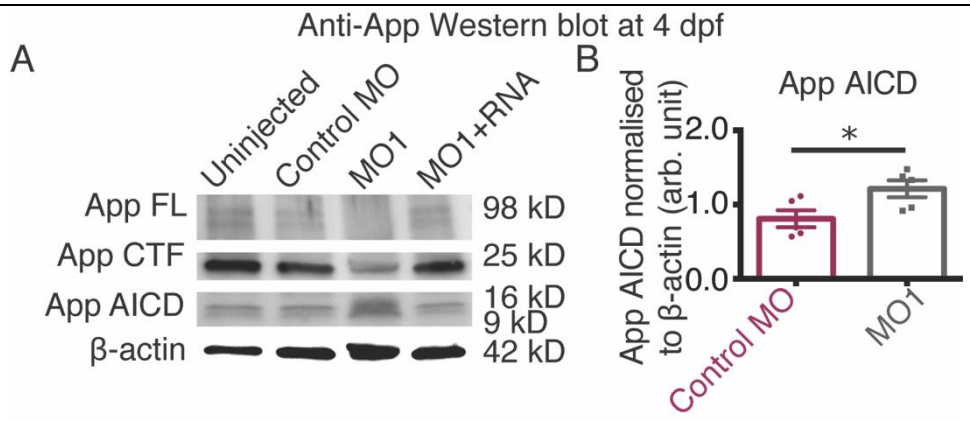

Figure 4.34: 36K Morphants might have more App cleavage. (A) Western blot showing cleaved App AICD, App CTFs and full-length App (App FL). (B) Quantification of different anti-App AICD western blots normalised to β-actin. Sample sizes: N=5. Unpaired two tailed t test with Welch's correction. P Value 0.0366 (*) for App AICD (B).

4.8. 36K knockdown altered membrane lipids

36K belongs to the short chain dehydrogenase (SDR) family (Morris et al., 2004). As some SDRs have been shown to be involved in lipid metabolism (Kavanagh et al., 2008; Persson et al., 2009), we further hypothesised that the activity of gamma secretase is altered due to an alteration in membrane lipids. Several studies have shown association between lipid alterations and their effect on the activity of gamma secretase (Osenkowski et al., 2008; Svennerholm and Gottfries, 1994). Disruptions in genes involved in ganglioside synthesis have also been shown to cause myelination defects (Sheikh et al., 1999). Considering all this, general lipid composition was analysed in 36K knockdown larvae.

4.8.1. 36K knockdown larvae showed reduction in a lipid comigrating with cerebrosides

With the aim of testing whether lipids are altered in MO1 larvae, thin layer chromatography (TLC) was performed in control MO larvae and MO1 larvae together with PD Dr. Matthias Eckhardt, Institute of Biochemistry and Molecular Biology, University of Bonn. In TLC, no changes were observed in total lipids (not shown). However, when sphingolipids were analysed, a weaker band for a lipid comigrating with cerebrosides standards was observed in the MO1 group in comparison to the control MO group (Figure 4.35A). The bands were quantified and the quantification showed a significant reduction in this lipid in the 36K knockdown larvae (MO1) in comparison to the control MO larvae (Figure 4.35B).

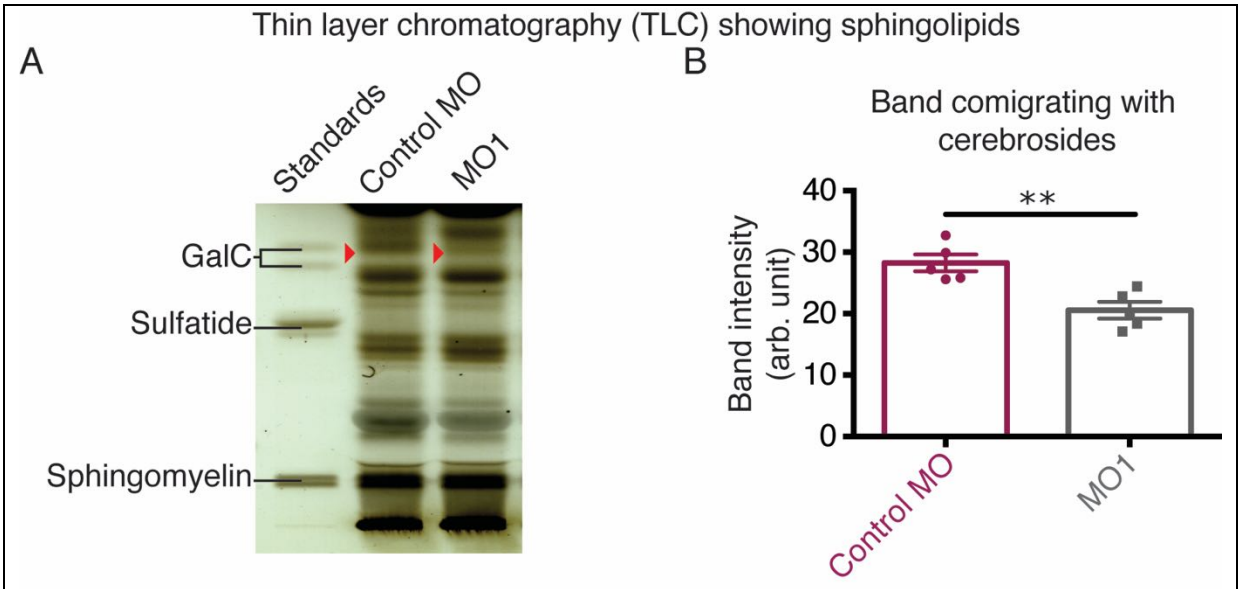

Figure 4.35: 36K knockdown larvae had a reduction in a lipid comigrating with cerebrosides. (A) A representative TLC showing sphingolipids in control MO and MO1 injected larvae at 5 dpf. TLC performed by PD Dr. Matthias Eckhardt. (B) Graph showing quantification of band intensity of the lipid comigrating with cerebrosides from TLC. Sample sizes: N = 5. Each N was from a lysate of 100 larvae per group. Mann Whitney two tailed test P value 0.0079 (**).

4.8.2. 36K knockdown led to an alteration in HexCer containing Sa/So ratio

For further confirming the TLC results and characterising the found lipid change further, liquid chromatography – tandem mass spectrometry (LC-MS/MS) was performed together with PD. Dr. Roger Sandhoff, Lipid Pathobiochemistry Group, German Cancer Research Centre, Heidelberg. When Ceramides (Cer), dihexosylceramides (Hex2Cer), Dihexosylceramides (Hex2Cer) and sulfatides (SM4s) were analysed by LC-MS/MS, no changes were revealed (Figure 4.36A). However, the ratio of hexosylceramides containing a saturated sphingoid base (NdS) over hexosylceramides containing a monosaturated sphingoid base (NS) was reduced in 36K MO1 larvae (Figure 4.36B). Saturated sphingoid base (NdS) is sphinganine (Sa) while monosaturated sphingoid base (NS) is sphingosine (So). The specific molecular mechanism underlying this reduction in hexosylceramides containing Sa/So ratio in 36K knockdown larvae is yet to be studied.

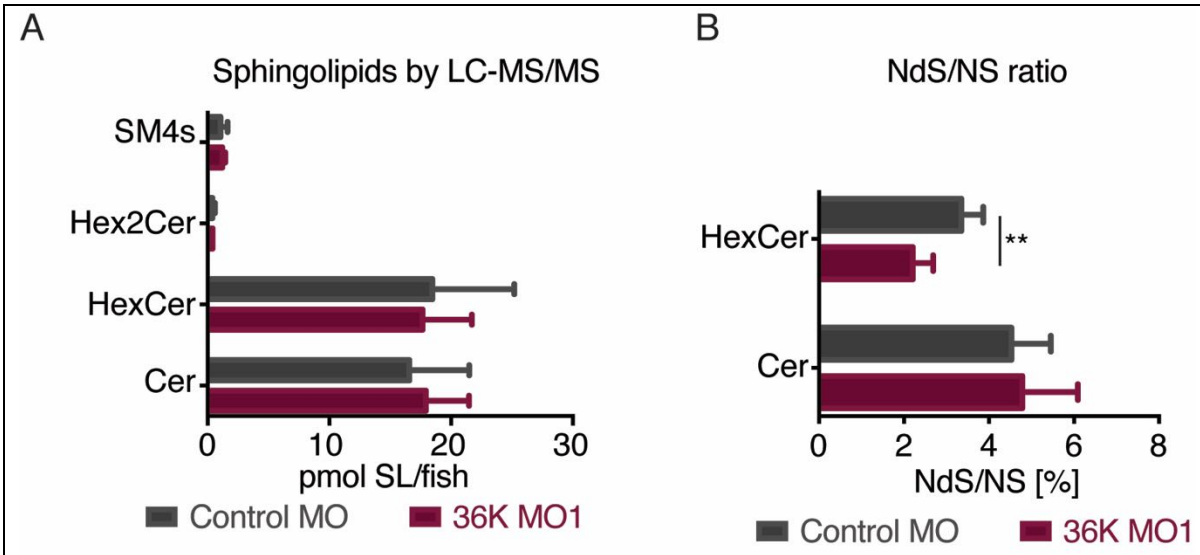

Figure 4.36: 36K knockdown leads to a change in HexCer containing NdS/NS ratio. (A) Graph showing Cer, HexCer, Hex2Cer, SM4s in control MO, MO1 larvae from Mass spectrometry. N=4. (B) HexCer containing a saturated sphingoid base (sphinganine) over those containing a monounsaturated sphingoid base (sphingosine) decreased to 2/3rd in the 36K MO1 zfl. N=4. 2-way ANOVA P ≤ 0.0001 followed by Tukey's multiple comparisons test for HexCer P Value 0.0052 (**). LC-MS/MS performed by PD. Dr. Roger Sandhoff.

5. Discussion

36K can be suggested to have two functions. At an early time point, a small amount of the protein seems sufficient for regulating the membrane lipid composition and thereby Notch activation to influence oligodendrocyte differentiation as described in this study. At a later time point, a high abundant amount of protein might be needed for a structural function similar to Mbp for compaction of CNS myelin.

5.1. 36K, a short chain dehydrogenase is specifically expressed in zebrafish CNS

36K, a protein belonging to the short chain dehydrogenase family (Morris et al., 2004) has been shown to be specifically expressed in the central nervous system (Jeserich and Waehneldt, 1986; Morris et al., 2004). Our custom-made antibodies, which were raised specifically against zebrafish 36K, were tested for specificity within cell culture experiments and MO Knockdown experiments. Further with these antibodies, 36K localization could be confirmed mainly in CNS tissue of larvae and adult zebrafish, which is in accordance with previous studies (Jeserich and Waehneldt, 1986; Morris et al., 2004). Owing to the abundance of 36K, these antibodies can be used as a CNS specific myelin marker in immunostaining even at early larval stages when it is still difficult to visualise other myelin markers.

5.2. 36K Morpholino specifically knocks down 36K expression and causes a behaviour phenotype

Morpholino MO1 could efficiently knock down 36K expression as depicted by western blots and immunostaining. Further confirming the specificity of MO1, and thereby ruling out unknown off-targets, MO phenotypes could be rescued when animals were co-injected with 36K mRNA containing a mutated non-matching MO1 binding site. A second independent

translation blocking Morpholino MO2 caused very similar length phenotype further signifying the specificity of our observations.

36K knockdown resulted in less responsive larvae as demonstrated by stimulated behaviour tests. 36K knockdown larvae swim similar initial distances if they respond in stimulated swim tests. No obvious changes have been found in motor neurons as shown from microarray analysis data and presynaptic innervation as shown using anti-Sv2 staining. Using a fluorescent reporter line and tracing axons would have been a better way to analyse axonal innervation. Mauthner axons are the axons initiating the C-start escape response in zebrafish (Liu and Fetcho, 1999). If they are not properly myelinated, escape response cannot be initiated in the knock down larvae. If motor neurons would have been affected, the swimming response following a stimulus would not be equal (Sonnack et al., 2015). Less startle responses have been previously reported in hypo-myelinated mice models (Poggi et al., 2016; Tanaka et al., 2009). Altogether, this points towards neural conduction or myelination defects rather than muscular defects. Disruption of myelin as shown by *in vivo* imaging using *Mbp* reporters and reduced expression of myelin genes shown by qPCR and microarray analysis data further support myelination defects.

5.3. 36K could have an early role in oligodendrocyte differentiation through Notch and later another role in compact myelin

Fewer claudinK+ oligodendrocytes and fewer dorsally migrated olig2+ OPCs have been observed in 36K knockdown larvae. We observed increased proliferation and no change in apoptotic cell numbers in the 36K knockdown larvae in microarray analysis and immunostaining. This suggests fewer dorsally migrated OPCs could not be due to less proliferation but instead less differentiation towards the oligodendrocyte lineage, as further confirmed by fewer ClaudinK+ and Mbp+ cells. The increased proliferating cells differentiate rather into astrocytes or radial glia than oligodendrocytes as there is an up-regulation of Notch. Notch up-regulation has been shown to promote differentiation towards astrocytes

and radial glia while suppressing oligodendrocyte differentiation (Artavanis-Tsakonas, 1999; Fortini et al., 1993; Grandbarbe, 2003; Kim et al., 2008). Furthermore, differentiation of oligodendrocytes from olig2+ OPCs is favoured by down-regulation of Delta Notch signalling (Louvi and Artavanis-Tsakonas, 2006; Park and Appel, 2003; Tallafuss et al., 2010). Increase in Gfap expression and fewer dorsally migrated olig2+ OPCs in 36K knockdown larvae fit with the hypothesis that 36K alters OPC differentiation through Notch. Increase in Gfap expression could be observed using *TgBAC(gfap:gfap-GFP)* reporter line at 3 dpf and with anti-Gfap staining at 4 dpf. This however could not be confirmed with Western blot (not shown) or in the microarray analysis data. One of the possibilities for this could be because whole larvae were taken for Western blots and microarray analysis, while with the reporter lines and with immunostaining, spinal cord regions were specifically observed. The increase in Gfap expression is likely due to a cell fate change rather than due to reactive astrogliosis, as genes involved in immune response were not found to be altered in the microarray analysis data. Staining for anti-microglial markers or other immune markers could have further confirmed if there is no reactive astrogliosis. Since fewer dorsally migrated olig2+ OPCs were observed at 3 dpf, when there is very little compact myelin yet, and Notch was found to be upregulated, these point towards 36K having an early role in oligodendrocyte differentiation through Notch.

On the other hand, 36K has been shown to be highly expressed in compact myelin (Morris et al., 2004). The expression of 36K was strongest after 7 dpf as shown by qPCR and western blot during development. At 7 dpf most of the CNS myelin is already compacted (Brösamle and Halpern, 2002). This points towards an additional function for 36K at later stages. When zebrafish larvae were treated with TSA from 36 hpf, a histone deacetylase inhibitor which amongst other effects inhibits migration and differentiation of oligodendrocytes (Takada and Appel, 2010), complete absence of 36K was observed as depicted by western blot. Presence of 36K in compact myelin (Morris et al., 2004), disrupted compaction in 36K knockdown larvae as shown by TEM and absence of 36K when there were no differentiated

oligodendrocytes could argue for a later function for 36K in differentiated oligodendrocytes and compact myelin. Further, 36K is a highly basic protein similar to Mbp. The pI value of 36K is 9.6, while that of Mbp is 12. Based on the highly basic nature and globular structure, 36K might have a structural role similar to Mbp in compaction of myelin as previously suggested by (Jeserich and Rauen, 1990). The two possible functions of 36K are depicted in Figure 5.1.

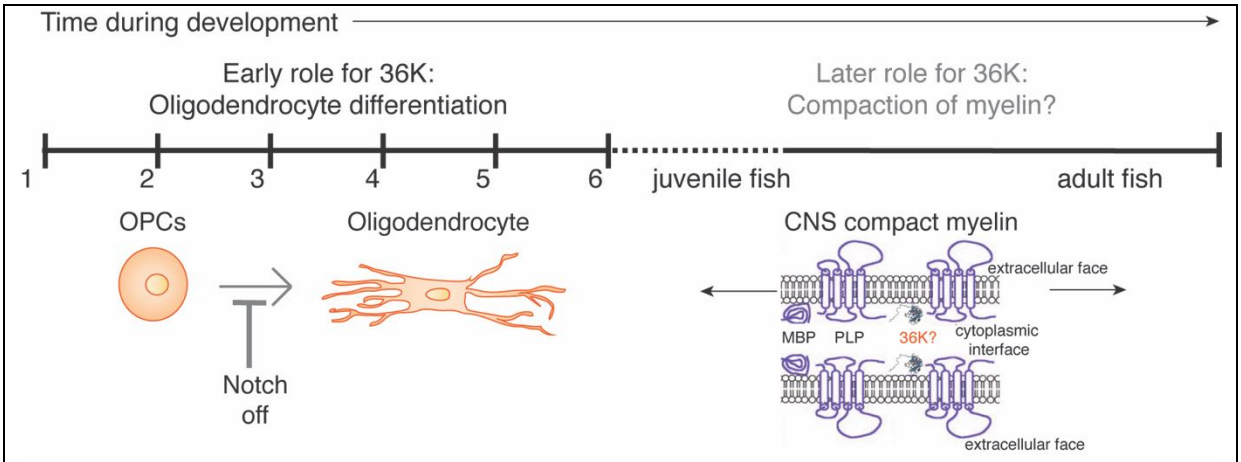

Figure 5.1: 36K might possibly have two functions. At an early time point we show that 36K aids in oligodendrocyte differentiation by directly or indirectly keeping/switching Notch off. At a later time point, 36K might be needed in differentiated oligodendrocytes to compact myelin. It may be involved in structural compaction of myelin similar to Mbp. Schematic includes the structure of compact myelin adapted from (Baumann and Pham-Dinh, 2001) and 36K structure predicted from RaptorX (Ma et al., 2012; Peng and Xu, 2011a, 2011b).

5.4. 36K has a role in OPC differentiation through upregulated Notch

DAPT, a gamma secretase inhibitor, has been shown to indirectly down-regulate Notch (Geling, 2002; Salta et al., 2014). The number of dorsally migrated olig2+ OPCs could be rescued in 36K knockdown larvae, when treated with DAPT, further supporting that 36K regulates CNS myelination through Notch. Higher concentrations of DAPT have been shown to cause defects in somitogenesis (Arslanova et al., 2010). However, a dose dependent titration assay showed that a concentration of 5 µg/mL could rescue/counteract the up-regulation of Notch targets (Salta et al., 2014). We also assessed somite numbers and they

were not found to be altered in 36K knockdown larvae (not shown). Hence this concentration of DAPT was chosen for our experiments and this could rescue the MO effects.

Since the gamma secretase inhibitor DAPT can rescue the 36K MO phenotypes, one might speculate there is an increased activity of gamma secretase in the 36K knockdown larvae. Increased gamma secretase activity is also demonstrated by the increase in App AICD as shown by western blot. However, it cannot be discarded that as a second additional possibility there is also an up-regulation in Notch ligands in 36K knockdown larvae. It can be speculated that the increased Notch ligands might come from the increased number of astrocytes. It is also known that axons coordinate communication with oligodendrocytes during myelin development (Barres and Raff, 1999; Boiko and Winckler, 2006; Piaton et al., 2010; Simons and Trajkovic, 2006). It might also be speculated that less myelinated axons try to establish increased contact with oligodendrocytes in an attempt to increase myelin since there are fewer differentiated oligodendrocytes and less myelin in the knockdown larvae, which might also have played a role in increase in Notch ligands.

Increase in Notch ligands and increased activity of gamma secretase together lead to an up-regulation of Notch signalling and further target genes in 36K knockdown larvae.

5.5. 36K knockdown alters lipid metabolism

Short chain dehydrogenases (SDRs) have been shown to regulate lipid metabolism (Kavanagh et al., 2008; Persson et al., 2009). Since 36K belongs to SDRs (Morris et al., 2004), and Notch ligands and gamma secretase processing of Notch happens within the membrane, we studied membrane lipid alterations in 36K knockdown larvae. Performing thin layer chromatography (TLC) experiments, we observed a reduction in a lipid band co-migrating with cerebrosides standard. The actual identity of the altered lipids could not yet be characterised at the molecular level. With liquid chromatography – tandem mass spectrometry (LC/MS-MS), no change could be observed in sphingomyelin. However, the

ratio of hexosylceramides containing a saturated sphingoid base (sphinganine Sa) over those containing a monounsaturated sphingoid base (sphingosine So) was reduced to two-third in 36K knockdown larvae.

The schematic (Figure 5.2) depicts the possible lipid alterations in 36K knockdown larvae. Galactosylceramides (part of cerebrosides) constitute about 20 % lipid dry weight in mature myelin (Baumann and Pham-Dinh, 2001). The lipid analysis was performed at 5 dpf, when myelin starts to get compacted and is not completely mature yet. This timepoint was chosen to check for early effects on lipids due to the Morpholino knockdown. Since there is no change in ceramides or hexosylceramides when sphingolipids were analysed by LC-MS/MS, but the ratio of hexosylceramides containing sphinganine (hexosylceramide Sa) to hexosylceramides containing sphingosine (hexosylceramide So) is reduced, this could be either due to an increase in hexosylceramides containing sphingosines or a reduction of hexosylceramides containing sphinganines. This might also be due to a reduction in the degradation of hexosylceramide containing sphingosines. However, the exact reasoning and molecular mechanisms in context with the function of 36K are yet to be studied. The reduction in the lipid band co-migrating with cerebrosides standards from TLC might be a yet unknown cerebroside in zebrafish.

Several studies have previously shown an association between lipid alterations and their effects on the activity of gamma secretase and vice versa (Grimm et al., 2006, 2014; Holmes et al., 2012; Oikawa et al., 2012; Osenkowski et al., 2008; Svennerholm and Gottfries, 1994). Lipid alterations can also influence the accessibility and amount of Notch ligands directly (Chillakuri et al., 2013). This can in turn result in up-regulating the Notch pathway together or independent of gamma secretase activity. As there are alterations in membrane lipids in 36K knockdown larvae, although they could not yet be characterised at the molecular level, it is not unreasonable to suggest that 36K regulates lipid metabolism. However, future work is essential to identify if 36K is directly involved in lipid regulation, or whether the observed

changes in lipids are a secondary effect to a change in cell fate or myelin. Performing lipid analysis with mass spectrometry at an even earlier timepoint like 3 dpf might also reveal if the changes in lipids might have caused the changes in Notch or if they might be a secondary effect. Also, the precise molecular mechanisms underlying how and what lipid alterations could affect gamma secretase activity is currently unknown and needs further investigation.

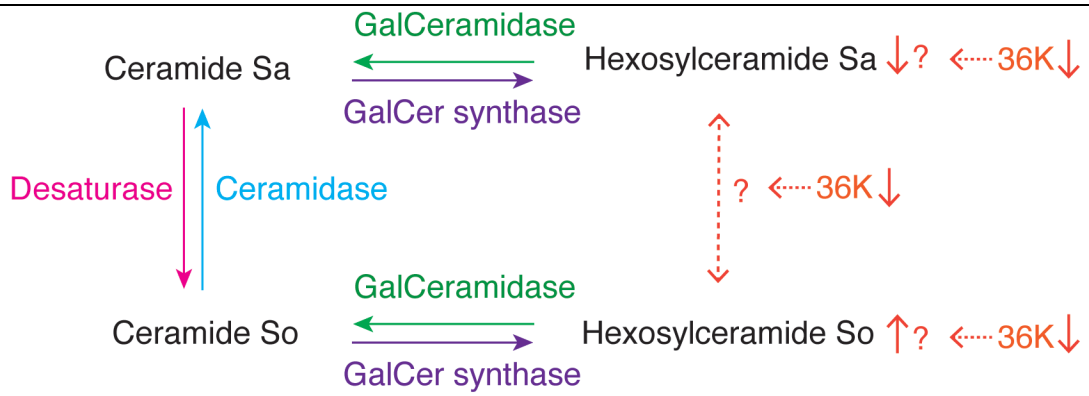

Figure 5.2: Lipid alterations in 36K knockdown larvae. Ceramide Sa is formed from Sa and can be converted to ceramide So by desaturase. These are not altered in 36K knockdown larvae. Ceramide Sa and ceramide So in the presence of GalCer synthase can be converted into hexosylceramide Sa and hexosylceramide So, respectively. The ratio of HexCer Sa to HexCer So is reduced in 36K knockdown larvae which could be due to a reduction in HexCer Sa or increase in HexCer So or an unknown interconversion step between HexCer Sa and HexCer So. Possible changes in the 36K knockdown larvae are marked by red arrows and a question symbol.

In order to further specifically study if 36K alters lipids through its short chain dehydrogenase activity, following 36K knockdown with Morpholino, rescue of 36K expression could be attempted with different mutated forms of *36k* mRNA with mutations in the cofactor binding motif and other conserved cysteine sites.

5.6. Is 36K involved in remyelination?

The usage of two independent Morpholinos against the same target and the rescue experiments confirm the specificity of the observations in the study. Human orthologue SDR12 mRNA could not rescue the effects of MO1 in zebrafish larvae. This might be due to

various possibilities including less similarity between the two orthologues. It could also be that the human orthologue could not be expressed efficiently in zebrafish, or due to differences in functions of SDR12 in humans in comparison to 36K in zebrafish.

In contrast to humans and other mammals, zebrafish exhibit excellent regenerating and remyelinating capacities following injury (Becker and Becker, 2008; Münzel et al., 2012, 2014). One of the reasons for efficient regeneration and remyelination in zebrafish is due to the lack of glial scar formation following injury (Goldshmit et al., 2012). It remains unclear if novel mechanisms or molecules are also necessary for enhancing replacement of oligodendrocytes in adult regeneration and remyelination following injury. Studying remyelination in an essentially non-regenerating system is more difficult than in zebrafish. Zebrafish has been increasingly used as a model for studying myelination and remyelination in the CNS (for review, see Buckley et al., 2008; Preston and Macklin, 2015). Despite certain indisputable limitations for any model, zebrafish are a powerful tool to study developmental myelination as well as remyelination. While much has been learned already from studies in rodents, tractability of the zebrafish nervous system might allow to study *in vivo* cellular behaviour, their response to injury. This might help identify fundamental mechanisms driving white matter repair.

In the future, it will therefore be very interesting to study the possible role of 36K in remyelination. The genes and pathways active during the initial development of myelin might be reactivated following lesion or injury during regeneration of myelin (Dias et al., 2012; Münzel et al., 2012; Park et al., 2008; Reimer et al., 2009, 2013). There is currently no knockout fish-line for 36K available. Generating a knockout mutant for 36K would possibly allow us to follow the function of 36K at later time-points and also to study remyelination. As a complete 36K knockout might very well not be viable, an inducible cell type specific knockout would need to be generated which however, would involve the challenge of identifying a cell type specific promoter or the 36K promoter itself.

During early development, 36K has been shown to have an early function in regulating the differentiation of oligodendrocyte precursor cells into oligodendrocytes through Notch pathway (this study). Initial cell fate decision of an Olig2+ motor neuronal progenitor from pMN region to differentiate into motor neuron or to maintain the precursor state to differentiate into oligodendrocyte later has been shown to be influenced by Delta-Notch signalling (Park and Appel, 2003). 36K might hence play an essential role in cell fate decisions through Notch signalling during development. In the future, colocalising 36K, Notch ligands and/or NICD using fluorescent reporters or combined with immunostaining might confirm further on the direct regulation of 36K on Notch signalling. Notch pathway has also been shown to be reactivated during regeneration (Dias et al., 2012). Indeed, Notch activation has been shown in some case to have detrimental effects on neurogenesis following injury (Yamamoto et al., 2001; for review, see Ables et al., 2011; Pierfelice et al., 2011). Studying the role of 36K on notch signalling and oligodendrocyte differentiation following injury using the above-mentioned knockout mutant when available, might help identify fundamental mechanisms of the role of 36K during regeneration.

5.7. Summary

36K knockdown larvae have alterations in membrane lipids as shown by thin layer chromatography and liquid chromatography - tandem mass spectrometry (LC-MS/MS). The precise mechanisms of how and which lipids are altered by 36K remains however unclear yet. Increased Notch ligands have been observed by microarray analysis and RT-PCR. Increased gamma secretase activity has been shown by increased App AICD. The found lipid alterations might cause an increase in transmembrane Notch ligands and/or enhance the activity of gamma secretase although the precise molecular mechanisms here stay unclear at the moment. These increased Notch ligands and increased gamma secretase activity in turn up-regulates Notch signalling. Since Notch is activated, oligodendrocyte differentiation is inhibited, while astrocyte differentiation is favoured. As there are less

differentiated oligodendrocytes, there is in turn less myelin as shown through myelin reporters. There are also defects in compaction of myelin as shown by transmission electron microscopy which might be due to a later structural function in compaction for 36K similar to that of Mbp.

The observations from this study can be summarized in the following model (Figure 5.3). When 36K is at endogenous levels, lipids and gamma secretase activity remain unaltered, Notch is not activated. OPCs differentiate into oligodendrocytes (Figure 5.3A). When 36K is knocked down, membrane lipids are altered – in a yet to be determined way - which increases Notch ligands and/or the access or activity of gamma secretase. This in turn increases the release of Notch intracellular domain and hence upregulate Notch targets. When Notch is upregulated, oligodendrocyte differentiation is inhibited, and instead more astrocytes are formed (Figure 5.3B). This suggests a role for 36K in balanced regulation of OPC differentiation through its enzymatic activity and further through the Notch pathway during development. Further, in the later stages, 36K might have a structural role in compact myelin like Mbp as suggested by the absence of 36K when there are no differentiated OPCs, which, however needs further investigation.

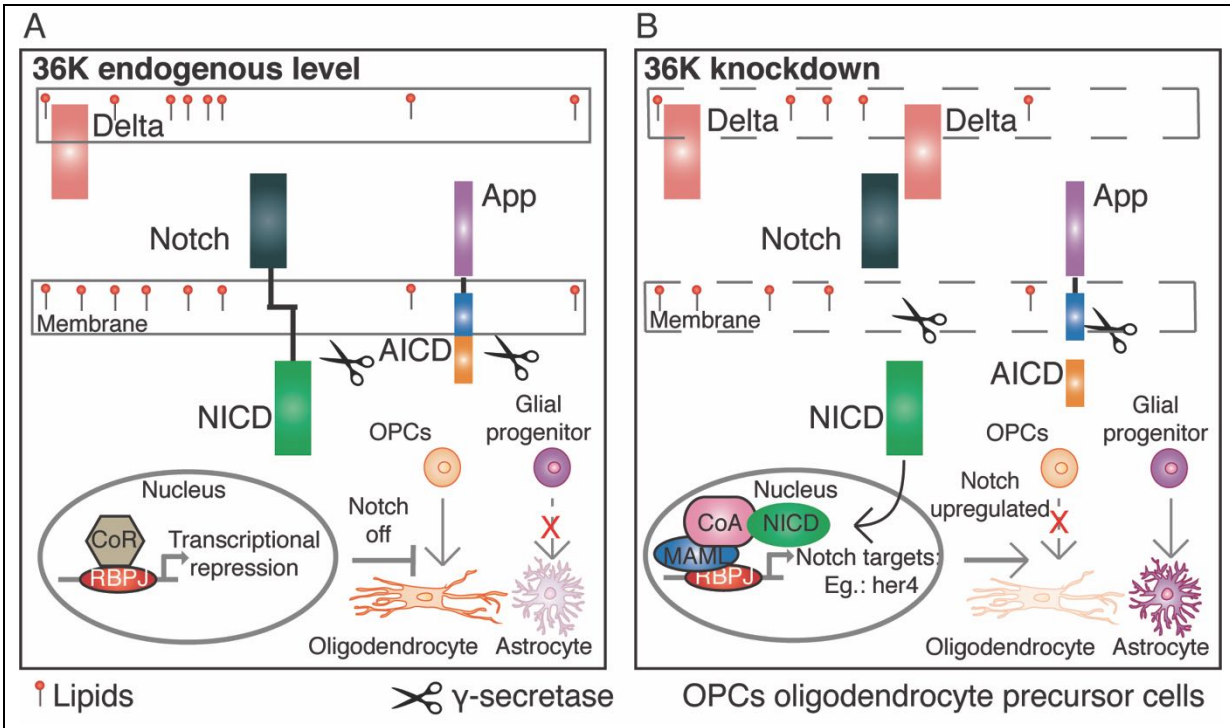

Figure 5.3: 36K down-regulation alters lipids hence increasing Notch ligands and gamma secretase activity finally up-regulating Notch. (A) When 36K is at endogenous amounts, lipids in the membrane are unaltered, access and hence activity of gamma secretase is normal / not increased. Oligodendrocytes differentiate normally. (B) When 36K is knocked down, lipids in the membrane are altered. This might lead to an increased access of Notch ligands and activity of gamma secretase leading to an increased release of NICD, thereby up-regulating Notch. Notch up-regulation in turn inhibits oligodendrocyte differentiation, further leading to less myelin. (Schematic used in Nagarajan et al., in submission, 2018).

5.8. Conclusions

The findings from this study revealed possible functions for 36K in CNS myelin in zebrafish. This study shows an early involvement for 36K in oligodendrocyte differentiation through the Notch signalling pathway, which might be due to an enzymatic role of 36K in lipid metabolism. Since lipids are altered in the membrane in 36K knockdown zebrafish larvae, Notch ligands and gamma secretase activity is increased, further up-regulating Notch cleavage and thereby regulating oligodendrocyte differentiation. In the future, in addition to investigating the direct role of 36K on lipid metabolism, it will be interesting to study the role

of 36K during remyelination in zebrafish. The pathways utilized during initial myelin development to generate and specify cell types might often be reactivated following lesions or pathologies in the adult. Understanding the function of 36K in zebrafish myelin during development and remyelination not only will increase our understanding of teleost myelin, but also potentially open opportunities to further understand demyelination and promote remyelination in human diseases.

Statement

I certify herewith that the dissertation here was completed and written independently by me and without outside assistance. References to the work of others have been cited and acknowledged completely. This work has never been submitted in this, or a similar form, at this or any other domestic or foreign institution of higher learning as a dissertation.

Bhuvaneswari Nagarajan

Publications

Publications

CNS myelin protein 36K regulates developmental oligodendrocyte differentiation (in submission); **Bhuvaneswari Nagarajan**, Alexander Harder, Anna Sophia Japp, Felix Häberlein, Enrico Mingardo, Henning Kleinert, Öznur Yilmaz, Angelika Zoons, Birgit Rau, Andrea Christ, Ulrich Kubitscheck, Britta Eiberger, Roger Sandhoff, Matthias Eckhardt, Dieter Hartmann, Benjamin Odermatt

Controlling Vibrations in Prosthetic Leg; *Lambert Academic Publishing* ISBN 978-3-659-14059-4 (Bachelor's Thesis published as a book), 2012; **Bhuvaneswari Nagarajan**, Janani Kasthurirengan

Main Conferences and Posters

Zebrafish CNS myelin protein 36K regulates developmental oligodendrocyte differentiation; Gordon Research Conference on Myelin, Ventura, CA, USA 2018; **Bhuvaneswari Nagarajan**, Alexander Harder, Anna Sophia Japp, Henning Kleinert, Ulrich Kubitscheck, Matthias Eckhardt, Dieter Hartmann, Benjamin Odermatt

Investigating the function of 36K – a major CNS myelin protein in zebrafish; Conference talk; Bonn International Graduate School of Neurosciences (BIGS) Neuroscience Student Symposium, Bacharach, Germany, 2017; **Bhuvaneswari Nagarajan**

Development of in vivo techniques to study myelination in zebrafish (2-photon light sheet microscopy); Bonn Brain 3, Bonn, Germany, 2015; Eugen Baumgart, **Bhuvaneswari Nagarajan**, Alexander Harder, Nicolai Pechstein, Jan-Hendrik Spille, Peter Königshoven, Ulrich Kubitscheck, Benjamin Odermatt

Establishing in vivo techniques to study myelination and remyelination in zebrafish CNS; Current topics in Myelin research, Kassel, Germany, 2015; **Bhuvaneswari Nagarajan**, Changsheng Liu, Benjamin Odermatt

Acknowledgements

I would like to first thank my academic supervisor Prof. Dr. Benjamin Odermatt for all the support, supervision, for being available for discussions whenever needed and eventually helping me learn to be independent.

I am greatly thankful to my second supervisor Prof. Dr. Ulrich Kubitscheck for all the support whenever needed and the inputs during the progress report sessions.

I would like to specially thank Prof. Dr. Rudolf Merkel for agreeing to be the Fachnahes Mitglied and PD. Dr. Elisabeth Mangold for agreeing to be the Fachfremdes Mitglied for my thesis committee.

I am thankful to BIGS neuroscience for providing a great opportunity for networking and for offering travel grant when needed. I am greatly indebted to Alexander Harder for his constant support with two-photon light sheet microscopy. Special thanks to all collaborators who contributed to the realisation of this work: Dr. Anna Japp, Prof. Dr. Dieter Hartmann, PD Dr. Matthias Eckhardt, PD Dr. Roger Sandhoff, Dr. Britta Eiberger. I am grateful to Prof. Dr. Schilling, Prof. Dr. Baader, Prof. Dr. Stein for the discussions during progress reports and journal club sessions.

Many thanks to all lab members for their support in various ways: Dr. Andrea Toledo for proof-reading my thesis and being a great friend; Öznur Yilmaz for all the help and support when needed; Caroline Kolvenbach, Nina-Katharina Schmitt for being there for discussions whenever needed both work-related and personal; Stephan Terporten, Caroline Kolvenbach, Felix Häberlein, Nina-Katharina Schmitt for the awesome Iceland trip; Enrico Mingardo, Felix Häberlein, Dr. Gabriel Dworschak, Nicoletta Czechowska for keeping me sane over the writing time; Tobias Lindenberg and zebrafish core facility; AG Odermatt for all the Mensa sessions; Dr. Henning Kleinert, for all the translations and help with Bureaucracy during my initial months in Bonn; Dr. Changsheng Liu, Magdalena Schmidt, Leonie Bourauel, Funda Turan, Thomas Hildebrandt, Andrea Christ and all other people at the institute for a very friendly and supportive working environment.

Sincere gratitude to my parents (Nagarajan, Uma) for their everlasting affection and confidence in me. Thanks to all my friends for all the encouragement during this work. Special thanks to Joshua for all the support and care.

Finally, I would like to thank everybody who contributed directly or indirectly to the successful realization of this work.

References

Ables, J.L., Breunig, J.J., Eisch, A.J., and Rakic, P. (2011). Not(ch) just development: Notch signalling in the adult brain. Nat. Rev. Neurosci. *12*, 269–283.

Ahrens, M.B., and Keller, P.J. (2013). Whole-brain functional imaging at cellular resolution using light-sheet microscopy.

Almeida, R.G., Czopka, T., and Lyons, D.A. (2011). Individual axons regulate the myelinating potential of single oligodendrocytes in vivo. *138*, 4443–4450.

Amores, A., Catchen, J., Ferrara, A., Fontenot, Q., and Postlethwait, J.H. (2011). Genome evolution and meiotic maps by massively parallel DNA sequencing: Spotted gar, an outgroup for the teleost genome duplication. Genetics *188*, 799–808.

Araya, C., Ward, L.C., Girdler, G.C., and Miranda, M. (2016). Coordinating cell and tissue behavior during zebrafish neural tube morphogenesis. Dev. Dyn. *245*, 197–208.

Arslanova, D., Yang, T., Xu, X., Wong, S.T., Augelli-Szafran, C.E., and Xia, W. (2010). Phenotypic analysis of images of zebrafish treated with Alzheimer's gamma-secretase inhibitors. BMC Biotechnol. *10*, 1–16.

Artavanis-Tsakonas, S. (1999). Notch Signaling: Cell Fate Control and Signal Integration in Development. Science (80-.). *284*, 770–776.

Avila, R.L., Tevlin, B.R., Lees, J.P.B., Inouye, H., and Kirschner, D.A. (2007). Myelin structure and composition in zebrafish. Neurochem. Res. *32*, 197–209.

Azim, K., and Butt, A.M. (2011). GSK3β negatively regulates oligodendrocyte differentiation and myelination in vivo. Glia *59*, 540–553.

Bai, Q., Sun, M., Stolz, D.B., and Burton, E.A. (2011). Major isoform of zebrafish P0 is a 23.5 kDa myelin glycoprotein expressed in selected white matter tracts of the central nervous system. J. Comp. Neurol. *519*, 1580–1596.

Barres, B.A. (2008). The Mystery and Magic of Glia: A Perspective on Their Roles in Health and Disease. Neuron *60*, 430–440.

Barres, B.A., and Raff, M.C. (1999). Axonal control of oligodendrocyte development. J. Cell Biol. *147*, 1123–1128.

Bauer, N.G., Richter-Landsberg, C., and Ffrench-Constant, C. (2009). Role of the oligodendroglial cytoskeleton in differentiation and myelination. Glia *57*, 1691–1705.

Baumann, N., and Pham-Dinh, D. (2001). Biology of oligodendrocyte and myelin in the mammalian central nervous system. Physiol. Rev. *81*, 871–927.

Becker, C.G., and Becker, T. (2008). Adult zebrafish as a model for successful central nervous system regeneration. Restor. Neurol. Neurosci. *26*, 71–80.

Benjamini, Y., and Hochberg, Y. (1995). Benjamini Y, Hochberg Y. Controlling the false discovery rate: a practical and powerful approach to multiple testing. J. R. Stat. Soc. B *57*, 289–300.

Benjamini, Y., and Hochberg, Y. (2000). On the Adaptive Control of the False Discovery Rate in Multiple Testing With Independent Statistics. J. Educ. Behav. Stat. *25*, 60–83.

Bill, B.R., Petzold, A.M., Clark, K.J., Schimmenti, L.A., and Ekker, S.C. (2009). A Primer for Morpholino Use in Zebrafish. Zebrafish *6*, 69–77.

Blader, P., Plessy, C., and Strähle, U. (2003). Multiple regulatory elements with spatially and temporally distinct activities control neurogenin1 expression in primary neurons of the zebrafish embryo. Mech. Dev. *120*, 211–218.

Blaumueller, C.M., Qi, H., Zagouras, P., and Artavanis-Tsakonas, S. (1997). Intracellular cleavage of Notch leads to a heterodimeric receptor on the plasma membrane. Cell *90*, 281–291.

Boiko, T., and Winckler, B. (2006). Myelin under construction - Teamwork required. J. Cell Biol. *172*, 799–801.

Boison, D., and Stoffel, W. (1994). Disruption of the compacted myelin sheath of axons of the central nervous system in proteolipid protein-deficient mice. Proc. Natl. Acad. Sci. U. S. A. *91*, 11709–11713.

Boison, D., Büssow, H., D'Urso, D., Müller, H.W., and Stoffel, W. (1995). Adhesive properties of proteolipid protein are responsible for the compaction of CNS myelin sheaths. J. Neurosci. *15*, 5502–5513.

Bolstad, B.M., Irizarry, R.A., Astrand, M., and Speed, T.P. (2002). A Comparison of Normalization Methods for High Density Oligonucleotide Array Data Based on Variance and Bias. Dev. Cell 1–9.

Bond, A.M., Bhalala, O.G., and Kessler, J.A. (2012). The dynamic role of bone morphogenetic proteins in neural stem cell fate and maturation. Dev. Neurobiol. *72*, 1068–1084.

Briscoe, J., and Novitch, B.G. (2008). Regulatory pathways linking progenitor patterning, cell fates and neurogenesis in the ventral neural tube. Philos. Trans. R. Soc. Lond. B. Biol. Sci. *363*, 57–70.

Brösamle, C., and Halpern, M.E. (2002). Characterization of myelination in the developing zebrafish. Glia *39*, 47–57.

Brou, C., Logeat, F., Gupta, N., Bessia, C., LeBail, O., Doedens, J.R., Cumano, A., Roux, P., Black, R.A., and Israël, A. (2000). A Novel Proteolytic Cleavage Involved in Notch Signaling. Mol. Cell *5*, 207–216.

Brown, D. (1981). Gene expression in eukaryotes. Science (80-.). *211*, 667–674.

Buckley, C.E., Goldsmith, P., and Franklin, R.J.M. (2008). Zebrafish myelination: a transparent model for remyelination? Dis. Model. Mech. *1*, 221–228.

Campagnoni, a T., and Macklin, W.B. (1988). Cellular and molecular aspects of myelin protein gene expression. Mol. Neurobiol. *2*, 41–89.

Chen, S.L., März, M., and Strähle, U. (2009). Gfap and Nestin Reporter Lines Reveal Characteristics of Neural Progenitors in the Adult Zebrafish Brain. Dev. Dyn. *238*, 475–486.

Chillakuri, C.R., Sheppard, D., Ilagan, M.X.G., Holt, L.R., Abbott, F., Liang, S., Kopan, R., Handford, P.A., and Lea, S.M. (2013). Structural Analysis Uncovers Lipid-Binding Properties of Notch Ligands. Cell Rep. *5*, 861–867.

Cochran, F.B., Yu, R.K., and Ledeen, R.W. (1982). Myelin Gangliosides in Vertebrates. J. Neurochem. *39*, 773–779.

Cornell, R.A., and Eisen, J.S. (2002). Delta/Notch signaling promotes formation of zebrafish neural crest by repressing Neurogenin 1 function. Development *129*, 2639–2648.

Czopka, T. (2016). Insights into Mechanisms of Central Nervous System Myelination Using Zebrafish.

Czopka, T., and Lyons, D. a (2011). Dissecting mechanisms of myelinated axon formation using zebrafish. (Elsevier Inc.).

Dias, T.B., Yang, Y.-J., Ogai, K., Becker, T., and Becker, C.G. (2012). Notch signaling controls generation of motor neurons in the lesioned spinal cord of adult zebrafish. J. Neurosci. *32*, 3245–3252.

Duncan, I.D., Hammang, J.P., and Trapp, B.D. (1987). Abnormal compact myelin in the myelin-deficient rat: absence of proteolipid protein correlates with a defect in the intraperiod line. Proc. Natl. Acad. Sci. U. S. A. *84*, 6287–6291.

Edgar, J.M., and Nave, K.-A. (2009). The role of CNS glia in preserving axon function. Curr. Opin. Neurobiol. *19*, 498–504.

Edwards, a M., Ross, N.W., Ulmer, J.B., and Braun, P.E. (1989). Interaction of myelin basic protein and proteolipid protein. J. Neurosci. Res. *22*, 97–102.

Fetcho, J.R., Higashijima, S., and McLean, D.L. (2008). Zebrafish and motor control over the last decade. Brain Res. Rev. *57*, 86–93.

Fior, R., and Henrique, D. (2009). "Notch-Off": A perspective on the termination of Notch signalling. Int. J. Dev. Biol. *53*, 1379–1384.

Folch, J., and Lees, M. (1951). Proteolipides, a new type of tissue lipoproteins; their isolation from brain. J. Biol. Chem. *191*, 807–817.

Fortini, M.E., Rebay, I., Caron, L.A., and Artavanis-Tsakonas, S. (1993). An activated Notch receptor blocks cell-fate commitment in the developing Drosophila eye. Nature *365*, 555–557.

Franklin, R.J.M., and Ffrench-Constant, C. (2008). Remyelination in the CNS: from biology to therapy. Nat. Rev. Neurosci. *9*, 839–855.

Fuccillo, M., Joyner, A.L., and Fishell, G. (2006). Morphogen to mitogen: the multiple roles of hedgehog signalling in vertebrate neural development. Nat. Rev. Neurosci. *7*, 772–783.

Fünfschilling, U., Supplie, L.M., Mahad, D., Boretius, S., Saab, A.S., Edgar, J., Brinkmann, B.G., Kassmann, C.M., Tzvetanova, I.D., Möbius, W., et al. (2012). Glycolytic oligodendrocytes maintain myelin and long-term axonal integrity. Nature *485*, 517–521.

Gammill, L.S., and Bronner-Fraser, M. (2003). Neural crest specification: Migrating into genomics. Nat. Rev. Neurosci. *4*, 795–805.

Gebriel, M., Prabhudesai, S., Uleberg, K.-E., Larssen, E., Piston, D., Bjørnstad, A.H., and Møller, S.G. (2014). Zebrafish brain proteomics reveals central proteins involved in neurodegeneration. J. Neurosci. Res. *92*, 104–

115.

Geling, A. (2002). A gamma-secretase inhibitor blocks Notch signaling in vivo and causes a severe neurogenic phenotype in zebrafish. EMBO Rep. *3*, 688–694.

Ghavami, S., Hashemi, M., Ande, S.R., Yeganeh, B., Xiao, W., Eshraghi, M., Bus, C.J., Kadkhoda, K., Wiechec, E., Halayko, A.J., et al. (2009). Apoptosis and cancer: Mutations within caspase genes. J. Med. Genet. *46*, 497–510.

Giacomotto, J., and Ségalat, L. (2010). High-throughput screening and small animal models, where are we? Br. J. Pharmacol. *160*, 204–216.

Glasauer, S.M.K., and Neuhauss, S.C.F. (2014). Whole-genome duplication in teleost fishes and its evolutionary consequences. Mol. Genet. Genomics *289*, 1045–1060.

Goldshmit, Y., Sztal, T.E., Jusuf, P.R., Hall, T.E., Nguyen-Chi, M., and Currie, P.D. (2012). Fgf-dependent glial cell bridges facilitate spinal cord regeneration in zebrafish. J. Neurosci. *32*, 7477–7492.

Grandbarbe, L. (2003). Delta-Notch signaling controls the generation of neurons/glia from neural stem cells in a stepwise process. Development *130*, 1391–1402.

Gravel, M., Peterson, J., Yong, V.W., Kottis, V., Trapp, B., and Braun, P.E. (1996). Overexpression of 2 ,3 - Cyclic Nucleotide 3 -Phosphodiesterase in Transgenic Mice Alters Oligodendrocyte Development and Produces Aberrant Myelination. *466*, 453–466.

Griffiths, I., Klugmann, M., Anderson, T., Yool, D., Thomson, C., Schwab, M.H., Schneider, A., Zimmermann, F., McCulloch, M., Nadon, N., et al. (1998). Axonal swellings and degeneration in mice lacking the major proteolipid of myelin. Science (80-.). *280*, 1610–1613.

Grimm, M.O.W., Tschäpe, J.A., Grimm, H.S., Zinser, E.G., and Hartmann, T. (2006). Altered membrane fluidity and lipid raft composition in presenilin-deficient cells. Acta Neurol. Scand. *114*, 27–32.

Grimm, M.O.W., Hundsdörfer, B., Grösgen, S., Mett, J., Zimmer, V.C., Stahlmann, C.P., Haupenthal, V.J., Rothhaar, T.L., Lehmann, J., Pätzold, A., et al. (2014). PS Dependent APP Cleavage Regulates Glucosylceramide Synthase and is Affected in Alzheimer's Disease. Cell. Physiol. Biochem. *34*, 92–110.

Hartline, D.K. (2008). What is myelin? Neuron Glia Biol. *4*, 153–163.

Hellemans, J., Mortier, G., De Paepe, A., Speleman, F., and Vandesompele, J. (2007). qBase relative quantification framework and software for management and automated analysis of real-time quantitative PCR data. Dev. Cell *8*, R19.

Herce, H.D., Rajan, M., Laettig-Tünnemann, G., Fillies, M., and Cardoso, M.C. (2014). A novel cell permeable DNA replication and repair marker. Nucleus *5*, 590–600.

Hill, D.M. (2012). Neural System Development - UNSW Embryology.

Holmes, O., Paturi, S., Ye, W., Wolfe, M.S., and Selkoe, D.J. (2012). Effects of Membrane Lipids on the Activity and Processivity of Purified γ-Secretase. Biochemistry *51*, 3565–3575.

Howe, K., Clark, M., Torroja, C., Torrance, J., Berthelot, C., Muffato, M., Collins, J.E., Humphray, S., McLaren, K., Matthews, L., et al. (2013). The zebrafish reference genome sequence and its relationship to the human genome. Nature *496*, 498–503.

Huisken, J., and Stainier, D.Y.R. (2009). Selective plane illumination microscopy techniques in developmental biology. Development *136*, 1963–1975.

Jahn, O., Werner, H.B., and Nawaz, S. (2013). Molecular Evolution of Myelin Basic Protein , an Abundant Structural Myelin Component.

Jeserich, G. (1983). Protein analysis of myelin isolated from the CNS of fish: Developmental and species comparisons. Neurochem. Res. *8*, 957–970.

Jeserich, G., and Rauen, T. (1990). Cell cultures enriched in oligodendrocytes from the central nervous system of trout in terms of phenotypic expression exhibit parallels with cultured rat Schwann cells. Glia *3*, 65–74.

Jeserich, G., and Waehneldt, T. V (1986). Characterization of antibodies against major fish CNS myelin protein: Immunoblot analysis and immunohistochemical localization of 36K and IP2 proteins in trout nerve tissue. J. Neurosci. Res. *15*, 147–158.

Jonz, M.G., and Nurse, C.A. (2003). Neuroepithelial cells and associated innervation of the zebrafish gill: A confocal immunofluorescence study. J. Comp. Neurol. *461*, 1–17.

Kavanagh, K.L., Jörnvall, H., Persson, B., and Oppermann, U. (2008). Medium- and short-chain dehydrogenase/reductase gene and protein families: The SDR superfamily: Functional and structural diversity within a family of metabolic and regulatory enzymes. Cell. Mol. Life Sci. *65*, 3895–3906.

Kim, H., Shin, J., Kim, S., Poling, J., Park, H.-C., and Appel, B. (2008). Notch-regulated oligodendrocyte specification from radial glia in the spinal cord of zebrafish embryos. Dev. Dyn. *237*, 2081–2089.

Kirby, B.B., Takada, N., Latimer, A.J., Shin, J., Carney, T.J., Kelsh, R.N., and Appel, B. (2006). In vivo time-lapse imaging shows dynamic oligodendrocyte progenitor behavior during zebrafish development. Nat. Neurosci. *9*, 1506–1511.

Klugmann, M., Schwab, M.H., Pühlhofer, A., Schneider, A., Zimmermann, F., Griffiths, I.R., and Nave, K.A. (1997). Assembly of CNS myelin in the absence of proteolipid protein. Neuron *18*, 59–70.

Kopan, R., Schroeter, E.H., Weintraub, H., and Nyet, J.S. (1996). Signal transduction by activated mNotch: Importance of proteolytic processing and its regulation by the extracellular domain. Dev. Biol. *93*, 1683–1688.

Kotani, M., Kawashima, I., Ozawa, H., Terashima, T., and Tai, T. (1993). Differential distribution of major gangliosides in rat central nervous system detected by specific monoclonal antibodies. Glycobiology *3*, 137–146.

Krishnaswamy, S., Verdile, G., Groth, D., Kanyenda, L., and Martins, R.N. (2009). The structure and function of Alzheimer's gamma secretase enzyme complex. Crit. Rev. Clin. Lab. Sci. *46*, 282–301.

Kudoh, T., Wilson, S.W., and Dawid, I.B. (2002). Distinct roles for Fgf, Wnt and retinoic acid in posteriorizing the neural ectoderm. Development *129*, 4335–4346.

Lee, M.-J., Chen, C.J., Cheng, C.-H., Huang, W.-C., Kuo, H.-S., Wu, J.-C., Tsai, M.J., Huang, M.-C., Chang, W.-C., and Cheng, H. (2008). Combined treatment using peripheral nerve graft and FGF-1: changes to the glial environment and differential macrophage reaction in a complete transected spinal cord. Neurosci. Lett. *433*, 163–169.

Lee, Y., Morrison, B.M., Li, Y., Lengacher, S., Farah, M.H., Hoffman, P.N., Liu, Y., Tsingalia, A., Jin, L., Zhang, P., et al. (2012). Oligodendroglia metabolically support axons and contribute to neurodegeneration. Nature *487*, 443–448.

Lessman, C.A. (2011). The developing zebrafish (Danio rerio): A vertebrate model for high-throughput screening of chemical libraries. Birth Defects Res. Part C - Embryo Today Rev. *93*, 268–280.

Li, H., Lu, Y., Smith, H.K., and Richardson, W.D. (2007). Olig1 and Sox10 Interact Synergistically to Drive Myelin Basic Protein Transcription in Oligodendrocytes. J. Neurosci. *27*, 14375–14382.

Litingtung, Y., and Chiang, C. (2000). Control of Shh activity and signaling in the neural tube. Dev. Dyn. *219*, 143–154.

Liu, A., and Niswander, L. a (2005). Bone morphogenetic protein signalling and vertebrate nervous system development. Nat. Rev. Neurosci. *6*, 945–954.

Liu, K.S., and Fetcho, J.R. (1999). Laser ablations reveal functional relationships of segmental hindbrain neurons in zebrafish. Neuron *23*, 325–335.

Logeat, F., Bessia, C., Brou, C., LeBail, O., Jarriault, S., Seidah, N.G., and Israël, A. (1998). The Notch1 receptor is cleaved constitutively by a furin-like convertase. Proc. Natl. Acad. Sci. U. S. A. *95*, 8108–8112.

Louvi, A., and Artavanis-Tsakonas, S. (2006). Notch signalling in vertebrate neural development. Nat. Rev. Neurosci. *7*, 93–102.

Lu, Q.R., Yuk, D.I., Alberta, J.A., Zhu, Z., Pawlitzky, I., Chan, J., McMahon, A.P., Stiles, C.D., and Rowitch, D.H. (2000). Sonic hedgehog-regulated oligodendrocyte lineage genes encoding bHLH proteins in the mammalian central nervous system. Neuron *25*, 317–329.

Lu, Q.R., Sun, T., Zhu, Z., Ma, N., Garcia, M., Stiles, C.D., and Rowitch, D.H. (2002). Common developmental requirement for Olig function indicates a motor neuron/oligodendrocyte connection. Cell *109*, 75–86.

Lubman, O.Y., Korolev, S. V., and Kopan, R. (2004). Anchoring Notch genetics and biochemistry: Structural analysis of the ankyrin domain sheds light on existing data. Mol. Cell *13*, 619–626.

Lyons, D. a, Pogoda, H.-M., Voas, M.G., Woods, I.G., Diamond, B., Nix, R., Arana, N., Jacobs, J., and Talbot, W.S. (2005). Erbb3 and Erbb2 Are Essential for Schwann Cell Migration and Myelination in Zebrafish. Curr. Biol. *15*, 513–524.

Ma, J., Peng, J., Wang, S., and Xu, J. (2012). A conditional neural fields model for protein threading. Bioinformatics *28*, 59–66.

Maden, M. (2006). Retinoids and spinal cord development. J. Neurobiol. *DOI 10.100*, 726–738.

Maga, G., and Hübscher, U. (2003). Proliferating cell nuclear antigen (PCNA): a dancer with many partners. J. Cell Sci. *116*, 3051–3060.

Marshall, C.A.G. (2005). Olig2 Directs Astrocyte and Oligodendrocyte Formation in Postnatal Subventricular Zone Cells. J. Neurosci. *25*, 7289–7298.

Meijering, E., Dzyubachyk, O., and Smal, I. (2012). Methods for cell and particle tracking. Dev. Cell *504*, 183–200.

Meletis, K., Barnabé-Heider, F., Carlén, M., Evergren, E., Tomilin, N., Shupliakov, O., and Frisén, J. (2008). Spinal cord injury reveals multilineage differentiation of ependymal cells. PLoS Biol. *6*, 1494–1507.

Meyer, A. (1998). Hox gene variation and evolution. Nature *391*, 225,227-228.

Meyer, a, and Schartl, M. (1999). Gene and genome duplication in vertebrates: the one-to-four (-to eight in fish) rule and the evolution of novel gene functions. Curr. Opin. Cell Biol. *11*, 699–704.

Meyer, A., and Van De Peer, Y. (2005). From 2R to 3R: Evidence for a fish-specific genome duplication (FSGD). BioEssays *27*, 937–945.

Miller, R.H. (2010). Regulation of oligodendrocyte development in the CNS. Prog. Neurobiol. *67*, 1–17.

Miscevic, F., Rotstein, O., and Wen, X.-Y. (2012). Advances in zebrafish high content and high throughput technologies. Comb. Chem. High Throughput Screen. *15*, 515–521.

Monk, K.R., and Talbot, W.S. (2009). Genetic dissection of myelinated axons in zebrafish. Curr. Opin. Neurobiol. *19*, 486–490.

Morris, J.K., Willard, B.B., Yin, X., Jeserich, G., Kinter, M., and Trapp, B.D. (2004). The 36K protein of zebrafish CNS myelin is a short-chain dehydrogenase. Glia *45*, 378–391.

Morrison, B.M., Lee, Y., and Rothstein, J.D. (2013). Oligodendroglia: metabolic supporters of axons. Trends Cell Biol. *23*, 644–651.

Mumm, J.S., Schroeter, E.H., Saxena, M.T., Griesemer, A., Tian, X., Pan, D.J., Ray, W.J., and Kopan, R. (2000). A Ligand-Induced Extracellular Cleavage Regulates gamma-Secretase-like Proteolytic Activation of Notch1. Mol. Cell *5*, 197–206.

Münzel, E.J., Schaefer, K., Obirei, B., Kremmer, E., Burton, E. a, Kuscha, V., Becker, C.G., Brösamle, C., Williams, A., and Becker, T. (2012). Claudin k is specifically expressed in cells that form myelin during development of the nervous system and regeneration of the optic nerve in adult zebrafish. Glia *60*, 253–270.

Münzel, E.J., Becker, C.G., Becker, T., and Williams, A. (2014). Zebrafish regenerate full thickness optic nerve myelin after demyelination, but this fails with increasing age. Acta Neuropathol. Commun. *2*, 77.

Murphy, M., Reid, K., Dutton, R., Brooker, G., and Bartlett, P.F. (1997). Neural stem cells. J. Investig. Dermatology Symp. Proc. *2*, 8–13.

Nagarajan, B., Harder, A., Japp, A., Häberlein, F., Mingardo, E., Kleinert, H., Yilmaz, Ö., Zoons, A., Rau, B., Christ, A., Kubitscheck, U., Eiberger, B., Sandhoff, R., Eckhardt, M., Hartmann D., and Odermatt, B. (2018). CNS myelin protein 36K regulates developmental oligodendrocyte differentiation. In submission.

Nawaz, S., Sa, P., Schmitt, S., Schaap, I.A.T., Lyons, D.A., and Velte, C. (2015). Actin Filament Turnover Drives Leading Edge Growth during Myelin Sheath Formation in the Article Actin Filament Turnover Drives Leading Edge Growth during Myelin Sheath Formation in the Central Nervous System. 1–13.

Nikolopoulou, E., Galea, G.L., Rolo, A., Greene, N.D.E., and Andrew, J. (2017). Europe PMC Funders Group Neural tube closure : cellular , molecular and biomechanical mechanisms. *144*, 552–566.

Noll, E., and Miller, R.H. (1993). Oligodendrocyte precursors originate at the ventral ventricular zone dorsal to the ventral midline region in the embryonic rat spinal cord. Development *118*, 563–573.

Norton, W.T., and Poduslo, S.E. (1973). Myelination in Rat Brain: Changes in Myelin Composition During Brain Maturation. J. Neurochem. *21*, 759–773.

Oikawa, N., Goto, M., Ikeda, K., Taguchi, R., and Yanagisawa, K. (2012). The γ-secretase inhibitor DAPT increases the levels of gangliosides at neuritic terminals of differentiating PC12 cells. Neurosci. Lett. *525*, 49–53.

Ono, K., Bansal, R., Payne, J., Rutishauser, U., and Miller, R.H. (1995). Early development and dispersal of oligodendrocyte precursors in the embryonic chick spinal cord. Development *121*, 1743–1754.

Osenkowski, P., Ye, W., Wang, R., Wolfe, M.S., and Selkoe, D.J. (2008). Direct and potent regulation of γ-secretase by its lipid microenvironment. J. Biol. Chem. *283*, 22529–22540.

Park, H.-C. (2005). Oligodendrocyte Specification in Zebrafish Requires Notch-Regulated Cyclin-Dependent Kinase Inhibitor Function. J. Neurosci. *25*, 6836–6844.

Park, H.-C., and Appel, B. (2003). Delta-Notch signaling regulates oligodendrocyte specification. Development *130*, 3747–3755.

Park, H.C., Mehta, A., Richardson, J.S., and Appel, B. (2002). Olig2 Is Required for Zebrafish Primary Motor Neuron and Oligodendrocyte Development. Dev. Biol. *248*, 356–368.

Park, K.K., Liu, K., Hu, Y., Smith, P.D., Wang, C., Cai, B., Xu, B., Connolly, L., Kramvis, I., Sahin, M., et al. (2008). Promoting Axon Regeneration in the Adult CNS by Modulation of the PTEN/mTOR Pathway. Science (80-.). *322*, 963–966.

Patzkó, A., and Shy, M.E. (2011). Update on Charcot-Marie-Tooth disease. Curr. Neurol. Neurosci. Rep. *11*, 78–88.

Peng, J., and Xu, J. (2011a). A multiple-template approach to protein threading. Proteins Struct. Funct. Bioinforma. *79*, 1930–1939.

Peng, J., and Xu, J. (2011b). Raptorx: Exploiting structure information for protein alignment by statistical inference. Proteins Struct. Funct. Bioinforma. *79*, 161–171.

Persson, B., Kallberg, Y., Bray, J.E., Bruford, E., Dellaporta, S.L., Favia, A.D., Duarte, R.G., J??rnvall, H., Kavanagh, K.L., Kedishvili, N., et al. (2009). The SDR (short-chain dehydrogenase/reductase and related enzymes) nomenclature initiative. Chem. Biol. Interact. *178*, 94–98.

Petcherski, A.G., and Kimble, J. (2000). Mastermind is a putative activator for Notch [1]. Curr. Biol. *10*, 471–473.

Piaton, G., Gould, R.M., and Lubetzki, C. (2010). Axon-oligodendrocyte interactions during developmental myelination, demyelination and repair. J. Neurochem. *114*, 1243–1260.

Pierani, a, Brenner-Morton, S., Chiang, C., and Jessell, T.M. (1999). A sonic hedgehog-independent, retinoid-activated pathway of neurogenesis in the ventral spinal cord. Cell *97*, 903–915.

Pierfelice, T., Alberi, L., and Gaiano, N. (2011). Notch in the Vertebrate Nervous System: An Old Dog with New Tricks. Neuron *69*, 840–855.

Poggi, G., Boretius, S., Möbius, W., Moschny, N., Baudewig, J., Ruhwedel, T., Hassouna, I., Wieser, G.L., Werner, H.B., Goebbels, S., et al. (2016). Cortical network dysfunction caused by a subtle defect of myelination. Glia *64*, 2025–2040.

Postlethwait, J.H., Woods, I.G., Ngo-Hazelett, P., Yan, Y.L., Kelly, P.D., Chu, F., Huang, H., Hill-Force, A., and Talbot, W.S. (2000). Zebrafish comparative genomics and the origins of vertebrate chromosomes. Genome Res. *10*, 1890–1902.

Preston, M. a., and Macklin, W.B. (2015). Zebrafish as a model to investigate CNS myelination. Glia *63*, 177–193.

Price, S.R., and Briscoe, J. (2004). The generation and diversification of spinal motor neurons: signals and responses. Mech. Dev. *121*, 1103–1115.

Privat, A., Jacque, C., Bourre, J.M., Dupouey, P., and Baumann, N. (1979). Absence of the major dense line in myelin of the mutant mouse “shiverer.” Neurosci. Lett. *12*, 107–112.

Pruvot, B., Curé, Y., Djiotsa, J., Voncken, A., and Muller, M. (2014). Developmental defects in zebrafish for classification of EGF pathway inhibitors. Toxicol. Appl. Pharmacol. *274*, 339–349.

Quarles, R.H. (1997). Glycoproteins of myelin sheaths. J. Mol. Neurosci. *8*, 1–12.

Quarles, R.H., Macklin, W.B., and Morell, P. (2006). Myelin Formation, Sturcture, and Biochemistry. Basic Neurochem. 6th Ed. Mol. Cell. Med. Asp. 51–71.

Raphael, A.R., and Talbot, W.S. (2011). New Insights into Signaling During Myelination in Zebrafish. In Journal of the American College of Cardiology, pp. 1–19.

Ravanelli, A.M., and Appel, B. (2015). Motor neurons and oligodendrocytes arise from distinct cell lineages by progenitor recruitment. Genes Dev. *29*, 2504–2515.

Reimer, M.M., Sörensen, I., Kuscha, V., Frank, R.E., Liu, C., Becker, C.G., and Becker, T. (2008). Motor neuron regeneration in adult zebrafish. J. Neurosci. *28*, 8510–8516.

Reimer, M.M., Kuscha, V., Wyatt, C., Sörensen, I., Frank, R.E., Knüwer, M., Becker, T., and Becker, C.G. (2009). Sonic hedgehog is a polarized signal for motor neuron regeneration in adult zebrafish. J. Neurosci. *29*, 15073–15082.

Reimer, M.M., Norris, A., Ohnmacht, J., Patani, R., Zhong, Z., Dias, T.B., Kuscha, V., Scott, A.L., Chen, Y.-C., Rozov, S., et al. (2013). Dopamine from the Brain Promotes Spinal Motor Neuron Generation during Development and Adult Regeneration. Dev. Cell 1–14.

Richardson, W.D., Pringle, N., Mosley, M.J., Westermark, B., and Dubois-Dalcq, M. (1988). A role for platelet-derived growth factor in normal gliogenesis in the central nervous system. Cell *53*, 309–319.

Roach, A., Takahashi, N., Pravtcheva, D., Ruddle, F., and Hood, L. (1985). Chromosomal mapping of mouse myelin basic protein gene and structure and transcription of the partially deleted gene in shiverer mutant mice. Cell *42*, 149–155.

Rosenfeld, J., and Freidrich, V.L. (1983). Axonal swellings in jimpy mice: Does lack of myelin cause neuronal abnormalities? Neuroscience *10*, 959–966.

Roy, S., Lee, V.M.-Y., Trojanowski, J.Q., and Editor-in-Chief:Â Â Larry R. Squire (2009). Axonal Transport and Neurodegenerative Diseases. 1199–1203.

Rushton, W.A.H. (1951). A theory of the effects of fibre size in medullated nerve. J. Physiol. *115*, 101–122.

Salta, E., Lau, P., Frigerio, C.S., Coolen, M., Bally-cuif, L., and Strooper, B. De (2014). A Self-Organizing miR-132 / Ctbp2 Circuit Regulates Bimodal Notch Signals and Glial Progenitor Fate Choice during Spinal Cord Maturation. Dev. Cell *30*, 423–436.

Sasai, N., Kutejova, E., and Briscoe, J. (2014). Integration of Signals along Orthogonal Axes of the Vertebrate Neural Tube Controls Progenitor Competence and Increases Cell Diversity. PLoS Biol. *12*, e1001907.

Satoh, N., Rokhsar, D., and Nishikawa, T. (2014). Chordate evolution and the three-phylum system. Proc. R. Soc. B Biol. Sci. *281*, 20141729–20141729.

Schaefer, K., and Brösamle, C. (2009). Zwilling-A and -B, two related myelin proteins of teleosts, which originate from a single bicistronic transcript. Mol. Biol. Evol. *26*, 495–499.

Schebesta, M., and Serluca, F.C. (2009). olig1 Expression identifies developing oligodendrocytes in zebrafish and requires hedgehog and notch signaling. Dev. Dyn. *238*, 887–898.

Schmidt-Schultz, T., and Althaus, H.H. (1994). Monogalactosyl Diglyceride, a Marker for Myelination, Activates Oligodendroglial Protein Kinase C. J. Neurochem. *62*, 1578–1585.

Schweitzer, J., Becker, T., Schachner, M., Nave, K.-A., and Werner, H. (2006). Evolution of myelin proteolipid proteins: gene duplication in teleosts and expression pattern divergence. Mol. Cell. Neurosci. *31*, 161–177.

Sheikh, K. a, Sun, J., Liu, Y., Kawai, H., Crawford, T.O., Proia, R.L., Griffin, J.W., and Schnaar, R.L. (1999). Mice lacking complex gangliosides develop Wallerian degeneration and myelination defects. Proc. Natl. Acad. Sci. U. S. A. *96*, 7532–7537.

Sherman, D.L., and Brophy, P.J. (2005). Mechanisms of axon ensheathment and myelin growth. Nat. Rev. Neurosci. *6*, 683–690.

Shimeld, S.M., and Holland, P.W. (2000). Vertebrate innovations. Proc. Natl. Acad. Sci. U. S. A. *97*, 4449–4452.

Shin, J., Park, H.-C., Topczewska, J.M., Mawdsley, D.J., and Appel, B. (2003). Neural cell fate analysis in zebrafish using olig2 BAC transgenics. Methods Cell Sci. *25*, 7–14.

Simons, M., and Trajkovic, K. (2006). Neuron-glia communication in the control of oligodendrocyte function and myelin biogenesis. J. Cell Sci. *119*, 4381–4389.

Snaidero, N., Czopka, T., Hekking, L.H.P., Mathisen, C., Verkleij, D., Mo, W., Goebbels, S., Edgar, J., Merkler, D., Lyons, D.A., et al. (2014). Myelin Membrane Wrapping of CNS Axons by PI(3,4,5)P3-Dependent Polarized Growth at the Inner Tongue. 277–290.

Song, P., and Pimplikar, S.W. (2012). Knockdown of amyloid precursor protein in zebrafish causes defects in motor axon outgrowth. PLoS One *7*.

Sonnack, L., Kampe, S., Muth-Köhne, E., Erdinger, L., Henny, N., Hollert, H., Schäfers, C., and Fenske, M. (2015). Effects of metal exposure on motor neuron development, neuromasts and the escape response of zebrafish embryos. Neurotoxicol. Teratol. *50*, 33–42.

Stanford, S.C. (2007). The Open Field Test: Reinventing the wheel. J. Psychopharmacol. *21*, 134–135.

Stolt, C.C. (2002). Terminal differentiation of myelin-forming oligodendrocytes depends on the transcription factor Sox10. Genes Dev. *16*, 165–170.

Streisinger, G., Walker, C., Dower, N., Knauber, D., and Singer, F. (1981). Production of clones of homozygous diploid zebra fish (Brachydanio rerio). Nature *291*, 293–296.

Sugimoto, Y., Taniguchi, M., Yagi, T., Akagi, Y., Nojyo, Y., and Tamamaki, N. (2001). Guidance of glial procursor cell migration by selected cues in the developing optic nerve. Development *128*, 3321–3330.

Svennerholm, L., and Gottfries, C. -G (1994). Membrane Lipids, Selectively Diminished in Alzheimer Brains, Suggest Synapse Loss as a Primary Event in Early-Onset Form (Type I) and Demyelination in Late-Onset Form (Type II). J. Neurochem. *62*, 1039–1047.

Takada, N., and Appel, B. (2010). Identification of genes expressed by zebrafish oligodendrocytes using a differential microarray screen. Dev. Dyn. *239*, 2041–2047.

Takagi, M., Sueishi, M., Saiwaki, T., Kametaka, A., and Yoneda, Y. (2001). A Novel Nucleolar Protein, NIFK, Interacts with the Forkhead Associated Domain of Ki-67 Antigen in Mitosis. J. Biol. Chem. *276*, 25386–25391.

Takke, C., Dornseifer, P., v Weizsäcker, E., and Campos-Ortega, J.A. (1999). her4, a zebrafish homologue of the Drosophila neurogenic gene E(spl), is a target of NOTCH signalling. Development *126*, 1811–1821.

Tallafuss, A., Trepman, A., and Eisen, J.S. (2010). DeltaA mRNA and protein distribution in zfish nervous system. Dev. Dyn *238*, 3226–3236.

Tamura, K., Taniguchi, Y., Minoguchi, S., Sakai, T., Tun, T., Furukawa, T., and Honjo, T. (1995). Physical interaction between a novel domain of the receptor Notch and the transcription factor RBP-Jκ/Su(H). Curr. Biol. *5*, 1416–1423.

Tanaka, H., Ma, J., Tanaka, K.F., Takao, K., Komada, M., Tanda, K., Suzuki, A., Ishibashi, T., Baba, H., Isa, T., et al. (2009). Mice with Altered Myelin Proteolipid Protein Gene Expression Display Cognitive Deficits Accompanied by Abnormal Neuron-Glia Interactions and Decreased Conduction Velocities. J. Neurosci. *29*, 8363–8371.

van Tetering, G., and Vooijs, M. (2011). Proteolytic cleavage of Notch: “HIT and RUN”. Curr. Mol. Med. *11*, 255–269.

van Tetering, G., van Diest, P., Verlaan, I., van der Wall, E., Kopan, R., and Vooijs, M. (2009). Metalloprotease ADAM10 is required for Notch1 site 2 cleavage. J. Biol. Chem. *284*, 31018–31027.

Theret, N., Boulenguer, P., Fournet, B., Fruchart, J.C., Bourre, T.J.M., and Delbart, C. (1988). Acylgalactosylceramides in Developing Dysmyelinating Mutant Mice.

Traiffort, E., Zakaria, M., Laouarem, Y., and Ferent, J. (2016). Hedgehog: A Key Signaling in the Development of the Oligodendrocyte Lineage. J. Dev. Biol. *4*, 28.

Ulloa, F., and Martı, E. (2010). Wnt Won the War : Antagonistic Role of Wnt over Shh Controls Dorso-Ventral Patterning of the Vertebrate Neural Tube. 69–76.

De Vos, K.J., and Hafezparast, M. (2017). Neurobiology of axonal transport defects in motor neuron diseases: Opportunities for translational research? Neurobiol. Dis. *105*, 283–299.

De Vos, K.J., Grierson, A.J., Ackerley, S., and Miller, C.C.J. (2008). Role of Axonal Transport in Neurodegenerative Diseases. Annu. Rev. Neurosci. *31*, 151–173.

Wan, Q.F., Zhou, Z.Y., Thakur, P., Vila, A., Sherry, D.M., Janz, R., and Heidelberger, R. (2010). SV2 Acts via Presynaptic Calcium to Regulate Neurotransmitter Release. Neuron *66*, 884–895.

Weinstein, J.A. (2010). High-Throughput Sequencing of the Zebrafish Antibody Repertoire Joshua A. Weinstein,. Zebrafish *807*, 807–810.

Wilson, L., and Maden, M. (2005). The mechanisms of dorsoventral patterning in the vertebrate neural tube. Dev. Biol. *282*, 1–13.

Yamamoto, S., Nagao, M., Sugimori, M., Kosako, H., Nakatomi, H., Yamamoto, N., Takebayashi, H., Nabeshima, Y., Kitamura, T., Weinmaster, G., et al. (2001). Transcription factor expression and Notch-dependent regulation of neural progenitors in the adult rat spinal cord. J Neurosci *21*, 9814–9823.

Yu, W., McDonnell, K., Taketo, M.M., and Bai, C.B. (2008). Wnt signaling determines ventral spinal cord cell fates in a time-dependent manner. Development *135*, 3687–3696.

Zalc, B. (2016). The acquisition of myelin: An evolutionary perspective. Brain Res. *1641*, 4–10.

Zalc, B., Monge, M., Dupouey, P., Hauw, J.J., and Baumann, N.A. (1981). Immunohistochemical localization of galactosyl and sulfogalactosyl ceramide in the brain of the 30-day-old mouse. Brain Res. *211*, 341–354.

Zhou, Q., and Anderson, D.J. (2002). The bHLH transcription factors OLIG2 and OLIG1 couple neuronal and glial subtype specification. Cell *109*, 61–73.

Zhou, Q., Choi, G., and Anderson, D.J. (2001). The bHLH transcription factor Olig2 Promotes oligodendrocyte differentiation in collaboration with Nkx2.2. Neuron *31*, 791–807.

Zuchero, J.B., Fu, M., Sloan, S.A., Ibrahim, A., Olson, A., Zaremba, A., Dugas, J.C., Wienbar, S., Caprariello, A.V., Kantor, C., et al. (2015). CNS Myelin Wrapping Is Driven by Actin Disassembly. Dev. Cell 1–16.